Murine *in vivo* tumor models for investigating the anticancer potential of natural and synthetic compounds

von Carina Atzberger

Inaugural-Dissertation zur Erlangung der Doktorwürde der
Tierärztlichen Fakultät der Ludwig-Maximilians-Universität
München

Murine *in vivo* tumor models for investigating the anticancer potential of natural and synthetic compounds

von Carina Atzberger

aus Erding

München 2018

Aus dem Veterinärwissenschaftlichen Department der Tierärztlichen Fakultät

der Ludwig-Maximilians-Universität München

Lehrstuhl für Molekulare Tierzucht und Biotechnologie

Arbeit angefertigt unter der Leitung von Univ.-Prof. Dr. Eckhard Wolf

Angefertigt an:

Fakultät für Chemie und Pharmazie, Lehrstuhl für Pharmazeutische Biologie

der Ludwig-Maximilians-Universität München

Mentorin: Univ.-Prof. Dr. Angelika M. Vollmar

Gedruckt mit Genehmigung der Tierärztlichen Fakultät
der Ludwig-Maximilians-Universität München

Dekan:	Univ.-Prof. Dr. Reinhard K. Straubinger, Ph.D.
Berichterstatter:	Univ.-Prof. Dr. Eckhard Wolf
Korreferent/en:	Univ.-Prof. Dr. Hermann Ammer

Tag der Promotion: 27. Juli 2018

Meiner Familie

TABLE OF CONTENTS

ABBREVIATIONS

°C	degree Celsius
µl	microliter
AML	acute myeloid leukemia
BCS	body condition score
d	day(s)
DMEM	Dulbecco's Modified Eagle Medium
DMSO	dimethyl sulfoxide
DTC	differentiated thyroid carcinoma
e.g.	exempli gratia (for example)
EDTA	ethylenediamine tetra-acetic acid
FCS	fetal calf serum
FELASA	Federation of European Laboratory Animal Science Associations
G	gauge
h	hour(s)
H	height
HCC	hepatocellular carcinoma
HPLC	high performance liquid chromatography
i.p.	intraperitoneal(ly)
i.v.	intravenous(ly)
IVIS®	*in vivo* imaging system
kg	kilogram
KO	knock out
L	length
luc	luciferase
MED	minimum effective dose
mg	milligram
min	minute(s)
MTD	maximum tolerated dose
NAADP	nicotinic acid adenine dinucleotide phosphate
NSG	NOD *scid* gamma
NT	non-targeting
PBS	phosphate buffered saline
PDX	patient derived xenograft
PEG	polyethylene glycol
PFA	paraformaldehyde
Raf	rapidly accelerated fibrosarcoma
RCC	renal-cell carcinoma
resi	resistant
ROI	region of interest
rpm	revolutions per minute
RPMI	Roswell Park Memorial Institute
s.c.	subcutaneous(ly)
S.E.M.	standard error of the mean
SCID	severe combined immunodeficiency
si	small interfering
TPC	two-pore channel
W	width
wt	wildtype

I. INTRODUCTION

Cancer is one of the biggest health problems in our days and led to 14.1 million new cancer cases and 8.2 million cancer related deaths worldwide in 2012. The leading cause of cancer in males worldwide is lung cancer, followed by prostate and colorectal cancer. In females, breast cancer is the most frequently diagnosed form of cancer, followed by colorectal cancer and lung cancer [1]. Lung cancer causes the most cancer related deaths in males followed by liver cancer, whereas breast cancer is the major cause of cancer related deaths in females. Estimations of the American Cancer Society predict 21.7 million new cancer cases and 13 million cancer related deaths in 2030 due to growth and aging of the population and different other risk factors [1, 2]. These risk factors are omnipresent in our societies and are frequently increasing. According to the American Cancer Society, lung cancer is primarily caused by tobacco smoking and air pollution. Therefore, lung cancer could be prevented effectively by tobacco control and campaigns against smoking [1]. A further risk factor for various cancers like colon cancer or post-menopausal breast cancer could be detected in an excess body mass index and overweight [3]. Moreover, malnutrition with consuming large amounts of red and processed meat can increase the risk of developing for instance colorectal and lung cancer [4]. An increased alcohol intake, virus infections with hepatitis B and C virus, tobacco smoking and aflatoxin uptake are common risk factors for developing liver cancer [5, 6]. Also altered reproductive patterns can have influence on cancer development both in women and in children. Moreover, recent use of oral contraceptives slightly increases the risk of developing breast cancer in females [7]. At the same time, the risk to develop acute lymphoblastic leukemia in children is increased with older parental age [8].

The five-year survival in patients between 15 and 74 years diagnosed with liver cancer amounts 17%, 61% for leukemia, and 88% for breast cancer in females in Germany [9]. These survival rates combined with the expected increasing cancer cases in the future and omnipresent risk factors elucidate that novel cancer therapeutics are required.

Procedures taking place in humans or animals are hardly to imitate in cell culture or *in vitro* setups. Pharmacokinetics, i.e. resorption, distribution, metabolism and excretion have an important influence on a compound`s mode of action in animal models [10]. Furthermore, insights in efficacy and toxicity are gained by animal models in an early state of developing a compound. Finally, *in vivo* models can serve as an important source of information between *in vitro* testing and clinical application, but always being aware of animal experiments` limitations relating to their translation to clinical practice. Today, animal experiments represent the major preclinical tool of evaluating the potential of therapeutic cancer drugs. Therefore, *in vivo* models still remain a unique source of *in vivo* information, besides emerging translational alternatives [11]. Finally, even critical scientists support that “animal models can and have provided many crucial insights that have led to major advances in medicine” [12].

The aim of our lab is to contribute to finding new cancer therapeutics. Therefore, we use promising novel compounds and test them on their anticancer potential. Natural and sometimes synthetic compounds are tested on different tumor cell lines, patient derived xenograft cells or patient cells *in vitro*. In this project, the most promising of these compounds are tested *in vivo* as a further step of characterizing their potential.

1. Animal experiments in cancer research

According to the “Bundesministerium für Ernährung und Landwirtschaft” (BMEL) 2,753,051 laboratory animals were used for research purposes in Germany in 2015. 58.7% of all laboratory animals were used for basic research purposes, containing 6.7% for oncology research. Furthermore, 13.6% of all laboratory animals were used for translational and applied research purposes, containing 33.9% research on oncologic diseases. The biggest group of laboratory animals was represented by 2,005,097 mice [13]. Advantages of mice are their small size and therefore their uncomplicated maintenance. Moreover, they have high reproduction rates, a short life span and large litters [14, 15].

In terms of oncology research, there are different ways to classify murine cancer models. The first point to schedule tumor models are ectopic and

orthotopic models. Solid tumors can be generated by injecting tumor cells of different origin subcutaneously which is an often-used ectopic tumor model. Tumor cells injected directly into the organ they physiologically appear, like for example the mammary fat pad for breast cancer cells or the liver for hepatocellular carcinoma, create an orthotopic tumor model [16, 17]. By injecting tumor cells into the bloodstream an assay of colony formation, also called dissemination assay can be conducted. Moreover, it can be differentiated between syngeneic and xenograft transplantations of tumor cells. While syngeneic models work with tumor cells and mice with an identical genetic background, xenograft models combine cancer cells of one species (e.g. human cancer cells) with immunocompromised mice. In syngeneic tumor models, mice with an intact immune system are used, so the influence of the immune system on tumors can be considered [16]. In contrast the benefit of xenograft models is the closer relation to human patients, but as these mice are immunocompromised, the role of the immune system is reduced [18]. Highly immunocompromised mice are often used as humanized mouse models for tumors of the hematopoietic system and for research with patient-derived xenograft cells [19, 20]. As the mouse genome was completely sequenced in 2002, genetical manipulations are also conducted in mice [21]. Besides of injecting cancer cells into mice to create a tumor, research on transgenic mouse models is done to get insights in genes responsible for cancer formation. By genetic modification of these genes, it is also possible that mice develop tumors spontaneously and therefore represent a better model of human cancer patients [18]. To evaluate novel chemotherapeutics also genetically altered mice are used to predict chemotherapy response in human patients [22].

According to the German animal welfare act, animals have to be alimented, maintained, and housed suitable to their species [23]. Therefore, interactions with laboratory animals and use of them always has to be based on ethical and humane standards and is protected by the German animal protection law.

In this thesis, different murine tumor models were used to investigate the potential of natural and synthetic compounds against cancer cells *in vivo*. These tumor models give the opportunity to evaluate variable modes of action a compound showed *in vitro* before, as e.g. inhibition of tumor cell

proliferation, inhibition of metastasis formation, or inhibition of tumor cell migration, *in vivo*.

Tumor dissemination assays are often used as a first step of *in vivo* characterization of compounds, which showed promising effects on tumor cell migration and invasion *in vitro*. Thus, dissemination assays show if a compound has general influence on tumor formation *in vivo*.

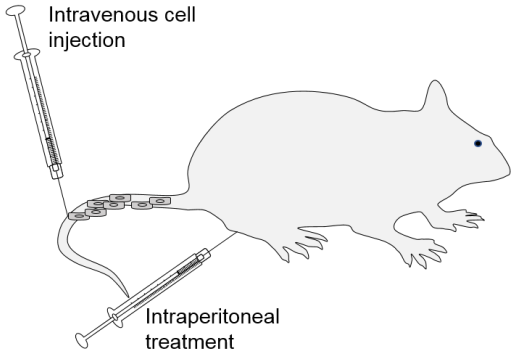

Figure 1: Tumor dissemination model

In ectopic tumor models, the influence on tumor proliferation and tumor growth of a compound can be evaluated via measurements with a digital caliper or bioluminescence imaging using the IVIS® spectrum.

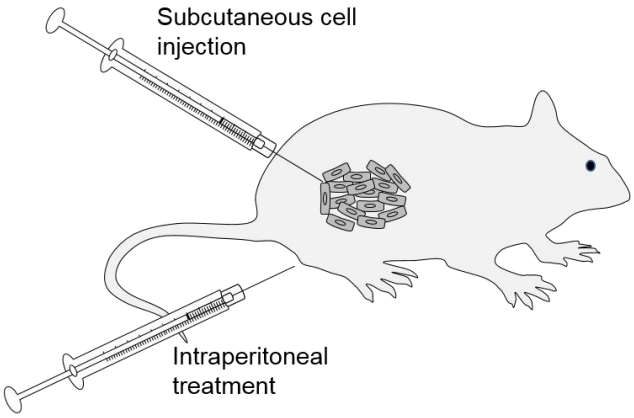

Figure 2: Ectopic tumor model

In a leukemia model the situation of leukemic tumor burden distributed in the whole body is mimicked to test compounds on their efficiency to reduce the number of leukemic tumor cells in an organism. The leukemic tumor burden is measured via bioluminescence of the tumor cells with the IVIS® spectrum.

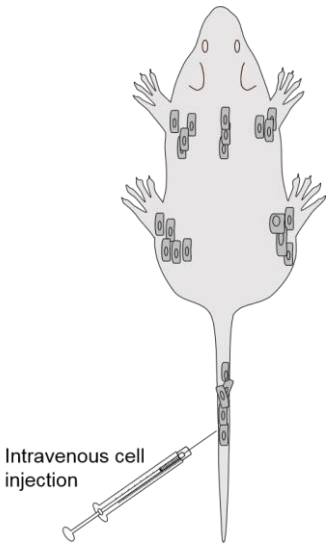

Figure 3: Leukemia model

An intrahepatic metastasis model offers the chance to investigate metastasis formation of liver cancer cells from the spleen to the liver. In this orthotopic tumor model compounds with promising effects against tumor cell metastasis can be evaluated *in vivo*.

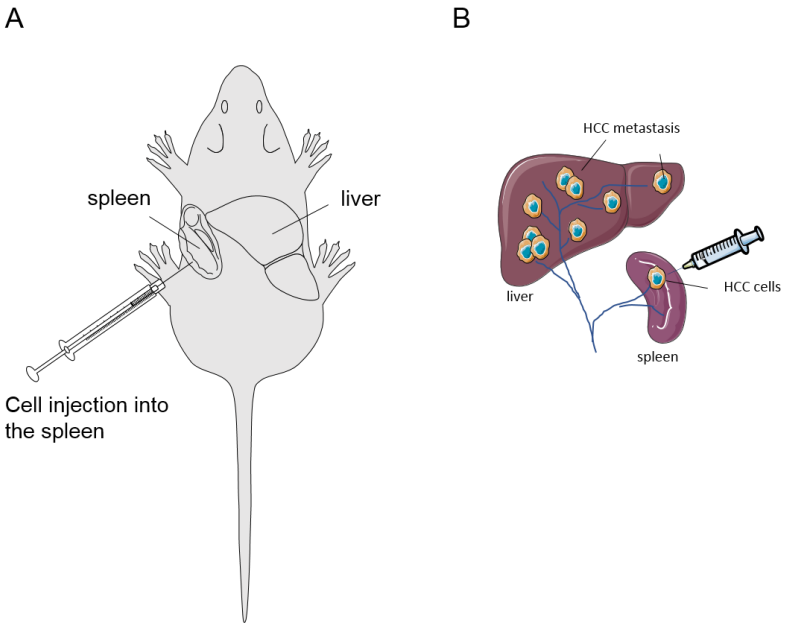

Figure 4: Intrahepatic metastasis model. A) Cell injection into the spleen. **B)** Metastasis formation. Figure created by Prof. Dr. Johanna Pachmayr (Paracelsus Medical University, Austria).

2. Problems in cancer treatment

Common cancer treatment in human patients consists of a variable combination of surgery, chemotherapy, radiation, and immunotherapy [24]. As the aim in cancer treatment in human medicine is often a curative therapy and therefore associated with high dosages of chemotherapeutic agents or radiation, different wearing and stressful side effects can occur during and after the treatment [25]. Besides the anesthetic risk that is attended by surgical interventions, amputation of the affected part of the body such as the breast via mastectomy can lead to depression in many cases [26]. Concerning immunotherapy with monoclonal antibodies, side effects as acute anaphylactic reactions, cardiotoxicity, and gastrointestinal perforations can occur as reviewed by Hansel et al. [27]. Radiation therapy can lead to local or loco-regional side effects, which can become manifest within a few weeks after the treatment, like erythema and desquamation of the skin or nausea. Late effects of radiation therapy can appear up to years after the treatment, represented by radiation-induced fibrosis, neural damage, and even radiation-induced malignancies [25]. Chemotherapeutic treatment mainly causes systemic side effects as emesis, nausea, and hair loss [28]. A further problem concerning chemotherapy is the development of drug resistance in cancer cells. In metastatic cancer, drug resistance is believed to cause more than 90% of treatment failure in human patients [29]. This drug resistance can be of intrinsic or acquired origin, with molecular resistance mechanisms as e.g. increased drug efflux, decreased drug influx, drug inactivation, alteration in drug targets, and evasion of apoptosis [29, 30]. To overcome chemo-resistance and sensitize cancer cells to treatment with chemotherapeutic drugs, as well as to find options in cancer treatment without severe side effects, new chemotherapeutic drugs are investigated in our lab. These new compounds were tested in combination with approved chemotherapeutic drugs to improve their effects or tested on their single treatment potential *in vivo*.

3. Compounds for *in vivo* experiments

Natural and synthetic compounds as well as approved drugs were tested in our lab to discover new options for anticancer therapy. In our lab compounds were tested *in vitro* on their anti-cancer activity. In this project the most promising of these compounds were tested *in vivo* to investigate their potential in a mammalian. In the cell, these compounds react on several important targets, which are still unknown for some of the tested compounds. On the one hand our compounds can be applied as novel drugs for cancer treatment. On the other hand, they represent important tools for target identification.

3.1. Natural compounds

The group of natural compounds consists of compounds and products from plants, microbes, and animals [31]. They can be subdivided in unaltered natural products, botanical drugs, biological macromolecules, and natural product derivatives [32]. Natural products are characterized by a high diversity of chemical structures and biological attributes [33]. They play an important role in the chemotherapy of cancer and are used for their anti-infective functions [31, 33]. Difficulties in access and supply and an often effortful product chemistry of natural products are major problems in natural product research [31]. A solution for this can be found in developing fragments of natural products with a reduced structural complexity. Their chemical synthesis needs less steps, but results in a similar or even higher potent compound [34]. Natural compounds are the origin of a multitude of active ingredients in medicines [31, 33]. Of the between 1981 and 2014 newly approved drugs, 42% had their origin in natural products, containing 4% unaltered natural products. Moreover, 52% of all drugs with anticancer effects approved within this period had their source in natural products [32]. These data elucidate that natural compounds are an important source for novel therapeutics and offer new treatment options for various diseases. So far unknown compounds which showed promising effects *in vitro* in our lab were evaluated in mouse models to proof their capability *in vivo* in this project.

3.1.1. Neocarzilin A

Neocarzilin A belongs to a group of chlorinated polyenones named neocarzilins. In addition to neocarzilin A also neocarzilin B and C are members of these polyenones isolated by the myxobacterium *Streptomyces carzinostaticus* var. F-41 [35, 36]. *Streptomyces carzinostaticus* also produces neocarzinostatin, which shows antitumoral activities *in vitro* and *in vivo* [37]. Neocarzilin A itself has high potent activity against K562 chronic myelogenous leukemia with IC_{50} values of 0.06 µg/ml *in vitro* [36]. Moreover, an acute toxicity in Institute of Cancer Research (ICR) mice is known with LD_{50} values of 88.1 mg/kg. Moreover, chemical synthesis of neocarzilin A is possible with L-isoleucine as first reactant [38]. In our lab neocarzilin A showed promising antiproliferative and anti-metastatic effects against various tumor cell lines *in vitro*. Furthermore, there is first evidence that neocarzilin A interacts with the synaptic vesicle membrane protein VAT-1 (unpublished data).

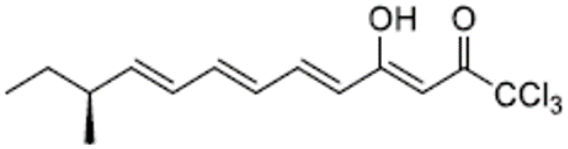

Figure 5: Chemical structure of neocarzilin A [35]

3.1.2. CA1

The pseudonym CA1 is used for a natural compound due to pending patent application. CA1 is known for its antibacterial effects and approved for the treatment of various infections. *In vivo* mouse models showed that CA1 is active against different tumor cells as well as sensitizes cancer cells to chemotherapy.

3.1.3. Jasplakinolide

Jasplakinolide is a natural compound isolated from the marine sponge *Jaspis johnstoni* [39]. Its mode of action consists of inducing actin polymerization and stabilizing actin filaments [40]. As reviewed by Allingham et al. the ratio between monomeric and filamentous actin in the cell can be

regulated and influenced by different proteins. Due to its filaments, actin plays an important role in locomotion, division and growth of cells [41]. In the beginning, jasplakinolide was investigated because of its antifungal activity against *Candida species* [42]. In terms of cancer it shows antiproliferative effects on human prostate carcinoma cells *in vitro* [43]. *In vivo*, jasplakinolide shows antitumor effects in mouse xenograft experiments on prostate carcinoma and Lewis lung carcinoma, also working as a radiation sensitizer [44]. Application in mice is reported via subcutaneous and intraperitoneal injection, subcutaneous continuous infusion as well as oral administration. Mortal toxicity is reached with a single 4 mg/kg subcutaneous injection, whereas 1.5 mg/kg administered twice daily via intraperitoneal injection can be tolerated for one week [42, 44]. Jasplakinolide was also tested in zebrafish and did not cause acute toxicity in 0.5 µM concentration [45]. These *in vivo* data indicate that actin inhibitors show toxic properties even in low concentrations leading to challenges in adequate dosing.

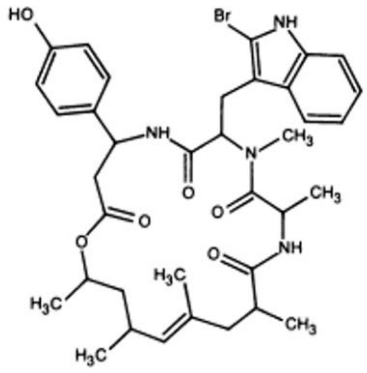

Figure 6: Chemical structure of jasplakinolide [42]

3.1.4. Latrunculin B

The natural compound latrunculin B is purified from red sea sponge *Negombata magnifica* (formerly *Latrunculia magnifica*) [46]. *Negombata magnifica* produces also a second natural toxin named latrunculin A with similar effects as latrunculin B *in vitro* [47]. Latrunculins build a complex with G-actin and therefore disturb actin filament organization [47, 48]. Furthermore latrunculin B has a stabilizing effect on G-actin and inhibits shift from G-actin into F-actin [46]. Latrunculins influence the actin organization

and cell morphology in mouse neuroblastoma cells and hamster fibroblast cells [47, 49]. *In vivo*, latrunculin A shows antitumor effects in peritoneal dissemination assays against human gastric cancer cell lines [50].

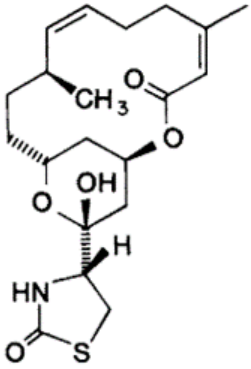

Figure 7: Chemical structure of latrunculin B [49]

3.2. Synthetic compounds

Synthetic compounds represent another important group of compounds in development of pharmaceuticals with anticancer activities. Today, chemical libraries with improving quality can be screened for one million compounds in a few months [51]. Screening properties are for example 3D-shape and electrostatic attributes [52]. Synthetic compounds tested *in vitro* in our lab with promising anticancer effects were tested *in vivo* afterwards in this project.

3.2.1. Ned-19

Ned-19 was found by screening a chemical library (ZINC) for compounds to do research on NAADP signaling [52]. Ned-19 works as a noncompetitive antagonist for NAADP and inhibits NAADP signaling in sea urchin eggs and in mammalian cells [52]. As NAADP is a potent second messenger for Ca^{2+} release, Ned-19 is able to inhibit Ca^{2+} release [53, 54]. NAADP also activates two-pore channels (TPCs), which are Ca^{2+} permeable cation channels in the endolysosomal system of cells. TPCs play an important role in the regulation of the endocytic transport and therefore have an influence on integrin trafficking in a cell [55]. As elucidated in nature reviews, integrins are important for cell migration and hence for tumor metastasis [56]. Therefore, Ned-19 is able to reduce tumor cell migration in melanoma cells

in vitro. Moreover, Ned-19 has a reducing influence on tumor metastasis, tumor vascularization, and tumor growth *in vivo* [57]. Furthermore, Ned-19 inhibits platelet aggregation and secretion, as well as whole-blood aggregation [54]. *In vivo*, mice tolerate Ned-19 i.p. injections every second day with a dose of 5 mg/kg over four weeks [57].

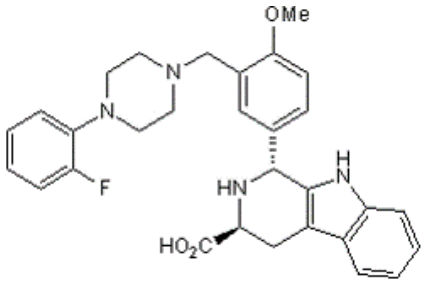

Figure 8: Chemical structure of Ned-19 [58]

3.2.2. PS89

The small molecule PS89 belongs to the compound class T8 which was identified as a promising candidate for chemo-sensitization by screening of a commercial compound library. In combination with the chemotherapeutic drug etoposide, PS89 sensitizes cancer cells towards chemotherapy and therefore leads to an increased apoptosis *in vitro* [59]. PS89 works as a reversible and specific protein disulfide isomerase (PDI) inhibitor and in this way is able to influence the unfolded protein response [60]. In comparison to original T8 an azid group replaces a fluorine in PS89 and therefore PS89 perfectly fits into the binding grooves of PDI. Thus, PS89 has the best sensitizing effects on etoposide treatment of the T8 family *in vitro* [59].

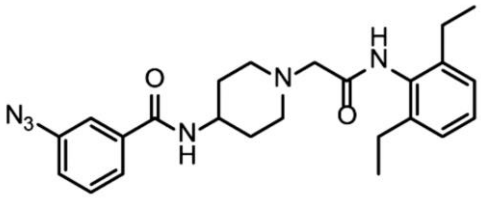

Figure 9: Chemical structure of PS89 [59]

3.2.3. Dinaciclib

Dinaciclib (SCH 727965) was identified by an *in vivo* screening system in search of CDK inhibitors which combine “potency, pharmacokinetic,

efficacy, and safety parameters" [61]. *In vitro*, dinaciclib inhibits CDK1, CDK2, CK5, and CKD9 with IC_{50} values between 1 and 4 nmol/l. Compared with flavopiridol, another well-known CDK inhibitor, the inhibition of CDK1 and CDK9 by dinaciclib is similar but the inhibition of CDK2 and CDK5 is 12-fold and 14-fold stronger, respectively [62]. Dinaciclib also has inhibitory effects on the unfolded protein response by interrupting the IRE1 (inositol-requiring enzyme 1) arm [63]. It is known that short dinaciclib treatment causes long running effects *in vitro*. Moreover, dinaciclib shows antitumoral effects against a multitude of different human tumor cell lines *in vitro*. The MTD for seven days daily intraperitoneal injection is higher than 60 mg/kg, the MED is 5 mg/kg in nude mice [62]. Antitumor effects are reported against ovarian cancer [62], triple negative breast cancer in a PDX model [64], acute myeloid leukemia [65], human melanoma [66], and human pancreatic cancer [67] *in vivo*. Dinaciclib was also tested in phase II clinical studies for acute myeloid leukemia [68], non-small cell lung cancer [69], and advanced breast cancer [70]. Since 2011 dinaciclib is granted orphan designation for the treatment of chronic lymphocytic leukemia [71].

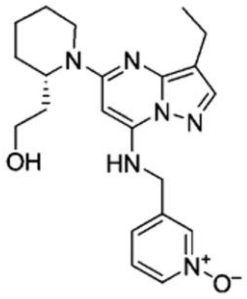

Figure 10: Chemical structure of dinaciclib [62]

3.2.4. Sorafenib

Sorafenib (BAY 43-9006) is an oral multikinase inhibitor, which is approved as Nexavar®. Bayer and Onyx identified through high-throughput screening for Raf1 kinase inhibitors 3-thienyl urea as a promising compound and chemically modified it with sorafenib as result. Sorafenib inhibits receptor tyrosine kinase signaling and activation of Raf. This leads to apoptosis, inhibition of metastasis formation, as well as inhibition of cell proliferation and neovascularization as reviewed by Wilhelm et al. [72]. Antitumor effects are shown in different *in vivo* experiments, for example in xenograft models

of human colon cancer, non-small cell lung cancer, and breast cancer [73]. Efficacy against tumors is also shown in xenograft tumor models of malignant melanoma [74], differentiated thyroid carcinoma (DTC) [75], renal-cell carcinoma (RCC) [76], and hepatocellular carcinoma (HCC) [77]. In mice, sorafenib is administered orally or via intraperitoneal injection in doses up to 100 mg/kg daily or twice a day [73, 74]. Sorafenib was tested in phase III clinical trial for RCC [78], HCC [79-81], and DTC [82]. In patients with advanced HCC, sorafenib prolongs median overall survival for about three months in comparison to placebo [79, 81]. In humans, 400 mg sorafenib is administered twice daily by oral treatment [79]. According to the European Medicines Agency, Nexavar® is approved as first line therapy against HCC and second line therapy against RCC and DTC [83]. Moreover, Nexavar® is the only approved drug for treating advanced HCC [84].

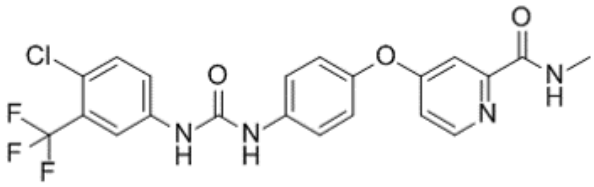

Figure 11: Chemical structure of sorafenib [85]

3.3. Compounds for combination therapy

Clinical approved compounds might be enhanced by the combination with an experimental compound. Our experimental compounds were tested on their chemo-sensitizing effects to improve the therapeutic effects of approved drugs. Therefore, daunorubicin and doxorubicin, two long known chemotherapeutics, were combined with experimental compounds. Expectable effects after promising *in vitro* testing of these combinations might be synergistic or additive antitumoral effects.

3.3.1. Daunorubicin

The anthracycline antibiotic daunorubicin is a natural product of *Streptomyces peucetius* var. *caesius* [86]. The main mechanisms of function are DNA intercalation, generation of free radicals, and inhibition of topoisomerase II, which leads to DNA strand breaks, as summed up by Gewirtz et al. [87]. Daunorubicin is administered in dose of 60 mg/m^2 in

human patients [88]. Daunorubicin hydrochloride is approved for combination treatment of acute myeloid leukemia and acute lymphatic leukemia in children and adults [89]. *In vivo* mouse models show that liposomal daunorubicin (DaunoXome®) increases steadily in the tumor, whereas free daunorubicin shows a peak level in short time after the injection. Moreover, liposomal daunorubicin is more specific to tumor tissue than free daunorubicin [90]. Therapeutic efficacy of liposomal formulation of daunorubicin is increased in comparison to free daunorubicin *in vivo* [91]. In phase III clinical trial liposomal daunorubicin reduces late relapses and therefore is considered to improve overall survival and disease-free intervals [92]. Liposomal daunorubicin has orphan disease designation for the treatment of acute myeloid leukemia [93].

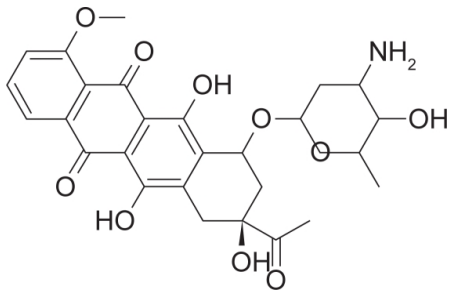

Figure 12: Chemical structure of daunorubicin [94]

3.3.2. Doxorubicin

Doxorubicin also belongs to the group of anthracycline antibiotics and is produced by *Streptomyces peucetius* var. *caesius* [86]. Its mode of action consists on DNA intercalation, covalent binding to DNA, inhibition of the topoisomerase II and therefore stabilization of the cleavage complex. Doxorubicin also produces free radicals by redox cycling. These free radicals cause cardiotoxic effects of doxorubicin, which leads to a restriction in dose frequency. It also causes acute bone marrow toxicity, which leads to a reduced dose intensity, as reviewed by Cummings et al. [95]. Furthermore, doxorubicin causes myopathy in cardiac muscle cells *in vitro* and *in vivo* by a decrease of muscle specific genes [96]. To circumvent negative side effects of doxorubicin, polyethylene glycol (PEG)-liposomal doxorubicin is a new option to use doxorubicin. PEG-liposomal doxorubicin has different pharmacokinetic characteristics as well as a longer circulation

time in the blood and an increased accumulation in tumors, as reviewed by Sharpe et al. [97]. *In vivo*, liposomal doxorubicin shows a higher residence time as free doxorubicin. Moreover, it has a stronger effect on tumor growth inhibition. Mice treated with liposomal doxorubicin show a constant body weight, compared with a decreasing body weight of mice treated with free doxorubicin. Free doxorubicin causes higher peak plasma concentrations after intratumoral injection, which can lead to acute cardiac toxicity [98]. According to the European Medicines Agency, liposomal doxorubicin hydrochloride (Caelyx®) is approved for breast neoplasm, multiple myeloma, ovarian neoplasm, and Kaposi`s sarcoma [99].

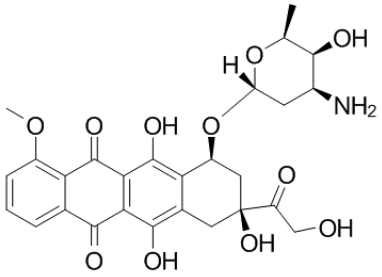

Figure 13: Chemical structure of doxorubicin [100]

4. Aim of the thesis

The aim of the thesis was the *in vivo* evaluation of promising compounds concerning their antitumor activity to find out novel therapeutic options against cancer. Compounds which showed potent anticancer effects *in vitro* were selected for testing in suitable mouse models. In the first part of the thesis the aim was to find out appropriate dosages of compounds which did not have negative effects on the general condition of the mice. In the second part we aimed to characterize compounds in more detail by elucidating their pharmacokinetic profile. In the main part of the thesis the influence of different compounds on tumor cell dissemination, tumor growth, and tumor metastasis was investigated. In tumor dissemination models the impact of compounds and cellular mechanisms on cell distribution after intravenous injection was tested. In subcutaneous tumor models the growth of different tumor cell lines was described. Moreover, the effects of compounds on tumor growth were tested with subcutaneous tumor models as well as with an intravenous leukemia model. Furthermore, the influence of compounds on tumor metastasis was tested in an intrahepatic metastasis model, which was conducted for the first time in our working group. Whenever possible, tumor load was detected by measurement of bioluminescence signals of tumor cells via the IVIS® spectrum. It was part of the thesis to create experimental setups, find suitable mouse models, plan *in vivo* experiments always considering animal welfare and legislation of animal protection, to perform the experiments, and to analyze the obtained data.

II. MATERIALS, MICE, AND METHODS

1. Materials

1.1. Compounds

DaunoXome®	kindly provided by Prof. Dr. Irmela Jeremias (Helmholtz Center Munich, Germany)
Dinaciclib	Selleckchem (Munich, Germany)
Doxorubicin	Sigma Aldrich Chemie GmbH (Steinheim, Germany)
Jasplakinolide	Bioz (Palo Alto, USA)
Latrunculin B	Sigma Aldrich Chemie GmbH (Steinheim, Germany)
Ned-19	Tocris Bioscience (Bristol, United Kingdom)
Neocarzilin A	Prof. Stephan Sieber (TUM Munich, Germany)
PS89	Prof. Uli Kazmaier (University of Saarland, Germany)
Sorafenib	Enzo Life Sciences GmbH (Lörrach, Germany)

1.2. Cells

AML-372	kindly provided by Prof. Dr. Irmela Jeremias (Helmholtz Center Munich, Germany)
Hep55c-luc cells	kindly provided by Dr. Lars König (LMU Munich, Germany)
HUH7 wt cells	Japanese Collection of Research Bioresources (Osaka, Japan)
HUH7 resi(+) cells	generated by Maximilian Ardelt (LMU Munich, Germany)

HUH7 resi(+)-luc cells	luciferase transfected by Martina Meßner (LMU Munich, Germany)
HUH7 resi(-) cells	generated by Martina Meßner (LMU Munich, Germany)
McA-RH7777 cells	kindly provided by PD Dr. Hans Zischka (Helmholtz Centre Munich, Germany)
Ril175-luc cells	kindly provided by Dr. Lars König (LMU Munich, Germany)
Ril175-luc Cdk5 KO cells	generated by Maximilian Ardelt (LMU Munich, Germany)
Ril175-luc TPC2 KO cells	generated by Martin Müller (LMU Munich, Germany)
4T1-luc cells	Perkin Elmer (Rodgau, Germany)
4T1-luc siTPC2 cells	transfected by Dr. Ong Nam Phuong Nguyen (LMU Munich, Germany)
4T1-luc siNT cells	transfected by Dr. Ong Nam Phuong Nguyen (LMU Munich, Germany)

1.3. Cell culture

Cell culture flasks	Sarstedt AG & Co. (Nümbrecht, Germany)
Fetal calve serum	Biochrom AG (Berlin, Germany)
DD medium	provided by Prof. Dr. Irmela Jeremias
DMEM medium	PAA Laboratories (Pasching, Austria)
DMSO	Sigma Aldrich Chemie GmbH (Steinheim, Germany)
EDTA	Carl Roth GmbH und Co. KG (Karlsruhe, Germany)
Kolliphor EL® (solutol)	Sigma Aldrich Chemie GmbH (Steinheim, Germany)

PBS (ph 7.4)	132.2 mM NaCl + 10.4 mM Na_2HPO_4 + 3.2 mM KH_2PO_4 + H_2o
RPMI 1640 medium	Pan-Biotech GmbH (Aidenbach, Germany)
Trypsin	Pan-Biotech GmbH (Aidenbach, Germany)
Trypsin/EDTA	Trypsin 0.05%, EDTA 0.20%, PBS

1.4. *In vivo* experiments

Anexate®	Cheplapharm (Mesekenhagen, Germany)
Antisedan®	Vetoquinol (Ismaning, Germany)
Bepanthen® Augensalbe	Bayer Vital GmbH (Leverkusen, Germany)
Betaisodona® Lösung	Mundipharma GmbH (Limburg, Germany)
Buprenovet®	Bayer AG (Leverkusen, Germany)
BD Micro-Fine™ 0.3 ml	BD Medical (Le Pont de Claix, France)
Cotton swabs	Heinz Herenz Medizinalbedarf GmbH (Hamburg, Germany)
Cutasept® Hautdesinfektion	Paul Hartmann AG (Heidenheim, Germany)
D-Luciferin (sodium salt)	Biomol GmbH (Hamburg, Germany)
Dorbene®	Zoetis (Berlin, Germany)
Dormicum®	La Roche (Basel, Switzerland)
EDTA blood tubes	Sarstedt AG & Co. (Nümbrecht, Germany)
Ethanol 70%	Brenntag GmbH (Mühlheim an der Ruhr, Germany)
Hamilton syringe	Sigma-Aldrich (Taufkirchen, Germany)
Isofluran CP	CP-Pharma® (Burgdorf, Germany)
Needles	Terumo (Eschborn, Germany)
Paraformaldehyde	AppliChem (Darmstadt, Germany)

Restrainer	Agnthos (Lidingö, Sweden)
Surgipro™ Monofilament Polypropylene 5-0	Covidien (Dublin, Ireland)
Syringes	Henry Schein VET GmbH (Hamburg, Germany)

1.4.1. Environmental enrichment

Aspen bricks	Plexx B.V. (Elst, The Netherlands)
Arbocel Crinklets Natural	J. Rettenmaier & Söhne GmbH und Co. KG (Rosenberg, Germany)
Fast-Trac®	Plexx B.V. (Elst, The Netherlands)
Fruit Crunchies	Plexx B.V. (Elst, The Netherlands)
Litter	Plexx B.V. (Elst, The Netherlands)
Mouse igloo	Plexx B.V. (Elst, The Netherlands)
Mouse tunnel	Plexx B.V. (Elst, The Netherlands)
Nestlets	Plexx B.V. (Elst, The Netherlands)
Wire hanger	Plexx B.V. (Elst, The Netherlands)

1.7 Instruments

Canon EOS 450D	Canon Deutschland GmbH (Krefeld, Germany)
Centrifuge Mikro 220 R	Hettrich (Tuttlingen, Germany)
Digital Caliper	Emil Lux GmbH & Co. KG (Wermelskirchen, Germany)
Gas Anesthesia System XGI-8	Caliper Life Sciences GmbH (Rüsselsheim, Germany)
Grundig MC4541 shaver	Grundig GmbH (Nürnberg, Germany)
Heating pad	Terra exotica (Alfeld, Germany)
IVIS® spectrum	Caliper Life Sciences GmbH (Rüsselsheim, Germany)

Megafuge 1.0 RS	Heraeus Holding GmbH (Hanau, Germany)
Olympus CK30 microscope	Olympus Deutschland GmbH (Hamburg, Germany)
Scale TE601	Sartorius AG (Göttingen, Germany)
Scale PB160P	Sartorius AG (Göttingen, Germany)
Infrared- lamp	Philips GmbH (Hamburg, Germany)
Vi-Cell TM XR	Beckmann Coulter GmbH (Krefeld, Germany)

1.8 Software

Microsoft Office 2016	Microsoft (Redmond, USA)
Graph Pad Prism 7	GradPad Software, Inc. (San Diego, USA)
Living Image 4.4	Caliper Life Sciences (Rüsselsheim, Germany)

2. Mice

2.1. Laboratory mouse strains

All laboratory mice were bred for experimental use and kept in captivity since birth. For the *in vivo* experiments female mice were used only. Mice were purchased in an age between five to six weeks from Envigo or Charles River.

2.1.1. BALB/c

The BALB/cOlaHsd mice are inbred albino mice which were obtained from Envigo. They were born in the Netherlands. BALB/c mice have an intact innate and adaptive immune system. These gentle mice are often used in experiments concerning oncology, teratology and pharmacology [101]. They were also used as sentinel animals for health monitoring examinations in our animal facility.

2.1.2. C57BL/6

The C57BL/6JOlaHsd strain is the most widely used inbred strain from Envigo. The breeding takes place in the Netherlands. This mouse strain has a completely intact immune system. They are often used in oncology research and as background for genetically modified mice models [101].

2.1.3. C57BL/6 albino

The C57BL/6BrdCrHsd-Tyr^{c} mice have the same genetic background as the C57BL/6 mice but with a mutation in the tyrosinase gene wherefore they are albino mice. They have an intact immune system. The mice were bred in France by Envigo. The advantage of this mouse strain in our animal experiments is the simple feasibility to image them without problems in the IVIS® spectrum [101].

2.1.4. Fox Chase SCID

The CB17/Icr-Prkdc^{scid}/IcrIcoCrl strain obtains mice which have a genetic autosomal recessive mutation. Therefore, they have a severe immunodeficiency affecting B and T lymphocytes, but they still have functional natural killer cells, macrophages, and granulocytes. Due to their immunodeficiency, a lot of human cancer cell lines can be monitored in these mice *in vivo*. Charles River breeds these mice in Germany [102].

2.1.5. NOD *scid* gamma (NSG)

The JAX™ mouse strain NOD.Cg-Prkdc^{scid}Il2rg^{tm1Wjl}/SzJ has a severe immunodeficiency concerning B cells, T cells and natural killer cells as well as cytokine signaling due to an IL2 receptor gamma chain deficiency. For this reason, the NSG mice are often used for xenograft models with hematopoietic stem cells and cancer stem cells. It is also possible to use them for patient-derived xenograft cell experiments. Charles River delivers these mice from the Jackson Laboratory in France to our animal facility [102].

2.2. Housing

All mice used for the *in vivo* experiments were kept in a special air-conditioned room with a twelve hours day and night cycle. The mice were housed in individually ventilated cages (IVC, type II long, Tecniplast) with a maximal occupancy of five mice per cage and a minimal occupancy of two mice per cage. All over the time the mice had *ad libitum* access to autoclaved water and autoclaved food (complete feed for rat and mice-maintenance, sniff®). The cages and the water were changed once a week. In terms of environmental enrichment every cage was equipped with litter, crinklets, nestlets, one mouse igloo, one mouse tunnel, a wire hanger, aspen bricks and one exercise wheel (Fast-Trac®).

The health status of the animals was monitored according to the FELASA guidelines four times a year. During the work for this thesis all health monitoring reports were negative. Therefore, negative influence on the *in vivo* experiments caused by bacteria, virus or parasites can be excluded.

All mice at least had one week to acclimatize to their new housing after the shipping before they were used for the *in vivo* experiments. During an experiment, the mice were controlled daily.

All animal experiments were performed according to German legislation for the protection of animals and were approved by the government of Upper Bavaria (approval numbers 55.2-1-54-2532-107-13, 55.2-1-54-2532-22-2016).

3. Methods

3.1. Cell culture

Murine breast adenocarcinoma cells (4T1-luc) stably expressing luciferase were cultivated in RPMI 1640 medium containing 10% FCS. Similarly, 4T1-luc siTPC2 cells and 4T1-luc siNT cells (generated by Dr. Ong Nam Phuong Nguyen, LMU Munich) were cultivated in RPMI 1640 medium containing 10% FCS. The patient-derived xenograft acute myeloid leukemia cells AML-372 were cultured in DD medium, which was kindly provided by Prof. Dr. Irmela Jeremias. Rat hepatoma cell line McA-RH7777 (provided by PD Dr. Hans Zischka, Helmholtz Centre Munich), murine hepatocellular carcinoma cells expressing luciferase (Ril175-luc) (provided by Lars König, LMU Munich), Ril175-luc Cdk5 KO cells (generated by Maximilian Ardelt, LMU Munich), Ril175-luc TPC2 KO cells (generated by Martin Müller, LMU Munich), murine hepatocellular carcinoma cell line Hep55c-luc and all HUH7 cells (human hepatocellular carcinoma cell line) were cultivated in DMEM medium containing 10% FCS. HUH7 resi(+) cells, HUH7 resi(+)-luc cells, and HUH7 resi(-) cells were generated by Maximilian Ardelt and Martina Meßner (both LMU Munich). Through permanent treatment with sorafenib below their IC_{50} value the sorafenib resistant cell line HUH7 resi(+) was generated. After months of increasing the sorafenib dose, the HUH7 resi(+) cells tolerate 10 µM sorafenib in DMEM. To receive HUH7 resi(-) cells, the HUH7 resi(+) cells were cultured without sorafenib for 72 hours.

All cells were cultured under constant humidity at 37° C and with 5% CO_2.

In general, to use adherent cells (4T1-luc, Hep55c-luc, HUH7, Ril175-luc, McA-RH7777) for an *in vivo* experiment the first step was to remove the medium. Afterwards the cells were washed two times with PBS. Then the cells were incubated with trypsin/EDTA for 3 minutes at 37° C to detach them from the cell culture flask. To stop this reaction growth medium is added again into the flask. After counting the cells via Vi-Cell TM XR, the needed amount of them was taken out of the flask and centrifuged using the Megafuge 1.0 RS (1,000 rpm, 5 min, 20° C). In the end, the cell pellet was solved in PBS. In comparison, in case cells in suspension (AML-372) were used, the cells were counted via Vi-Cell TM XR without removing them from

medium. The needed amount of the solution was taken off and centrifuged (1,000 rpm, 5 min, 20° C). Afterwards the cells were resuspended in PBS.

3.2. Animal experiments

Laboratory mice were purchased from Envigo or Charles River at an age of five to six weeks and the experiments started with animals at an age of six to eight weeks. All mice acclimatized at least one week before entering an experiment. For subcutaneous, intraperitoneal, and intravenous injections 1 ml syringes and 27 G needles were utilized. To carry out intravenous injections a forward or a backward restrainer was used depending on the cooperation and the size of the mice. For subcutaneous injections, the mice were shaved before cell injection. Inhalation anesthesia for bioluminescence imaging was performed with 2 to 3% isoflurane in oxygen. During the anesthesia, the cornea was prevented from drying out with ophthalmic ointment (Bepanthen® Augensalbe). For cardiac puncture, BD Micro-Fine™ 0.3 ml were used. In the end of the animal experiments mice were sacrificed via cervical dislocation. When it was rational to keep the tumors, they were removed, photographed, and weighed. One part of them was frozen in liquid nitrogen and stored at - 80° C and the other part was fixed with 4% PFA, after three days transferred into 1% PFA, and three days later conserved in 70% ethanol and stored at 4° C.

3.2.1. Bioluminescence measurement in living animals - IVIS® spectrum *in vivo* imaging system

Bioluminescence measurements are based on an enzymatic reaction between luciferase tagged tumor cells and luciferin as its substrate. Under an ATP consuming reaction in the presence of oxygen luciferase catalyzes the reaction from luciferin into oxyluciferin. By returning from the excited state to the ground state oxyluciferin is emitting light [103]. This light can be detected by the IVIS® spectrum. With this sensitive way of optical imaging the total number of mice per group can be reduced because every single mouse can be imaged at different time points [104]. 6 mg luciferin sodium salt solved in 100 µl PBS were injected intraperitoneally in the mice before they were anesthetized. After the injection, the mice were put into a narcosis chamber flooded with 3% isoflurane in oxygen. The narcotized mice were

taken out of the narcosis chamber, got eye ointment applied to prevent their eyes from drying out, and were placed into the IVIS® spectrum. During the bioluminescence measurement, the mice are narcotized with 2% isoflurane in oxygen through a nose coin with gas anesthesia inlet and outlet ports. They were prevented from becoming hypothermic by laying on a hotplate (37° C). Mice were imaged in ventrodorsal position as standard and in dorsoventral or laterolateral position if there were specific indications. In every position four to eight readings were taken with intervals of one minute between each measurement. To evaluate the signal, the region of interest (ROI) was defined. With the Living Image 4.4 software the bioluminescence signal within the ROI was calculated in photons/second/cm². The bioluminescence signal is indicated in total flux/area. Shown is one timepoint out of the sequence. In this thesis the IVIS® spectrum is used for longitudinal monitoring of tumors in living mice as well as for control measurements and end point measurements of single organs at the end of an experiment.

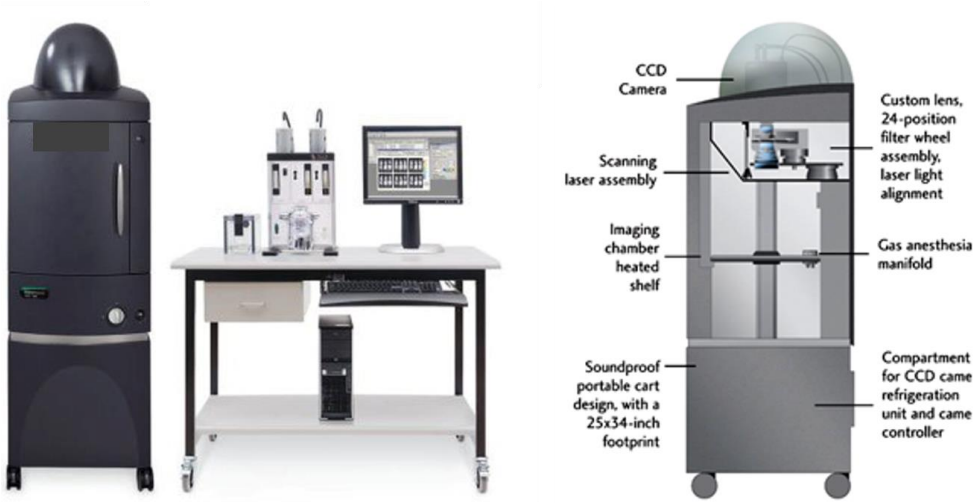

Figure 14: IVIS® spectrum *in vivo* imaging system [105]

3.2.2. Dose finding tests

Dose finding tests were performed to find out an adequate dose of a compound for an animal experiment. By these dose finding tests the highest possible dosage of a compound that does not harm the mice or lead to any abnormalities shall be found. For the dose finding experiment the same mouse strain was used as for the main experiment. The compounds were solved in 5% DMSO, 10% solutol, and 85% PBS and were injected

intraperitoneally using 1 ml syringes and 27 G needles. If intravenous injections were indicated, the compound was just solved in PBS. Every mouse was injected with a volume of 100 µl at most once a day. The intervals and the duration of testing the compounds depended on the plans for the following main experiment. The tested dosages depended on results of *in vitro* concentrations and, if available, published data. As the dosages published in literature are not generally appropriable because of other mouse strains or other routes of administration, the dosage given in literature can sometimes just be seen as a hint. After injection, the mice were monitored directly and after thirty minutes, two hours, and twenty-four hours and after that daily. In some dose finding experiments the mice were observed for a few days after the last injection of the compound to see if there are decelerated reactions on the treatment. During these experiments, the mice were examined concerning their general condition, their behavior, their appearance, their breathing, body condition score and weight. They were especially monitored for toxic effects of the compounds such as cyanoses, anorexia, icterus or any signs of pain. The exact treatment plan for the compounds used in dose finding tests can be seen in Table 1.

Table 1: Treatment plan for dose finding tests

Compound	Injection interval	Injections in total	Dosage	Way of injection	Mice	Mice/group
CA1	every second day	6	100 mg/kg	i.p.	SCID	3
Dinaciclib	daily	3	10 mg/kg 20 mg/kg 30 mg/kg	i.p.	C57BL/6	3
Doxorubicin	once	1	1 mg/kg 3 mg/kg	i.v.	BALB/c	3
Jasplakinolide + 3 mg/kg doxorubicin i.v.	once	1	0.25 mg/kg 0.5 mg/kg 1 mg/kg	i.p.	BALB/c	3
Latrunculin B + 3 mg/kg doxorubicin i.v.	once	1	0.05 mg/kg 0.1 mg/kg 0.5 mg/kg	i.p.	BALB/c	3
Neocarzilin A	daily	3	0.02 mg/kg 0.2 mg/kg 2 mg/kg 10 mg/kg 20 mg/kg	i.p.	BALB/c	3
Sorafenib	every second day	6	20 mg/kg 30 mg/kg	i.p.	SCID	2

3.2.3. Pharmacokinetic studies

In the pharmacokinetic studies we had a look at the blood plasma concentration of compounds at different time points after the injection. After the compound was injected, the mice were set back to their cage. After the demanded time, the mice were euthanized via cervical dislocation. Then the thorax was opened and blood was taken via cardiac puncture. The blood was filled into 2 ml EDTA-blood tubes and centrifuged at 1,000 rpm for ten minutes. The blood plasma was analyzed by Dr. Christoph Müller and Anna Niedrig (LMU Munich, Germany) using HPLC. Details of the experimental conditions can be found in Table 2.

Table 2: Conditions of pharmacokinetic studies

Compound	Dosage	Type of injection	Mice	Mice/ timepoint	Evaluated timepoints after injection (minutes)
PS89	10 mg/kg	i.v.	BALB/c	2	0, 5, 8, 10, 15
PS89	30 mg/kg	i.p.	NSG	4	15, 120

3.2.4. Dissemination assays

Dissemination assays were performed to evaluate the distribution of tumor cells after they were injected intravenously. As the cells were injected intravenously, the mice had to be restrained with a forward or a backward restrainer depending on their size and their cooperation on handling. The veins were dilated with an infrared lamp for about 15 seconds. Afterwards the tumor cells which were solved in 100 µl PBS were injected using 1 ml syringes and 27 G needles into the tail vein. As the cells are tagged with luciferase, it is possible to detect their bioluminescence signal afterwards in the IVIS® spectrum. For one thing, this assay can be used to evaluate the potential of compounds to reduce tumor dissemination. Therefore, the mice were treated with the compound before cell injection, not afterwards. For another thing, it is also possible to monitor tumor dissemination when the cells were pretreated or genetically modified before. So, it is not necessary to treat the mice before cell injection. In both cases the mice were imaged one or two times in the week after the cell injection. A third option to measure in a dissemination assay concerns tumor cell distribution in general. There

is the possibility to image the bioluminescence signal in short times after the tumor cell injection to evaluate the dissemination of the cells in the first hours in a living organism. Details for single dissemination experiments can be found in Table 3.

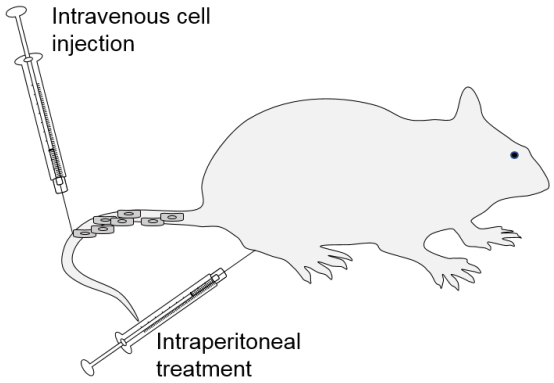

Figure 15: Tumor dissemination model. Tumor cells were injected into the tail vein, pretreatment of the mice via intraperitoneal injections.

Table 3: Conditions of dissemination experiments

Mice	Mice/ group	Cells	Number of cells	IVIS® measurements in total	Time between IVIS® measurements after cell injection	Compound	Dosage	Treatment (i.p.)
BALB/c	8	4T1-luc cells	$1x10^5$	2	5 days 8 days	Neocarzilin A	10 mg/kg	48 h, 24 h, and 0.5 h before cell injection
BALB/c	7	4T1-luc cells, pretreated with 150 µmol/L Ned-19 for 24 hours	$1x10^5$	2	5 days 8 days	Ned-19	/	/
BALB/c	8	siTPC2 4T1-luc cells	$1x10^5$	2	5 days 8 days	/	/	/
C57BL/6-Tyr	3	Ril175-luc cells	$1x10^5$ $2x10^5$	2	3 days 5 days	/	/	/
C57BL/6-Tyr	10	Ril175-luc TPC2 KO cells	$2x10^5$	1	3 days	/	/	/
C57BL/6-Tyr	10	Ril175-luc cells	$2x10^5$	1	3 days	Dinaciclib	10 mg/kg	48 h, 24 h, and 0.5 h before cell injection
C57BL/6-Tyr	10	Ril175-luc Cdk5 KO cells	$2x10^5$	1	3 days	/	/	/
BALB/c	5	4T1-luc cells	$5x10^6$	3	3 hours 6 hours 24 hours	/	/	/
BALB/c	2	4T1-luc cells	$1x10^6$ $2x10^6$	4	3 hours 6 hours 24 hours 48 hours	/	/	/

3.2.5. Ectopic tumor models for the evaluation of tumor growth

Ectopic tumor models were used to monitor the inhibiting effect of compounds on the growth of tumor cells or to evaluate the growth rate of subcutaneous tumors. Therefore, tumor cells were injected into the left flank of the mouse using 1 ml syringes and 27 G needles. Before cell injection the mice were shaved on the left lateral abdomen. After the cell injection, the tumor size was measured in three dimensions (L = length, longest side of the tumor, W = width, widest side of the tumor, and H = height, highest side of the tumor) using a digital caliper every two to three days. The tumor volume was calculated using the formula 1/6 x π x L x W x H. Another approach to measure the tumor load in ectopic tumor models was established for the first time in our lab during this thesis. Instead of just measuring the size of a subcutaneous tumor via a digital caliper, tumor cells were tagged with luciferase before the injection. Then it was possible to measure the bioluminescence signal of the subcutaneous tumors very precisely. These bioluminescence measurements were conducted biweekly using the IVIS® spectrum. In the end of the experiments, the tumors were resected, photographed, weighed, and measured. After that, one part was frozen at -80° C and the other part was conserved in 4% PFA. The detailed conditions for the implemented ectopic tumor models can be seen in Table 4.

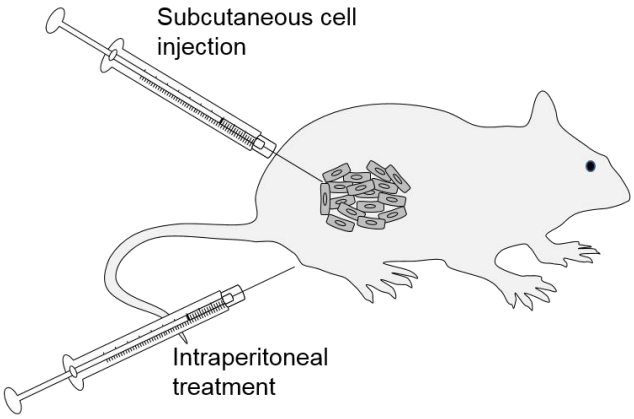

Figure 16: Ectopic tumor model. Tumor cells were injected subcutaneously, treatment via intraperitoneal injection.

Table 4: Details for the conditions chosen for ectopic tumor models

Compound	Dosage	Mice	Cells	Number of cells	Mice/group	Treatments in total	Treatment intervals	Aim of the experiment
/	/	BALB/c	4T1-luc	$1x10^6$	4	/	/	Preliminary experiment to evaluate the growth rate
/	/	SCID	McA-RH7777	$2x10^6$	4	/	/	Preliminary experiment to evaluate the growth rate
Sorafenib	20 mg/kg	SCID	HUH7 wt HUH7 resi(-) HUH7 resi(+)	$3x10^6$	3	7	3 times a week	Preliminary experiment to evaluate if the cells are able to grow in the mice
Sorafenib	20 mg/kg	SCID	HUH7 wt	$3x10^6$	8	8	Every second day	Evaluation of HUH7 wt growth reduction under treatment with 20 mg/kg sorafenib
Sorafenib	20 mg/kg	SCID	HUH7 resi(+)	$3x10^6$	10	8	Every second day	Characterization of HUH7 resi(+) growth with and without sorafenib treatment, characterization of rebound growth
CA1	100 mg/kg	SCID	HUH7 resi(+)-luc	$3x10^6$	5	5	3 times a week	Characterization of HUH7 resi(+)-luc growth under CA1 treatment, implementation of bioluminescence imaging in s.c. models

3.2.6. Patient derived xenograft cell model for monitoring leukemia

In this patient derived xenograft (PDX) cell model human leukemia cells (AML-372), which were provided by Prof. Dr. Irmela Jeremias and Dr. Binje Vick (both Helmholtz Centre, Munich), were monitored in NOD scid gamma mice (NSGs). Therefore, $1x10^5$ AML-372 cells were injected intravenously. As the AML-372 cells are tagged with luciferin, bioluminescence measurement in the IVIS® spectrum was possible to control the leukemic burden in the mice. 24 days after the first cell injection the mice received a second AML-372 cell injection with $1x10^5$ due to a very reduced growing of the tumor cells after the first injection. The mice were imaged in the IVIS® spectrum once a week until the tumor signal reached at least $1x10^8$ total flux/area. When this signal was exceeded the treatment of the mice began and the tumor burden was measured twice a week via the IVIS® spectrum. The mice were divided into four groups, from which one group

served as control group, one group was treated with PS89 (solved in 5% DMSO, 10% solutol, and 85% PBS), one group was treated with liposomal daunorubicin (solved in glucose 5%), and the fourth group received a combination treatment with PS89 and liposomal daunorubicin. The detailed treatment plan can be seen in Table 5. With this PDX model the proliferation of leukemia cells can be observed *in vivo* under treatment with different compounds and the effects of their combination can be evaluated. Whenever a control injection was recommended, a solvent of 5% DMSO, 10% solutol, and 85% PBS was used for the intraperitoneal injections and glucose 5% was used for the intravenous injections.

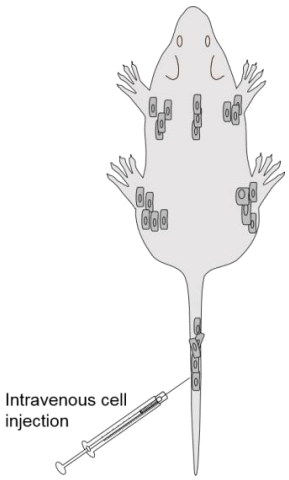

Figure 17: Leukemia model. After intravenous cell injection leukemic tumor cells are detectable in the whole mouse body.

Table 5: Classification of different groups in a PDX cell leukemia model

Group	Compounds and dosage	Mice	Cells
Control	Solvent i.p. Glucose 5% i.v.	NSG	$1x10^5$ AML-372
PS89	PS89 (30 mg/kg) i.p. Glucose 5% i.v.	NSG	$1x10^5$ AML-372
Daunorubicin	Solvent i.p. Daunorubicin (5 mg/kg) i.v.	NSG	$1x10^5$ AML-372
Combination	PS89 (30 mg/kg) i.p. Daunorubicin (5 mg/kg) i.v.	NSG	$1x10^5$ AML-372

3.2.7. Orthotopic tumor model for evaluation of metastasis

In this murine tumor model, the metastasis of liver cancer cells was observed. During a surgery liver cancer cells (Hep55c or Ril175-luc) were injected into the spleen. The narcosis of the mice consisted of 1 mg/kg medetomidine and 10 mg/kg midazolam. The antagonization consisted of 0.5 mg/kg flumazenil and 2.5 mg/kg atipamezole. For pre- and postoperative analgesia 0.125 mg/kg buprenorphine was used. The mice received buprenorphine for altogether four days. After the mice reached Stage III in the Guedel`s classification, their skin was shaved and disinfected. Then the skin and the muscles of the left lateral abdomen were opened one centimeter in length. On the open abdomen, the spleen was pushed outside with slight pressure by a cotton swab containing PBS. Cells solved in 50 µl PBS were slowly injected into the spleen using a Hamilton syringe. In the following the injection site was compressed with a cotton swab containing 70% ethanol. The peritoneum, the muscles and the skin were sutured in two layers. The described surgery was mainly done by Laura Posselt (LMU Munich, Germany). Afterwards the metastasis formation in the liver was measured using bioluminescence detection in the IVIS® spectrum. In this orthotopic *in vivo* assay, the anti-metastatic effects of a compound can be observed. Therefore, the mice were only treated before the cell injection. The detailed conditions for these experiments can be seen in Table 6.

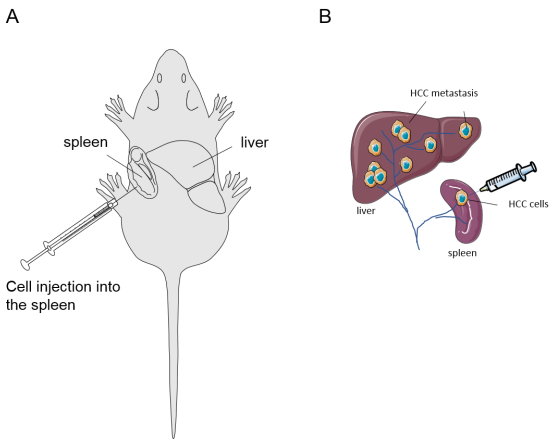

Figure 18: Intrahepatic metastasis model. A) Cell injection into the spleen. **B)** Metastasis formation. Injection of a primary tumor into the spleen and metastasis formation in the liver. Figure created by Prof. Dr. Johanna Pachmayr (Paracelsus Medical University, Austria).

Table 6: Conditions of orthotopic tumor models for the evaluation of metastasis formation in C57BL/6-Tyr mice

Cells	Number of cells	Number of animals	Compound and dosage	Treatments in total	Treatment plan	IVIS® measurements in vivo	Aim of the experiment
Hep55c-luc	$2x10^6$	3 (2 control 1 treated)	10 mg/kg dinaciclib	3	48 h, 24, 0,5 h before cell injection	3	Preliminary experiment
Ril175-luc	$1x10^6$	3 (2 control 1 treated)	10 mg/kg dinaciclib	3	48 h, 24, 0,5 h before cell injection	3	Preliminary experiment
Ril175-luc	$0.5x10^6$	4 (2 control 2 treated)	10 mg/kg dinaciclib	3	48 h, 24, 0,5 h before cell injection	3	Preliminary experiment
Ril175-luc	$1x10^6$	20 (10 control 10 treated)	10 mg/kg dinaciclib	3	48 h, 24, 0,5 h before cell injection	2	Main experiment

3.2.8. Statistical analysis

Results are expressed as mean value ± S.E.M. if not indicated otherwise. Statistical analysis was performed with unpaired t-tests using GraphPad Prism 7. P-values < 0.05 were considered as significant.

III. RESULTS

1. Evaluation of murine dose finding tests

Dose finding tests were performed to find out a well-tolerated dosage of our compounds. They were important to assure an uncomplicated procedure in following experiments. A detailed overview over the conditions gives Table 1 on page 27.

1.1. Neocarzilin A

Neocarzilin A was tested in three female BALB/c mice per group in dosages from 0.02 – 20 mg/kg via intraperitoneal injection. The compound was injected on three following days (from day 0 to day 3). The dosages 0.02 mg/kg and 0.2 mg/kg were tested by Dr. Melanie Ulrich (LMU Munich, Germany). The mice which received 0.02 up to 10 mg/kg had a good general condition and did not show any abnormalities. The mice which received 20 mg/kg had a reduced general condition directly after the second and third injection and did not put full weight on their left leg after the injection for 30 minutes. Therefore, these three mice were euthanized after the last treatment. All groups were constant in their body weight when comparing the first and the last day of the experiment (Figure 19) and stayed on BCS 3. These results led to the decision to use neocarzilin A in a dosage of 10 mg/kg for the following dissemination experiment to avoid the negative side effects we have seen in the higher dosage.

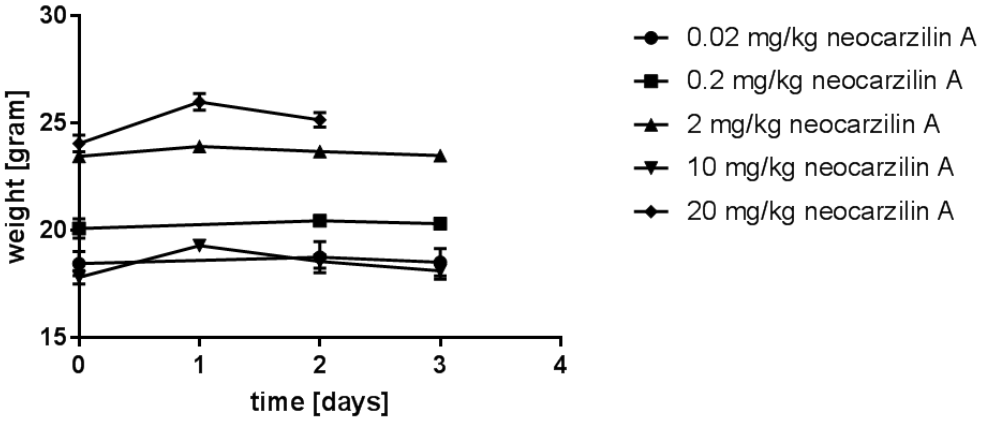

Figure 19: Body weight development over time. Weight of mice during the dose finding experiment with neocarzilin A injection on day 0, 1, and 2. Represented is the mean ± S.E.M. of three mice per group.

1.2. CA1

CA1 was tested in three female SCID mice in the dosage of 100 mg/kg via intraperitoneal injection every second day. After the first injection on day 0 the mice lost body weight but began to regain weight after day 2. After six injections in total and three days of observation after the last injection, the mean body weight was minimally higher (16.9 g) than at the beginning of the dose finding experiment (16.6 g) (Figure 20). Since the third CA1 injection the mice showed an extremely active and stressed behavior for 20 minutes after the treatment, but no typical signs of pain. Nevertheless, we decided to use 100 mg/kg CA1 for the ectopic tumor model, based on published data wherein CA1 treatment daily or twice a day in a dosage of 100 mg/kg was tolerated by mice. To reduce stress for the mice we decided to reduce the treatment interval and to inject the mice only three times a week with 100 mg/kg CA1 in the ectopic tumor model.

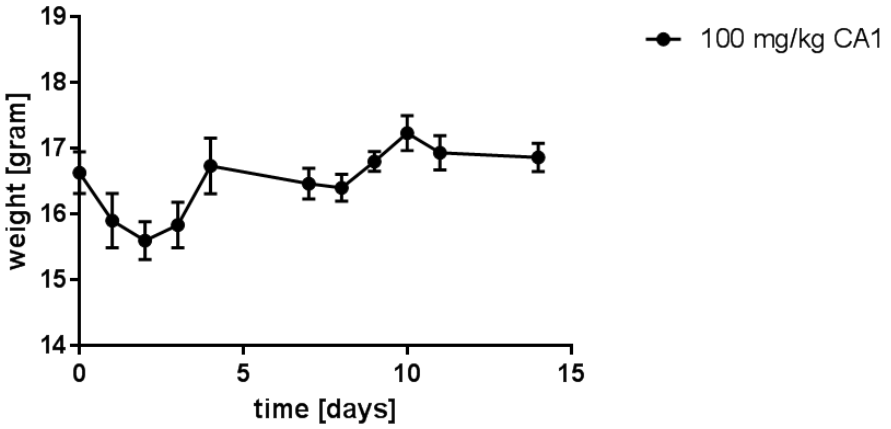

Figure 20: Body weight development over time. Weight of mice during the dose finding test with CA1 injections every second day. Represented is the mean ± S.E.M. of three mice per group.

1.3. Dinaciclib

Dinaciclib was tested in three female C57BL/6 mice per group in the dosages 10 mg/kg, 20 mg/kg, and 30 mg/kg via intraperitoneal injection. The mice received the injections on day 0, day 1, and day 2. During the three days of treatment the mice showed a good general condition without detectable abnormalities although the groups which received 20 mg/kg and 30 mg/kg lost weight during the three days of treatment (Figure 21). The

mice in the 30 mg/kg group recovered weight in the days after the treatment and reached their weight of day 0 whereas the mice in the 10 mg/kg group had a constant weight during the whole experiment. On day 9 one mouse of the 10 mg/kg group had to be euthanized because of a swollen leg and exuding wound at the intraperitoneal injection site. The other two mice treated with 10 mg/kg dinaciclib were euthanized on day 10 without detectable abnormalities and a good general condition. Two of the mice which received 20 mg/kg dinaciclib had to be euthanized on day 4 due to a bad general condition. The third mouse of this group was found dead in cage on day 7. In the 30 mg/kg dinaciclib group one mouse was euthanized because of bad general condition and a swollen leg on day 7. On day 8 and 9 the other two mice were euthanized because of swollen legs and exuding wounds at the intraperitoneal injection site. All abnormalities appeared suddenly and the mice were sacrificed immediately when they showed any wearing abnormalities. Due to the problems in the 20 mg/kg and the 30 mg/kg group we decided to use 10 mg/kg dinaciclib for the metastasis model and the dissemination assay.

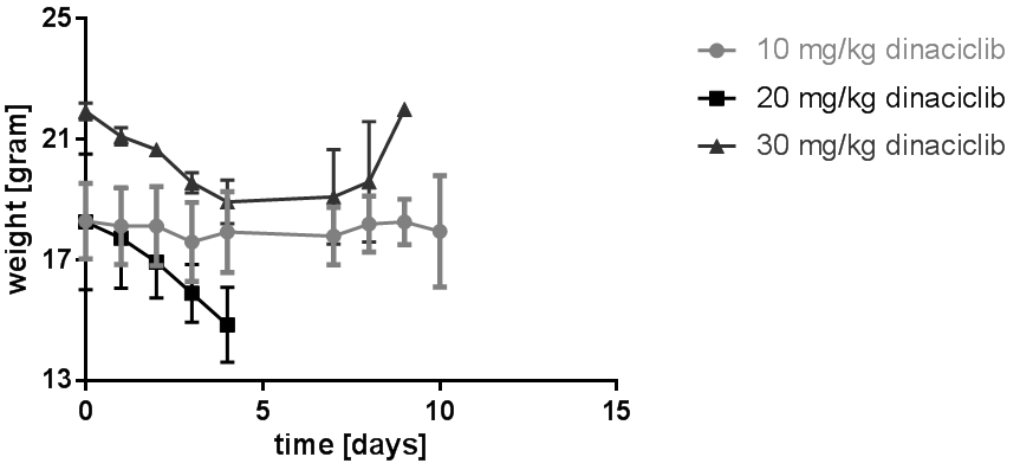

Figure 21: Body weight development over time. Weight of mice during the dose finding experiment with dinaciclib injections on day 0, 1, and 2. Represented is the mean ± S.E.M. of three mice per group.

1.4. Sorafenib

Sorafenib was tested in four SCID mice divided into two groups. One group received 20 mg/kg sorafenib, the other group received 30 mg/kg sorafenib for six injections in total. Injections took place every second day starting on day 0. All four mice gained weight during the experiment but reacted with a low-grade weight loss on the injections the following day (Figure 22). The general condition during the whole experiment was good in both groups and no abnormalities were detectable. As the body weight development of mouse 1 and mouse 2 was better during the injections than in the other two mice, the consequence was to use 20 mg/kg sorafenib in the tumor growth model.

A B

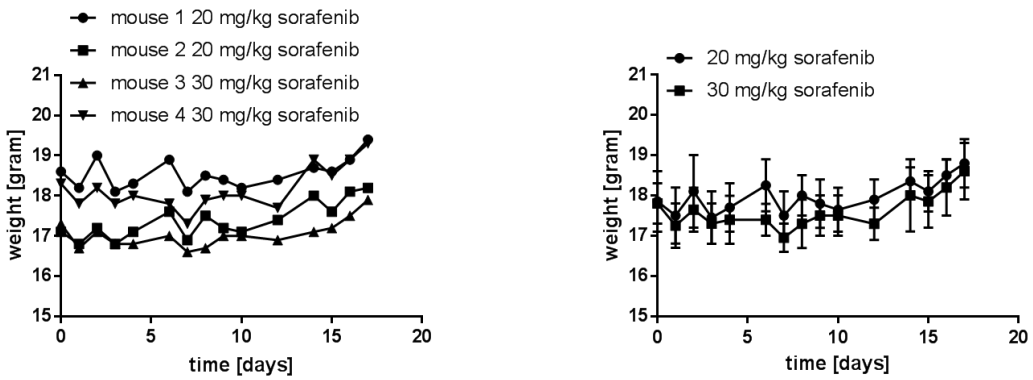

Figure 22: Body weight development over time. A) Weight of mice during the dose finding experiment with sorafenib injection on day 0, 2, 4, 6, 8, and 10. Each curve presents the body weight of one single mouse. **B)** Weight of mice during the dose finding experiment with sorafenib injection on day 0, 2, 4, 6, 8, and 10. Represented is the mean ± S.E.M. of two mice per group.

1.5. Doxorubicin

Doxorubicin was tested in six BALB/c mice divided into two groups. They were injected intravenously on day 0 with 1.5 mg/kg and 3 mg/kg doxorubicin, respectively. After the injection and for the following 48 hours of monitoring, the mice showed a good general condition without detectable abnormalities. Their body weight was nearly constant or even slightly increased (Figure 23). Therefore, we decided to use 3 mg/kg doxorubicin for further experiments.

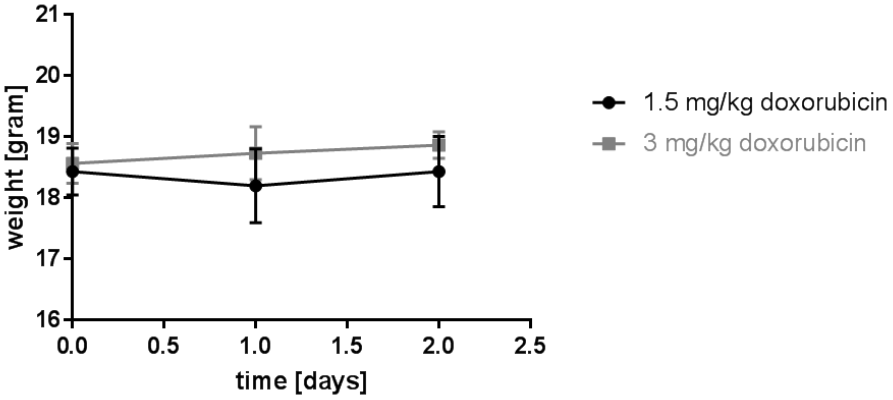

Figure 23: Body weight development over time. Weight of mice during the dose finding experiment with doxorubicin injection on day 0. Represented is the mean ± S.E.M. of three mice per group.

1.6. Latrunculin B

Latrunculin B was tested in three female BALB/c mice per group in dosages of 0.05 mg/kg, 0.1 mg/kg, and 0.5 mg/kg via singular intraperitoneal injection on day 0 in combination with 3 mg/kg doxorubicin injected intravenously 20 minutes after the latrunculin B injection. Injections with 0.05 mg/kg and 0.1 mg/kg latrunculin B were tolerated well, the mice showed a physiological general condition. In both groups the mice slightly lost weight during the observation period of 24 and 48 hours, respectively (Figure 24). All three mice injected with 0.5 mg/kg latrunculin B showed a severely reduced general condition including paralysis of the extremities 15 minutes after the injection, thus doxorubicin was not injected. These mice had to be euthanized immediately. Therefore 0.1 mg/kg latrunculin B combined with 3 mg/kg doxorubicin was used for further experiments.

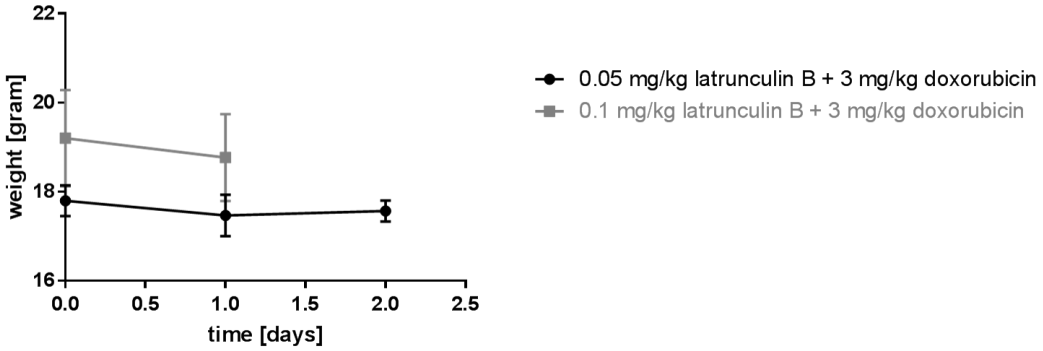

Figure 24: Body weight development over time. Weight of mice during the dose finding experiment with latrunculin B and doxorubicin injection on day 0. Represented is the mean ± S.E.M. of three mice per group.

1.7. Jasplakinolide

Jasplakinolide was tested in three female BALB/c mice per group in dosages of 0.25 mg/kg, 0.5 mg/kg, and 1 mg/kg via intraperitoneal injection in combination with 3 mg/kg doxorubicin injected intravenously 20 minutes after the jasplakinolide injection. The compound was injected on day 0 without further injections. All mice treated with 0.25 mg/kg and 0.5 mg/kg jasplakinolide tolerated the injections well and showed a good general condition during the whole dose finding experiment. The mice injected with 1 mg/kg jasplakinolide also had no detectable abnormalities after the injection and during the first six hours after the treatment, but 24 hours after the injection one mouse was found dead in cage, whereas the other two mice showed a good general condition. The body weight of the mice which were treated with 0.25 mg/kg jasplakinolide increased slightly, whereas the body weight of the group treated with 0.5 mg/kg stayed equal and the group treated with 1 mg/kg jasplakinolide showed a slightly decreasing body weight (Figure 25). Therefore, we decided to use 0.5 mg/kg jasplakinolide combined with 3 mg/kg doxorubicin for further experiments.

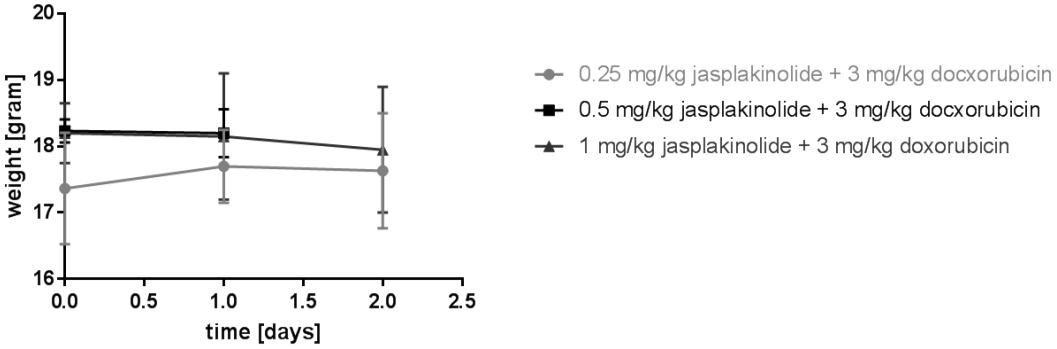

Figure 25: Body weight development over time. Weight of mice during the dose finding experiment with jasplakinolide injection on day 0. Represented is the mean ± S.E.M. of three mice per group.

2. Examination of pharmacokinetic studies

Knowledge of pharmacokinetic attributes is important to find the right dosage of a compound and to get an idea of its mode of action. Detailed experimental conditions can be seen in Table 2 on page 28.

2.1. Evaluation of PS89 in pharmacokinetic studies

Blood plasma concentrations of the compound PS89 were examined after intravenous and intraperitoneal injections. In the intravenous setup, the sample out of the pooled blood plasma taken directly after the injection contained 0.16 µg/µl PS89. Five and eight minutes after the injection 0.018 µg/µl PS89 were detected. After ten minutes 0.077 µg/µl PS89 was found in the blood plasma. 15 minutes after the injection 0.004 µg/µl PS89 were detected (Figure 26). In the intraperitoneal setup blood plasma concentrations were measured 15 minutes and 120 minutes after the injection. It was possible to detect 0.0023 µg/µl PS89 in the pooled blood plasma of four mice after 15 minutes. 120 minutes after the intraperitoneal injection PS89 was not detectable any more.

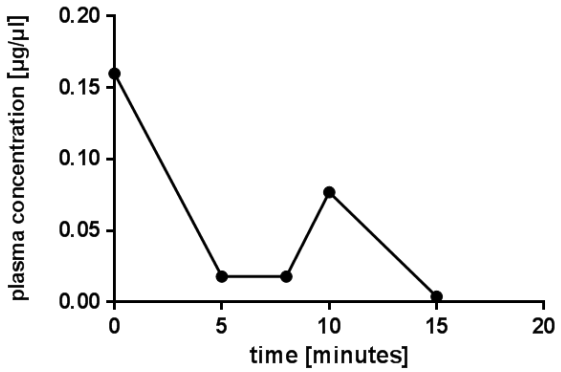

Figure 26: Blood plasma concentration after intravenous injection. Blood was taken 0, 5, 8, 10, and 15 minutes after 10 mg/kg PS89 was injected. Every measured value represents a pooled blood plasma sample of two mice. Measurement was done by Dr. Christoph Müller and Anna Niedrig.

3. *In vivo* tumor models to evaluate tumor dissemination

We conducted dissemination assays as a first step of *in vivo* characterization of new compounds, which showed promising effects on tumor cell migration and invasion *in vitro*. Hence, dissemination assays provide insights if a compound is able to influence tumor formation *in vivo*. Detailed experimental condition can be seen in Table 3 on page 29.

3.1. Examination of dissemination of 4T1-luc cells

Assays with bioluminescence measurements in the first hours after tumor cell injection were performed for the first time in our lab to implement a new imaging setup. In this new experimental setup, we focused on the procedures taking place short time after the intravenous cell injection. We wanted to detect a bioluminescence signal in the IVIS® spectrum already few hours after the cell injection. Therefore, we injected a significantly higher number of cells compared to established dissemination assays. In contrast to other dissemination assays, the mice were imaged at least once a day on consecutive days.

The first assay was performed with five BALB/c mice, which were injected with $5x10^6$ 4T1-luc cells (murine breast adenocarcinoma cells). The bioluminescence measurements took place 3 hours, 6 hours, and 24 hours after the cell injection. Due to lung embolism two mice had to be euthanized directly after the cell injection. In the three remaining mice, a clear tumor signal was visible since the first measurement. Three hours after the injection, the mean bioluminescence signal was $2.5x10^8$ total flux/area, then the signal decreased to $1.5x10^8$ total flux/area 6 hours after the injection and increased to $6.4x10^8$ total flux/area 24 hours after the cell injection (Figure 28B). The general condition of the three remaining mice was reduced. They also showed reduction of weight between 4.5% and 24.4% within 24 hours (Figure 28A).

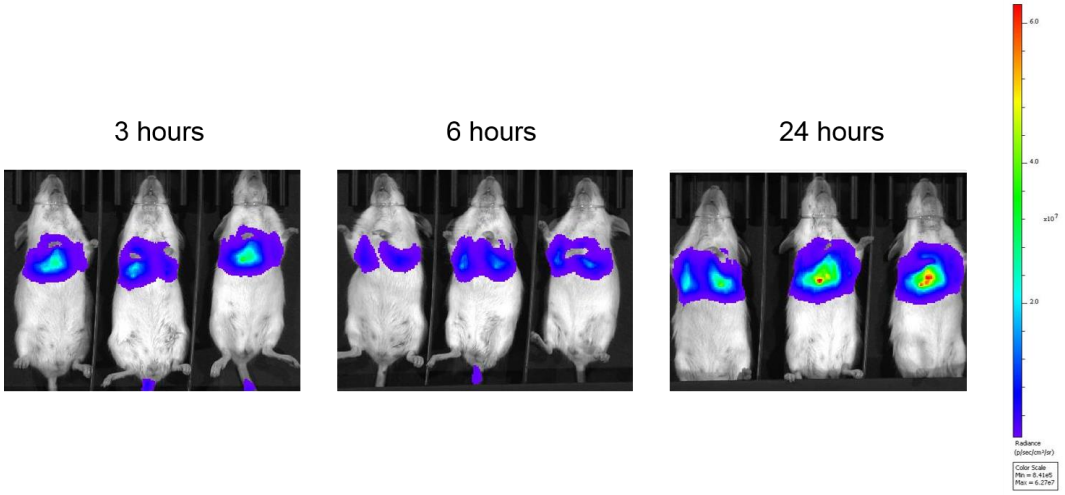

Figure 27: Bioluminescence imaging of 4T1-luc cells. Pictures of tumor burden in three BALB/c mice in ventrodorsal position 3, 6, and 24 hours after i.v. cell injection of $5x10^6$ 4T1-luc cells.

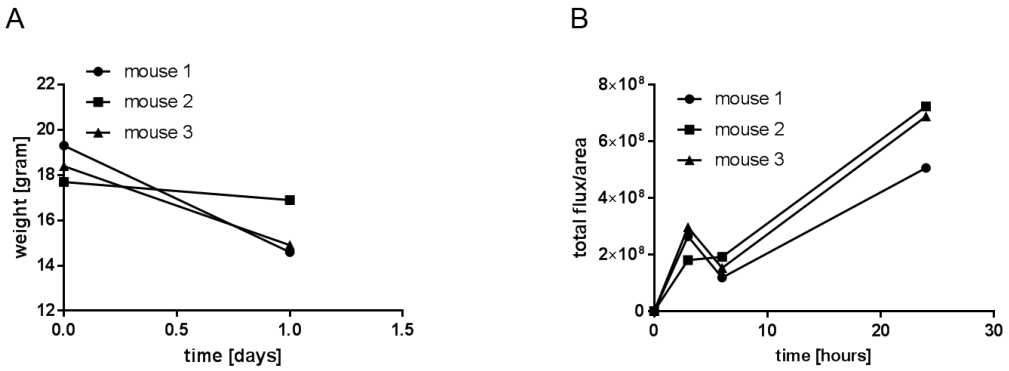

Figure 28: Body weight development and tumor growth. A) Body weight development. Decrease of mice` weight for 24 hours. Each curve represents one single mouse. **B)** Tumor burden in the lungs. The tumor burden was measured 3, 6, and 24 hours after i.v. cell injection. Each curve represents the tumor burden in total flux/area of one single mouse.

In a second approach, two BALB/ c mice were injected with $1x10^6$ 4T1-luc cells intravenously and two BALB/c mice were injected with $2x10^6$ 4T1-luc cells. In all mice, the tumor signal was most obvious in the lung, additionally one mouse which received $2x10^6$ 4T1-luc cells showed a tumor signal in the spleen after three hours (Figure 29). In the group which was injected with the higher number of cells the mean bioluminescence signal was $7.0x10^7$ total flux/area 3 hours after the injection, $7.4x10^8$ total flux/area after 6 hours, $1.0x10^8$ total flux/area after 24 hours and $3.5x10^8$ total flux/area after 48 hours. In the group which received the lower

number of cells, the mean bioluminescence signal was $2.6x10^7$ total flux/area after 3 hours, $1.8x10^7$ total flux/area after 6 hours, $2.8x10^7$ total flux/area after 24 hours, and $8.1x10^7$ total flux/area after 48 hours (Figure 30B). The general condition of the mice was good and without detectable abnormalities. The body weight increased low-grade during the 48 hours of the experiment (Figure 30A). The number of bioluminescence measurements as well as the injected number of cells was limited by the general condition of the mice. As the reduced general condition and the lung embolism in the group injected with $5x10^6$ 4T1-luc cells was not tolerable, we decided to use $2x10^6$ 4T1-luc cells for further experiments.

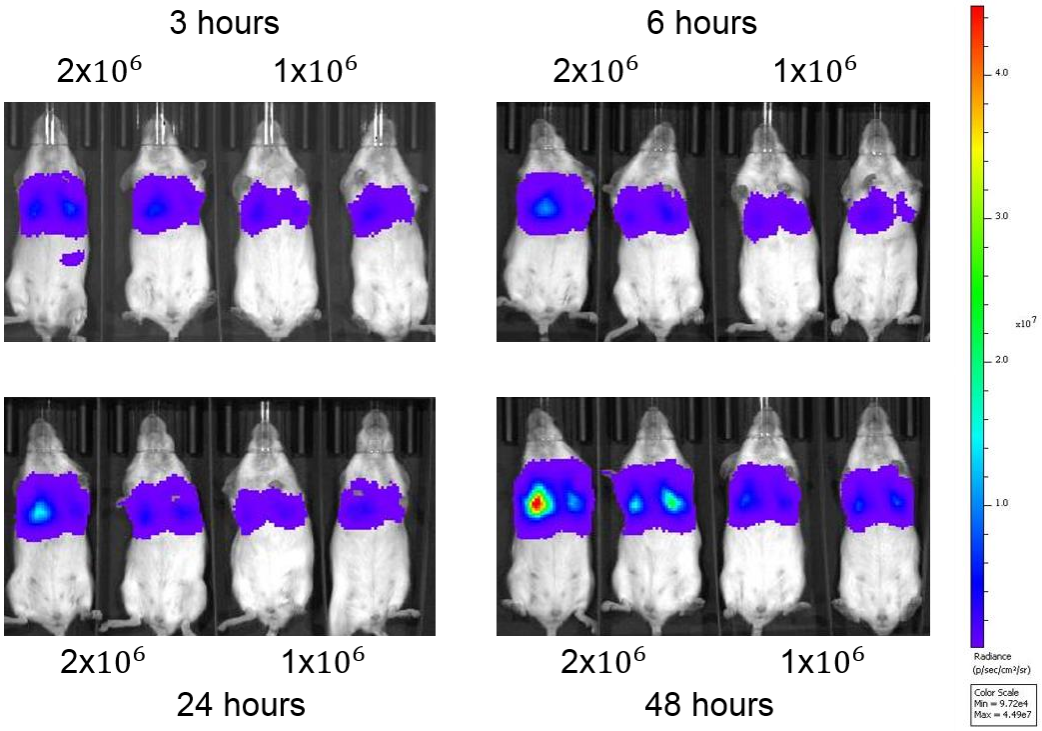

Figure 29: Bioluminescence imaging of 4T1-luc cells. Pictures of tumor burden in four BALB/c mice in ventrodorsal position 3, 6, 24, and 48 hours after i.v. cell injection of $1x10^6$ and $2x10^6$ 4T1-luc cells, respectively.

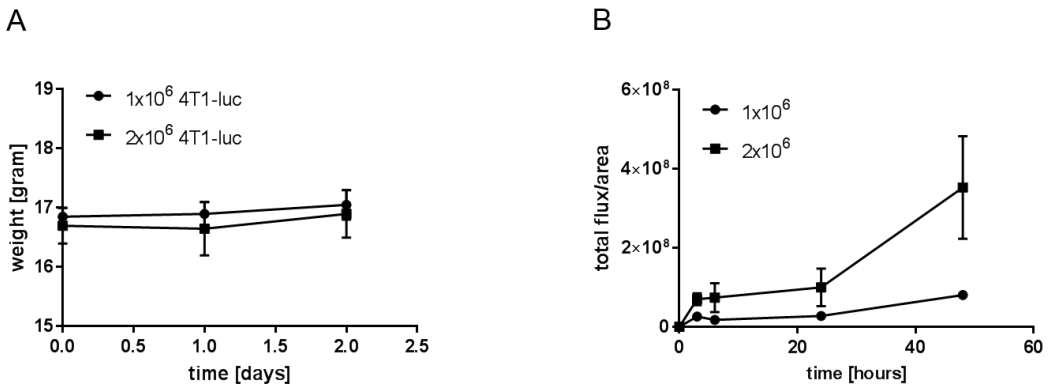

Figure 30: Body weight development and tumor growth. A) Development of mice` weight for 2 days. Each curve represents the mean ± S.E.M. of two mice per group. **B)** Tumor burden in the lungs. The tumor burden was measured 3, 6, 24, and 48 hours after i.v. cell injection. Each curve represents the mean tumor burden ± S.E.M. of two mice per group.

3.2. Effects of neocarzilin A on dissemination of 4T1-luc cells

The compound neocarzilin A was tested in a dissemination model with the dosage of 10 mg/kg. 16 BALB/c mice were divided into two groups, one control group and one neocarzilin A treated group. The mice were pretreated with 10 mg/kg neocarzilin A or just solvent 48 h, 24 h, and 0.5 h before the injection of $1x10^5$ murine breast adenocarcinoma 4T1-luc cells on day 0 (detailed conditions can be seen in Table 3 on page 29). The general condition of the mice was good during the experiment and no abnormalities were detectable. Body weight in both groups increased during the experiment (Figure 31). Bioluminescence signal was detectable in the lung of seven mice in the control group and in all mice in the neocarzilin A treated group. On day 5 and on day 8 the signal was higher in the control group in comparison to the treated group. The control group reached in mean $2.3x10^8$ total flux/area on day 5 and $1.9x10^9$ total flux/area on day 8, whereas the neocarzilin A treated group reached in mean $8.9x10^7$ total flux/area on day 5 and $1.2x10^9$ total flux/area on day 8 (Figure 32). Thus, neocarzilin A was able to reduce dissemination of murine breast cancer cells into the lung.

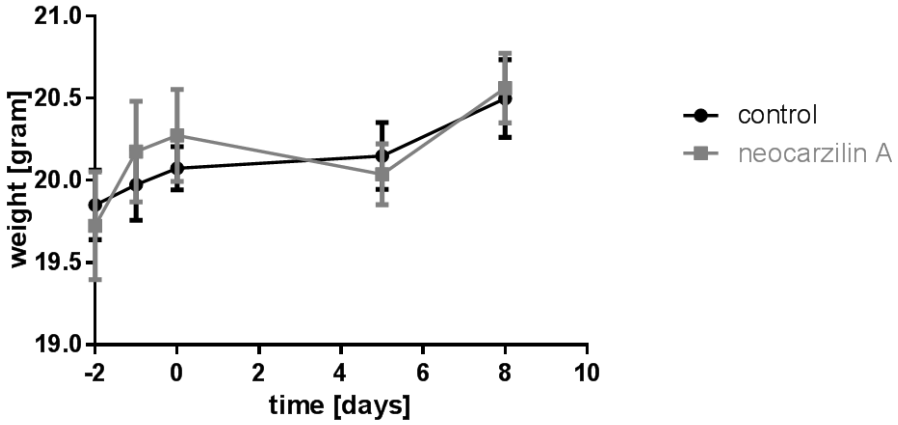

Figure 31: Body weight development. Weight of mice during the dissemination experiment. Represented is the mean ± S.E.M. of eight mice per group.

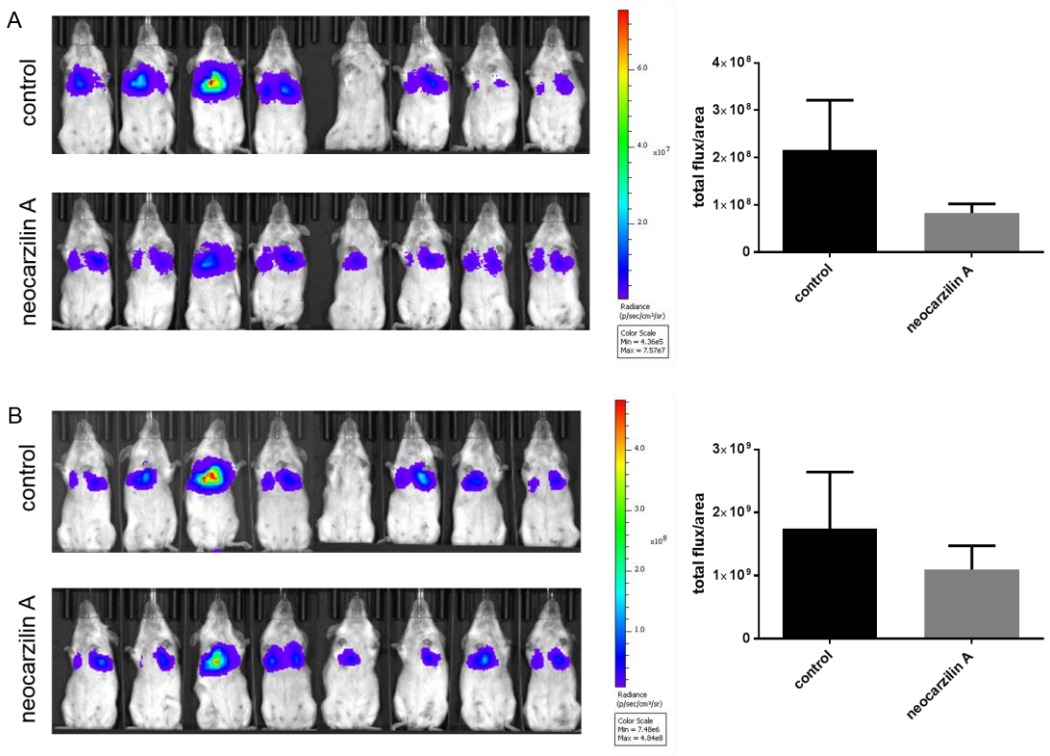

Figure 32: Bioluminescence imaging in BALB/c mice. A) Bioluminescence imaging on day 5. Measurement in ventrodorsal position five days after the i.v. injection of $1x10^5$ 4T1-luc cells. **B)** Bioluminescence imaging on day 8. Measurement in ventrodorsal position eight days after the i.v. injection of $1x10^5$ 4T1-luc cells. Represented is the mean ± S.E.M. of seven mice in the control group and eight mice in the neocarzilin A treated group.

3.3. Examination of Ril175-luc cell dissemination

The dissemination of murine liver cancer cells Ril175-luc was tested in six C57BL/6-Tyr mice, divided into two groups. One group received $1x10^5$ Ril175-luc cells, the other group received $2x10^5$ Ril75-luc cells on day 0. The bioluminescence measurements took place on day 3 and day 5. During this experiment, the general condition of all mice was unimpeded and the body weight stayed almost constant. On day 3 and on day 5 bioluminescence signals were detectable in the lungs of all six mice (Figure 33). The mean bioluminescence signal in the group injected with the lower number of Ril175-luc cells was $5.2x10^5$ total flux/area on day 3 and $2.6x10^6$ total flux/area on day 5. The mean bioluminescence signal in the group injected with the higher number of Ril175-luc cells was $3.0x10^6$ total flux/area on day 3 and $8.0x10^6$ total flux/area on day 5 (Figure 34B).
Thus, we could establish an imaging setup of murine liver cancer cells Ril175-luc with the IVIS® spectrum for the first time in our lab. For further dissemination experiments we decided to inject $2x10^5$ Ril175-luc cells into the tail vein.

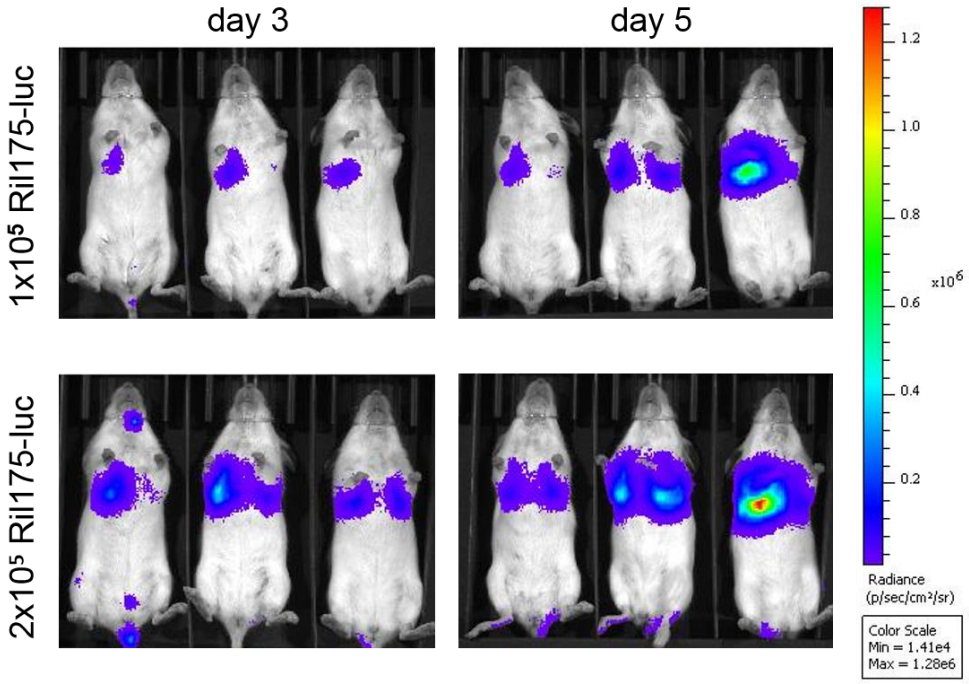

Figure 33: Bioluminescence imaging of Ril175-luc cells. The bioluminescence signal of both groups is shown on day 3 and on day 5 after i.v. injection of $1x10^5$ respectively $2x10^5$ Ril175-luc cells. The mice were imaged in ventrodorsal position.

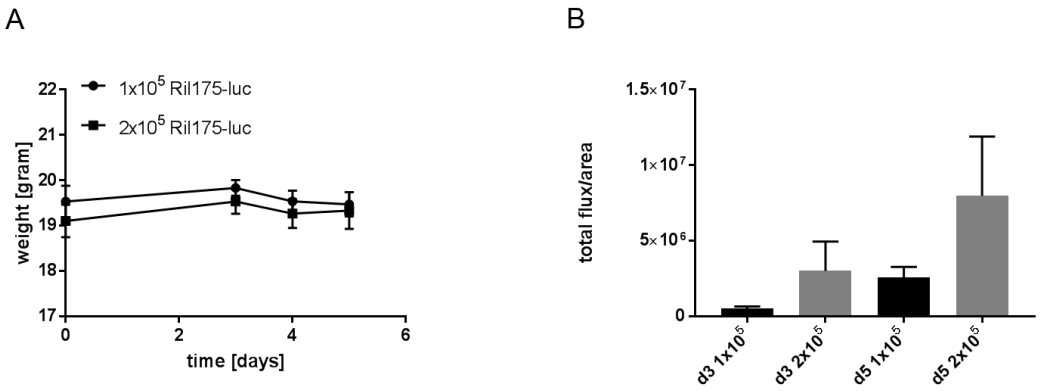

Figure 34: Body weight development and tumor growth. A) Body weight development over time. Weight of mice during the dissemination experiment. Represented is the mean ± S.E.M. of three mice per group. **B)** Bioluminescence signal of Ril175-luc cells. Measurements were performed on day 3 and on day 5. Represented is the mean ± S.E.M. of three mice per group.

3.4. Effects of Cdk5 inhibition on Ril175-luc cell dissemination

In the first part of this experiment the Cdk5 inhibitor dinaciclib was tested in a dissemination assay with 20 C57BL/6 albino mice, divided into two groups. Mice were pretreated with 10 mg/kg dinaciclib 48 h, 24 h, and 0.5 h before the intravenous injection of $2x10^5$ murine liver cancer cells Ril175-luc. Bioluminescence imaging was performed on day 3 after the tumor cell injection. During the experiment, the general condition of both groups was good and without detectable abnormalities in behavior. Both groups started the experiment with nearly equal body weight on day -2 (19.0 g in the mean in the control group and 18.8 g in the mean in the dinaciclib treated group), the control group was able to gain weight during the experiment (day 3: 19.4 g in the mean), whereas the dinaciclib treated group lost weight (day 3: 18.3 g in the mean) (Figure 36A). On day 3 the bioluminescence signal was significantly lower in the dinaciclib treated group ($3.6x10^6$ total flux/area) than in the control group ($2.0x10^6$ total flux/area) (Figure 36B). Thus, 10 mg/kg dinaciclib was sufficient to reduce tumor dissemination of murine liver cancer cells *in vivo*.

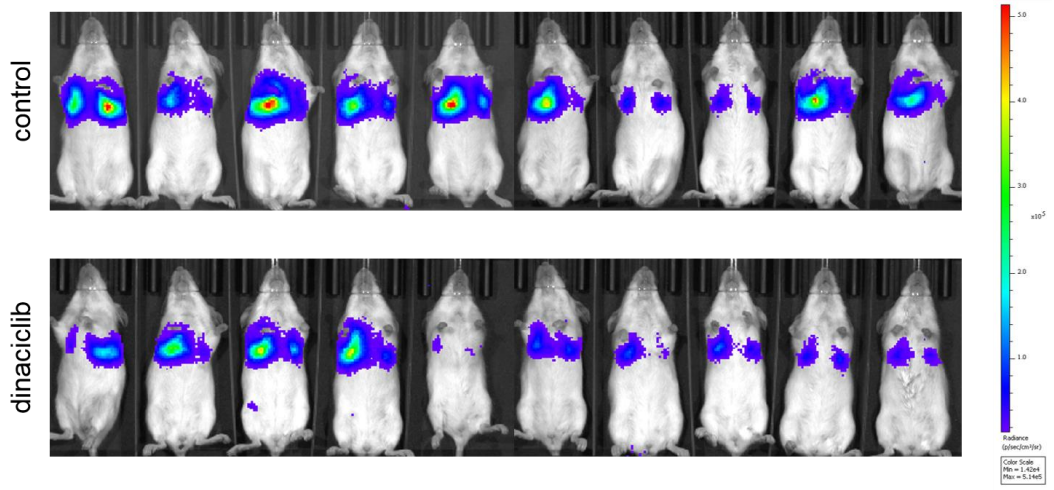

Figure 35: Bioluminescence imaging in C57BL/6 albino mice. Bioluminescence imaging on day 3. Measurement in ventrodorsal position three days after the i.v. injection of $2x10^5$ Ril175-luc cells.

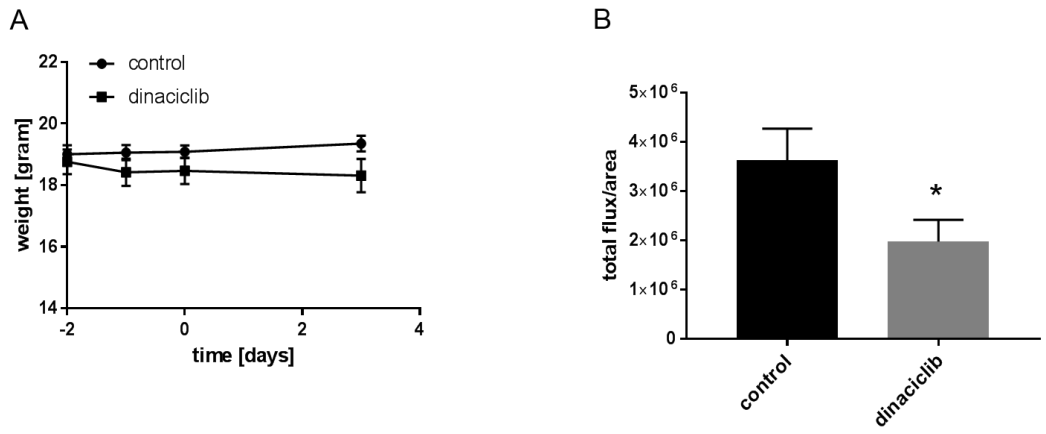

Figure 36: Effects of dinaciclib on tumor dissemination. A) Body weight development. Weight of mice during the dissemination experiment. Represented is the mean ± S.E.M. of ten mice per group. **B)** Tumor signal on day 3 after cell injection. Represented is the mean ± S.E.M. of ten mice per group. Significance was calculated by unpaired t-test (* $p < 0.05$).

In the second part of the experiment dissemination of murine liver cancer cells Ril175-luc with Cdk5 KO was tested. 10 mice per group were injected intravenously with $2x10^5$ Ril175-luc Cdk5 KO cells or Ril175-luc wt cells. The mouse weight during this experiment was nearly constant (Figure 39A), the general condition of the mice was without detectable abnormalities. Three days after the cell injection the cell dissemination was impaired by Cdk5 knockout ($1.2x10^6$ total flux/area) compared to wildtype cells

(4.8x10^6 total flux/area) (Figure 39B). Thus, this set of data shows that the influence of Cdk5 on dissemination of murine liver cancer cells could be proven.

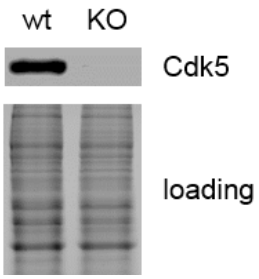

Figure 37: Cdk5 KO Ril175-luc cells. Western Blot showing the protein levels of Cdk5 in RiL175-luc wild-type cells and RiL175-luc Cdk5 KO cells generated via the CRISPR/Cas method by Maximilian Ardelt.

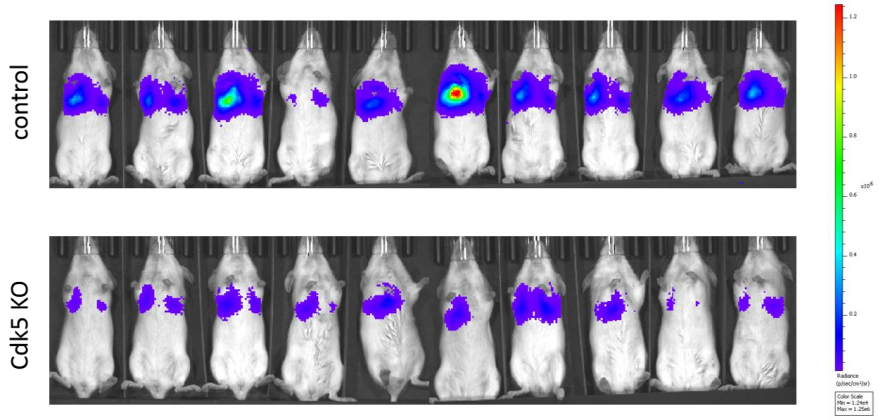

Figure 38: Bioluminescence imaging in C57BL/6 albino mice. Bioluminescence imaging on day 3. Measurement in ventrodorsal position three days after the i.v. injection of 2x10^5 Ril175-luc Cdk5 KO cells or Ril175-luc wt cells as control.

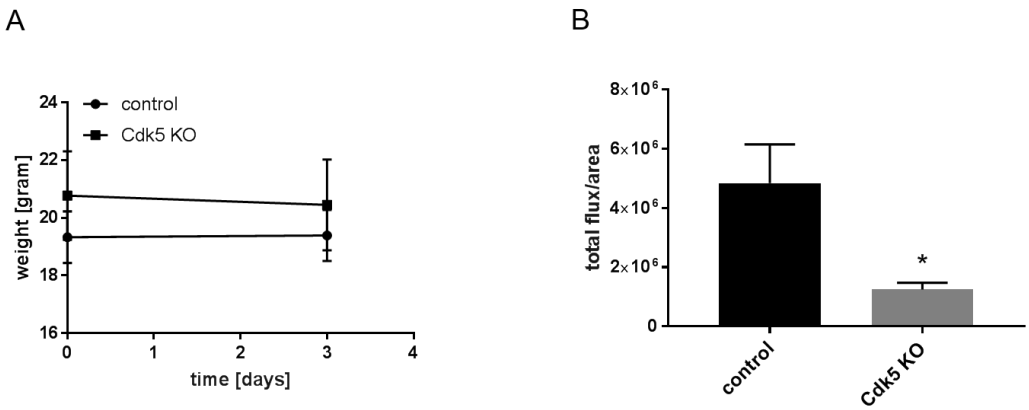

Figure 39: Effects of Cdk5 KO on tumor dissemination. A) Body weight development. Weight of mice during the dissemination experiment. Represented is the mean ± S.E.M. of ten mice per group. **B)** Tumor signal on day 3 after cell injection. Represented is the mean ± S.E.M. of ten mice per group. Significance was calculated by unpaired t-test (* $p < 0.05$).

3.5. Effects of TPC2 on tumor cell dissemination

The first part of this experimental setup consisted of a dissemination assay with Ned-19 pretreated cells. Therefore, murine breast adenocarcinoma cells 4T1-luc were pretreated with 150 µmol/L Ned-19 for 24 hours. Each of the seven BALB/c mice received $1x10^5$ 4T1-luc cells via intravenous injection on day 0. As control group seven BALB/c mice received $1x10^5$ 4T1-luc cells pretreated with DMSO for 24 hours. The mice were imaged on day 5. During the experiment, the general condition of the mice was good and their body weight was nearly constant (Figure 41A). The bioluminescence signal on day 5 was significantly lower in the Ned-19 group ($2.2x10^6$ total flux/area) than in the control group ($7.0x10^6$ total flux/area) (Figure 41B). Thus, Ned-19 pretreatment was able to reduce tumor dissemination in murine breast cancer cells significantly.

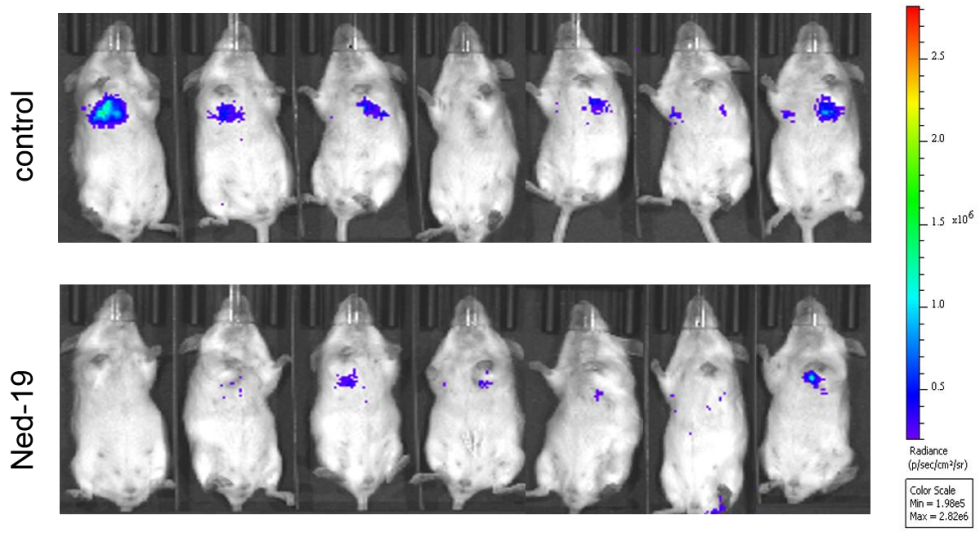

Figure 40: Bioluminescence imaging in BALB/c mice. Measurements in ventrodorsal position on day 5 after i.v. injection of $1x10^5$ 4T1-luc cells pretreated with 150 µmol/L Ned-19 or DMSO as control.

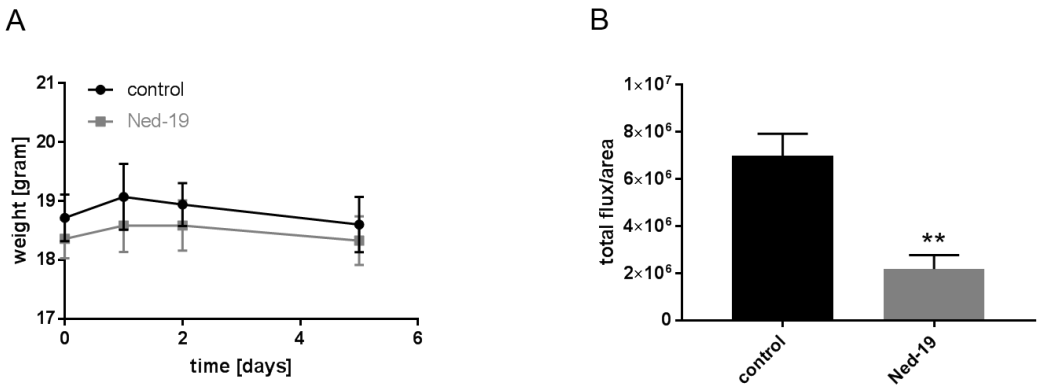

Figure 41: Effects of Ned-19. A) Body weight development over time. Weight of mice during the dissemination experiment. Represented is the mean ± S.E.M. of seven mice per group. **B)** Bioluminescence signal of 4T1-luc cells. Represented is the mean ± S.E.M. of seven mice per group. Significance was calculated by unpaired t-test (** $p < 0.01$). Statistical analysis was done by Dr. Ong Nam Phuong Nguyen [55].

In the second dissemination assay $1x10^5$ TPC2-silenced 4T1-luc cells (siTPC2) were intravenously injected in eight BALB/c mice. As control eight BALB/c mice received control transfected 4T1-luc cells (siNT). The mice were imaged on day 5 after the cell injection. All mice showed a good general condition and an increasing body weight during the experiment (Figure 43A). The bioluminescence signal of tumor cells in the lung in the siTPC2 group ($6.2x10^6$ total flux/area) was significantly lower than in the siNT group ($2.4x10^7$ total flux/area) (Figure 43B). Hence, silencing TPC2 reduced dissemination of murine breast cancer cells significantly.

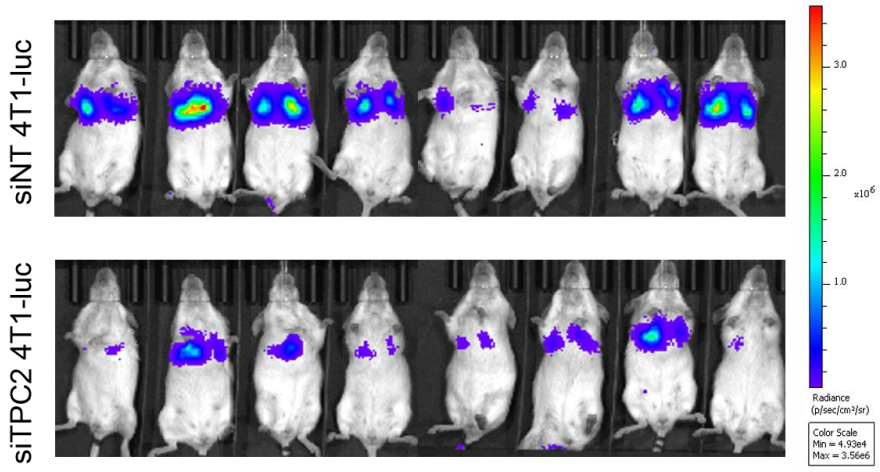

Figure 42: Bioluminescence imaging in BALB/c mice on day 5. Measurements in ventrodorsal position on day 5 after i.v. injection of $1x10^5$ siTPC2 4T1-luc cells or siNT 4T1-luc cells as control.

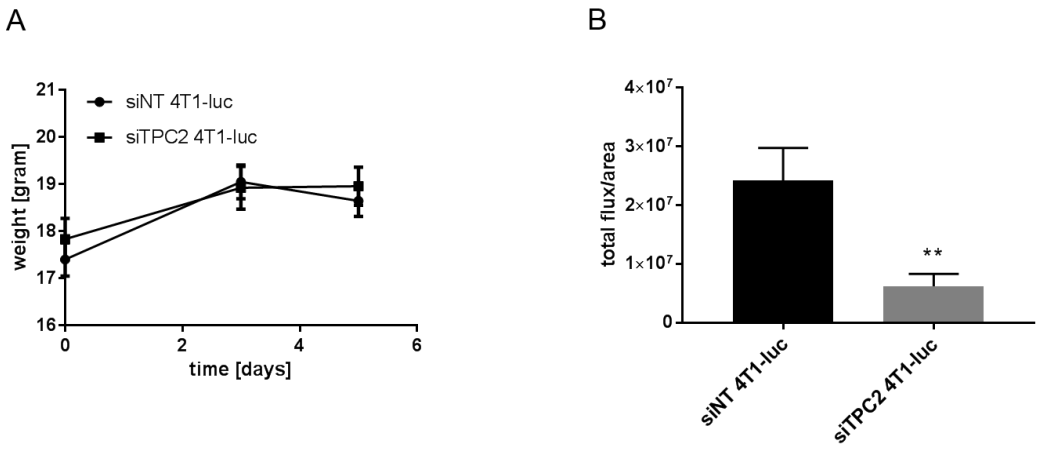

Figure 43: Effects of silencing TPC2. A) Body weight development over time. Weight of mice during the dissemination experiment. Represented is the mean ± S.E.M. of eight mice per group. **B)** Bioluminescence measurement of 4T1-luc cells. Represented is the mean ± S.E.M. of eight mice per group. Significance was calculated by unpaired t-test (** $p < 0.01$).

The following dissemination experiment was performed with murine liver cancer Ril175-luc TPC2 KO cells. One group of ten C57BL/6-Tyr mice was injected with $2x10^5$ Ril175-luc cells without genetical manipulation and served as control group, whereas ten other mice were injected with $2x10^5$ Ril175-luc TPC2 KO cells. During the experiment, the mice gained body weight and showed a good general condition (Figure 45A). On day 3 after the cell injection the bioluminescence signal of the TPC2 KO tumors was significantly lower ($2.3x10^6$ total flux/area) compared to the control group ($1.0x10^7$ total flux/area) (Figure 45B). Accordingly, it could be shown that TPC2 is a potential target to reduce tumor dissemination *in vivo*.

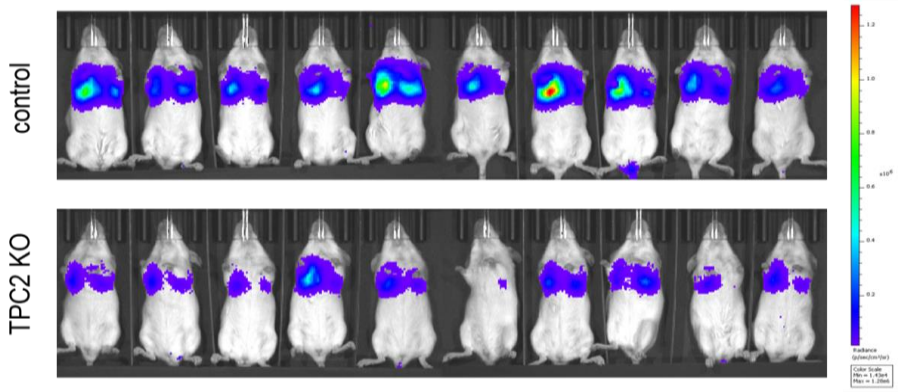

Figure 44: Bioluminescence imaging in C57BL/6 albino mice. Measurements in ventrodorsal position on day 3 after i.v. injection of $2x10^5$ Ril175-luc TPC2 KO cells or $2x10^5$ Ril175-luc cells as control.

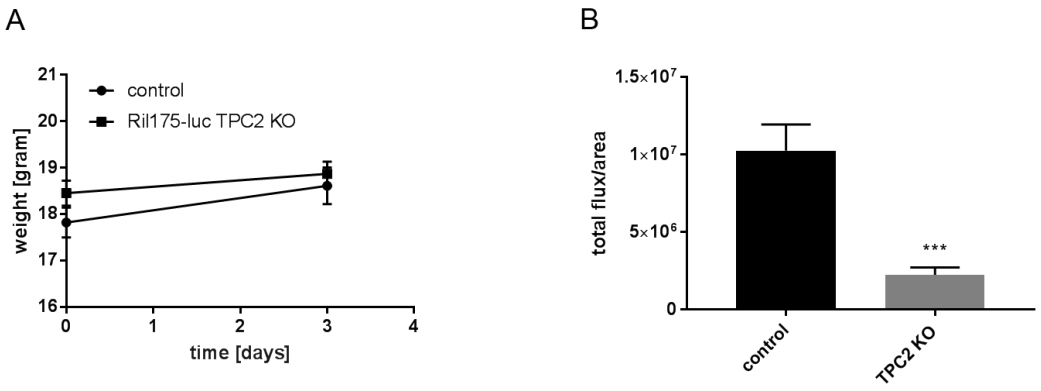

Figure 45: Effects of TPC2 KO. A) Body weight development over time. Weight of mice during the dissemination experiment. Represented is the mean ± S.E.M. of ten mice per group. **B)** Bioluminescence signal of Ril175-luc cells. Shown are the tumor signals of both groups in ventrodorsal position. Significance was calculated by unpaired t-test (*** $p < 0.001$).

4. Examination of murine ectopic tumor models

In ectopic tumor models the tumor growth of murine breast adenocarcinoma cells 4T1-luc, rat hepatoma cells McA-RH7777, and human hepatocellular carcinoma cells HUH7 was evaluated. In this model, it is possible to characterize the growth of different cell lines, find a suitable mouse strain for further experiments as well as to examine the influence of different compounds on subcutaneous tumor growth. Detailed information on the experimental conditions can be seen in Table 4 on page 31.

4.1. Preliminary growth experiment with 4T1-luc cells

In this preliminary growth experiment BALB/c mice were subcutaneously injected with $1x10^6$ murine breast adenocarcinoma cells 4T1-luc to determine the tumor growth rate for further experiments. Three days after the cell injection in three out of four mice subcutaneous tumors were visible. On day 6 after the cell injection all mice developed subcutaneous tumors with a mean tumor volume of 70 mm^3. In the end of the experiment on day 9, the mean tumor volume amounted 194 mm^3 (Figure 46B). During the whole experiment the general condition of the mice was good, they lost body weight after the cell injection but in the end gained weight compared to their initial weight (Figure 46A). Thus, 4T1-luc cells are suitable for breast cancer growth models.

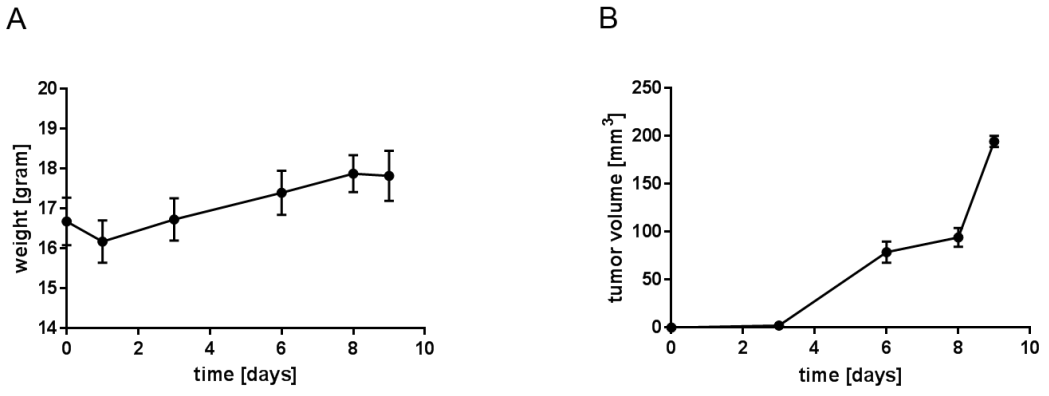

Figure 46: Results of preliminary growth experiment. A) Body weight development over time. Weight of mice during the experiment. Represented is the mean ± S.E.M. of four mice per group. **B)** Tumor growth over time. Represented is the mean ± S.E.M. of four mice per group.

4.2. Preliminary growth experiment with McA-RH7777 cells

In this growth experiment we wanted to find a suitable mouse strain for experiments with the rat hepatoma cell line McA-RH7777. As this cell line was used for the first time in an *in vivo* mouse model in our lab, no mouse strain was established. Therefore, it was of interest, if McA-RH7777 cells were able to form subcutaneous tumors in SCID mice. Four SCID mice were injected with $2x10^6$ McA-RH7777 cells on day 0. On day 7 tumors were visible in two of four mice. On day 9 tumors were visible in all four mice with a mean tumor volume of 49 mm^3. On the last day of the experiment the mean tumor volume was 145 mm^3 (Figure 47B) and the tumor weight was between 0.05 mg and 0.15 mg after resection (Figure 47C). The general condition of all four SCID mice was good during the whole experiment with a constant body weight (Figure 47A). Therefore, we demonstrated that McA-RH7777 cells grow subcutaneously in SCID mice and can be used for further tumor growth models.

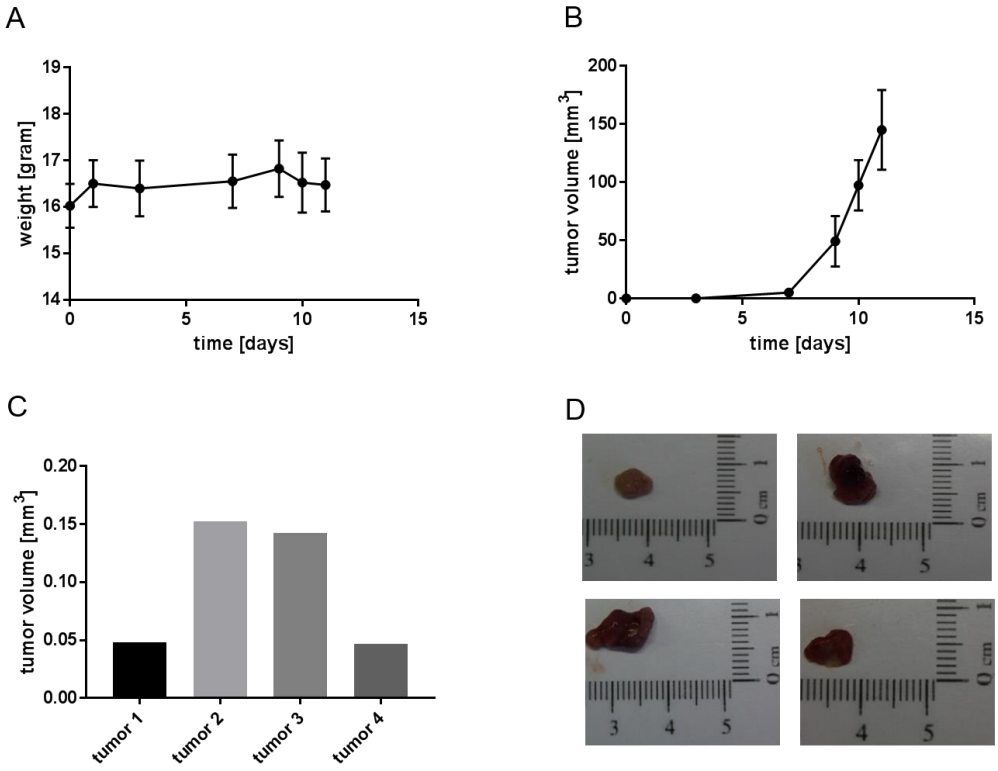

Figure 47: Results of growth experiment. A) Body weight development over time. Weight of mice during the experiment. Represented is the mean ± S.E.M. of four mice per group. **B)** Tumor growth over time. Represented is the mean ± S.E.M. of four mice per group. **C)** Tumor weight after resection on day 11. **D)** Pictures of tumors after resection.

4.3. Evaluation of HUH7 cells in a murine ectopic tumor model

The aim of the first part of this *in vivo* experiment was to find out, if all of the *in vitro* tested human hepatocellular carcinoma HUH7 cell lines are able to build subcutaneous tumors in SCID mice. *In vitro*, the proliferation of HUH7 wildtype (wt) and HUH7 sorafenib resistant cell lines HUH7 resi(+) and HUH7 resi(-) differ significantly. Whereas HUH7 wt and HUH7 resi(+) cells proliferated similarly *in vitro*, the doubling time of HUH7 resi(-) cells was less than half compared with the other HUH7 cells (unpublished data). In addition, HUH7 wildtype cells show a significantly higher average volume than HUH7 sorafenib resistant cells (unpublished data). To test their growth *in vivo*, $3x10^6$ HUH7 wt cells, HUH7 resi(-) cells, and HUH7 resi(+) cells were injected subcutaneously in three mice per group. The groups which were injected with HUH7 wt cells and the HUH7 resi(-) cells were treated with solvent. Two groups were injected with HUH7 resi(+) cells. One of this groups was treated with solvent the other group was treated with 20 mg/kg sorafenib i.p. three times a week (detailed conditions can be seen in Table 4 on page 31). During the experiment, the general condition of the mice was unimpeded and their body weight was nearly constant until day 6 after the cell injection. Since day 6 the whole HUH7 resi(-) group showed a loss of body weight and on day 11 a bad general condition, so that they had to be euthanized. The other groups showed constant body weight development until the end of the experiment on day 15, except for the HUH7 resi(+) group treated with solvent (Figure 48A). They had a reduced body weight on day 11 but anyhow a good general condition. Except for one mouse in the HUH7 wt cell group and one mouse in the HUH7 resi(+) cell group treated with solvent, in all mice tumor growth was visible. The HUH7 wt cells showed the biggest tumor growth *in vivo* with a tumor volume of 284 mm^3 in the mean on day 15 (Figure 48B). The HUH7 resi(+) group had a mean tumor volume of 55 mm^3 on day 15, the HUH7 resi(+) group which received sorafenib treatment had a mean tumor volume of 25 mm^3 on day 15. The HUH7 resi(-) group was euthanized on day 11 with a mean tumor size of 21 mm^3 (Figure 48C). In this preliminary experiment we could prove that all HUH7 cell lines are able to form subcutaneous tumors *in vivo*. Moreover, it was possible to show a slightly reduced tumor growth in HUH7 resi(+) cells treated with sorafenib *in vivo* compared to HUH7 resi(+) without further

treatment *in vivo*. Further, HUH7 wt cells formed tumors with the biggest volume after 15 days.

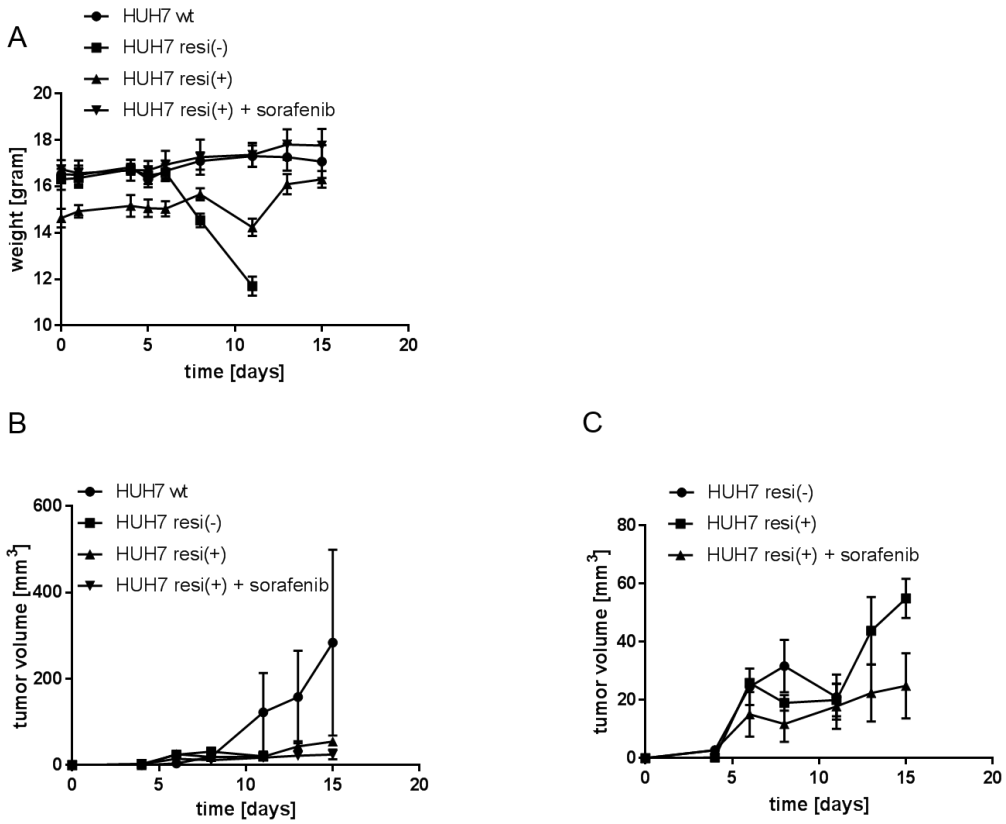

Figure 48: Results of the preliminary tumor growth experiment. A) Body weight development over time. Weight of mice during the experiment. Represented is the mean ± S.E.M. of three mice per group. **B)** Tumor growth over time. Tumor volume of different HUH7 cell lines treated just with solvent and HUH7 resi(+) cells treated with 10 mg/kg sorafenib three times a week. Each curve represents the mean ± S.E.M. of two or three mice per group. **C)** Tumor growth over time. Tumor volume of different HUH7 sorafenib resistant cell lines with and without sorafenib treatment. Each curve represents the mean ± S.E.M. of two or three mice per group.

In the second part of the ectopic tumor model, tumor growth was tested in HUH7 wt cells and HUH7 resi(+) cells with and without sorafenib treatment. Therefore 36 mice were divided into four groups. 16 mice received HUH7 wt cells and eight of them were treated with 20 mg/kg sorafenib every second day. 20 mice received HUH7 resi(+) cells and ten of them were treated with 20 mg/kg sorafenib every second day. During the whole experiment the body weight in all groups was constant. The general condition of the mice was without detectable abnormalities. On day 15 the HUH7 wt control cells showed the highest mean tumor volume of 533 mm^3.

On the same day the HUH7 wt cells which were treated with sorafenib showed a mean tumor volume of 134 mm^3. The HUH7 resi(+) control cells had a mean tumor volume of 228 mm^3 on day 15, and a mean tumor volume of 313 mm^3 on day 16. The HUH7 resi(+) cells with sorafenib treatment showed a mean tumor volume of 89 mm^3 on day 15, and a mean tumor volume of 178 mm^3 on day 16 (Figure 50B). After tumor resection (day 15 or day 16), the HUH7 wt control tumors had a mean weight of 0.32 g, the HUH7 wt tumors under sorafenib treatment had a mean weight of 0.07 g, the HUH7 resi(+) control tumors had a mean weight of 0.22 g, and the HUH7 resi(+) tumors under sorafenib treatment had a mean weight of 0.13 g (Figure 50C). Moreover, we observed an invasive tumor growth in both HUH7 sorafenib resistant cell lines. Relating to tumor weight after resection we could see a reduction of tumor volume in HUH7 wt tumors as well as in HUH7 resi(+) tumors under sorafenib treatment. Interestingly, in all mice, HUH7 wt tumors appeared deep red and well vascularized whereas all HUH7 resi(+) tumors appeared pale and exsanguinated (Figure 49) suggesting a reduced vascularization and thereby less blood supply in these tumors.

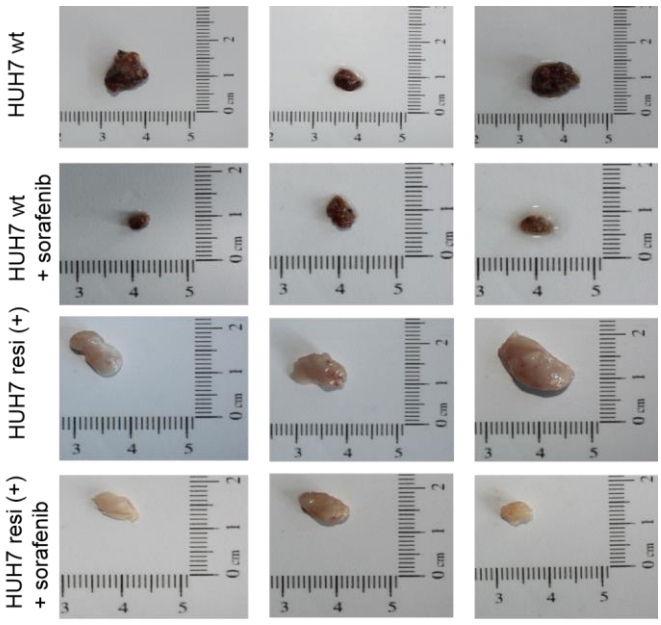

Figure 49: Solid HUH7 tumors after resection. After euthanasia the skin was opened and the subcutaneous tumors were resected, weighted and photographed. Represented are three representative tumors of each group.

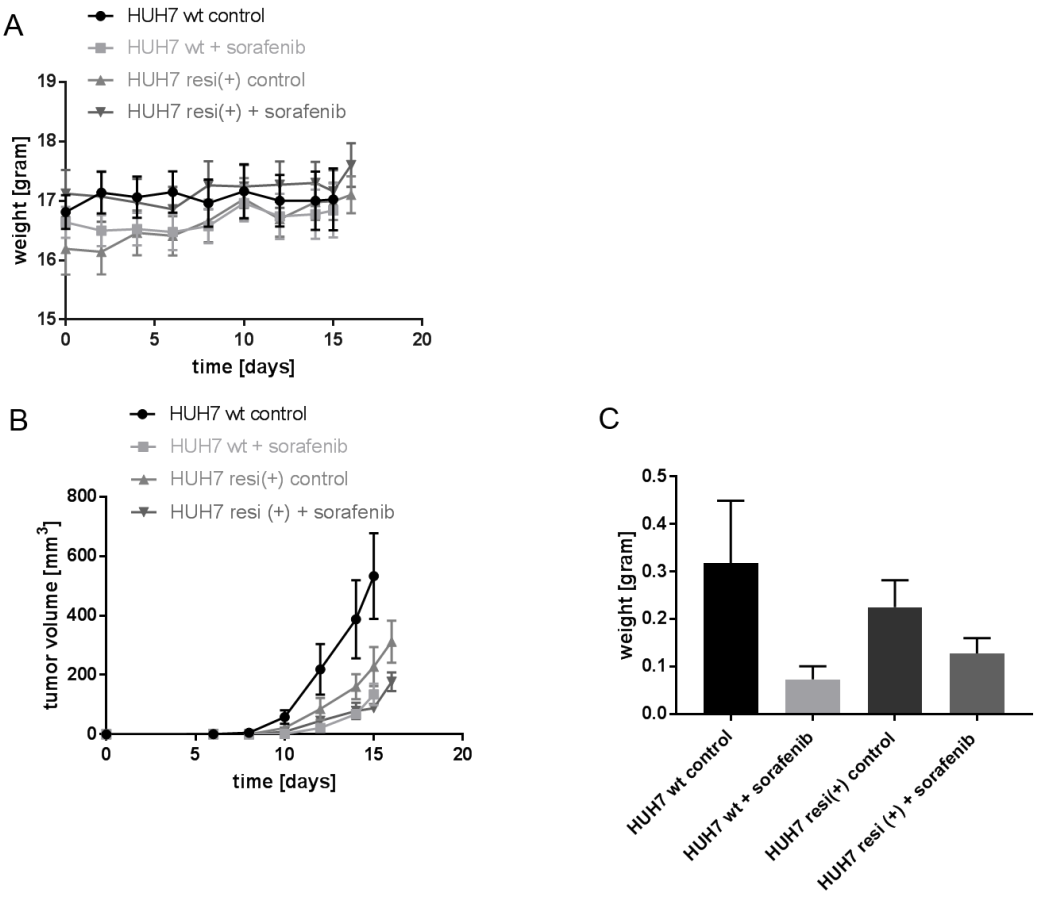

Figure 50: Results of HUH7 tumor growth experiment. A) Body weight development over time. Weight of mice during the experiment. Represented is the mean ± S.E.M. of eight respectively ten mice per group. **B)** Tumor growth over time. Tumor volume of HUH7 wt and HUH7 resi(+) cells with and without 20 mg/kg sorafenib treatment every second day. Each curve represents the mean ± S.E.M. of eight or ten mice per group. **C)** Tumor weight after resection. S.c. tumors were resected after euthanizing the mice and scaled. Represented is the mean ± S.E.M. of eight or ten mice per group.

In the third part of this project, HUH7 resi(+)-luc cells were injected subcutaneously to investigate the influence of treatment with the experimental natural compound CA1 on tumor growth. Therefore, 10 SCID mice were divided into two groups. One group just received treatment with solvent and served as control. The other group was intraperitoneally treated with 100 mg/kg CA1 three times a week. In contrast to the other ectopic tumor models, we changed our experimental setup and imaged the subcutaneous tumors twice a week using the IVIS® spectrum additionally to caliper measurements. The general condition of the mice was good during the experiment, except for a reduced general condition of the CA1 treated

mice for 15 minutes after the intraperitoneal injection. Bioluminescence signal was detectable already three days after the cell injection (Figure 51A). On day 3, both groups showed a nearly equal bioluminescence signal of $3.2x10^7$ total flux/area in the control group and $1.4x10^7$ total flux/area in the CA1 treated group. On day 7 and on day 10 the bioluminescence signal in the control group was $3.9x10^9$ total flux/area and $9.7x10^9$ total flux/area, respectively. In the CA1 treated group the bioluminescence signal was $3.0x10^8$ total flux/area on day 7 and $1.9x10^9$ total flux/area on day 10 (Figure 52B). Subcutaneous tumors were visible and measurable with the digital caliper since day 8. The tumor volume measured with the digital caliper was also higher in the control group compared to the CA1 treated group (Figure 52C). In the same way, tumor weight after resection was significantly higher in the control group compared to the CA1 treated group (Figure 52D). Therefore, we implemented a functional new imaging setup for HUH7-luc cells, which allows bioluminescence measurements in a short interval after the cell injection. Moreover, the natural compound CA1 significantly reduced subcutaneous tumor growth of HUH7 resi(+)-luc cells.

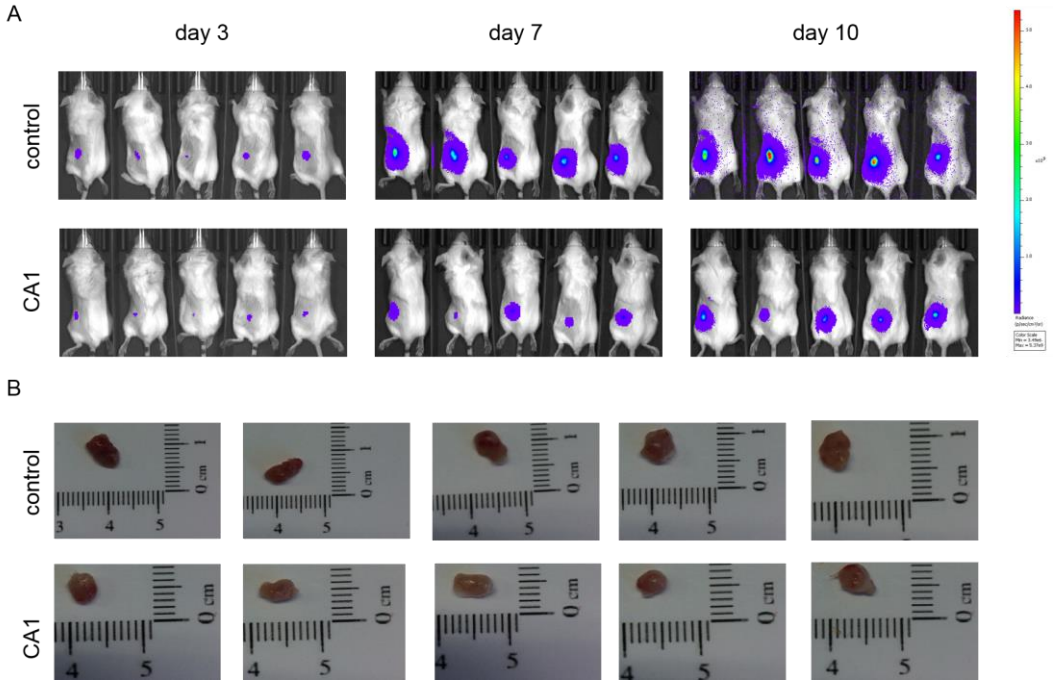

Figure 51: Subcutaneous tumor growth of HUH7 resi(+)-luc cells. A) Bioluminescence imaging in SCID mice. Measurements in dorsoventral position on days 3, 7, and 10 after s.c. injection of $3x10^6$ HUH7 resi(+)-luc cells. **B)** Pictures of tumors after resection on day 10.

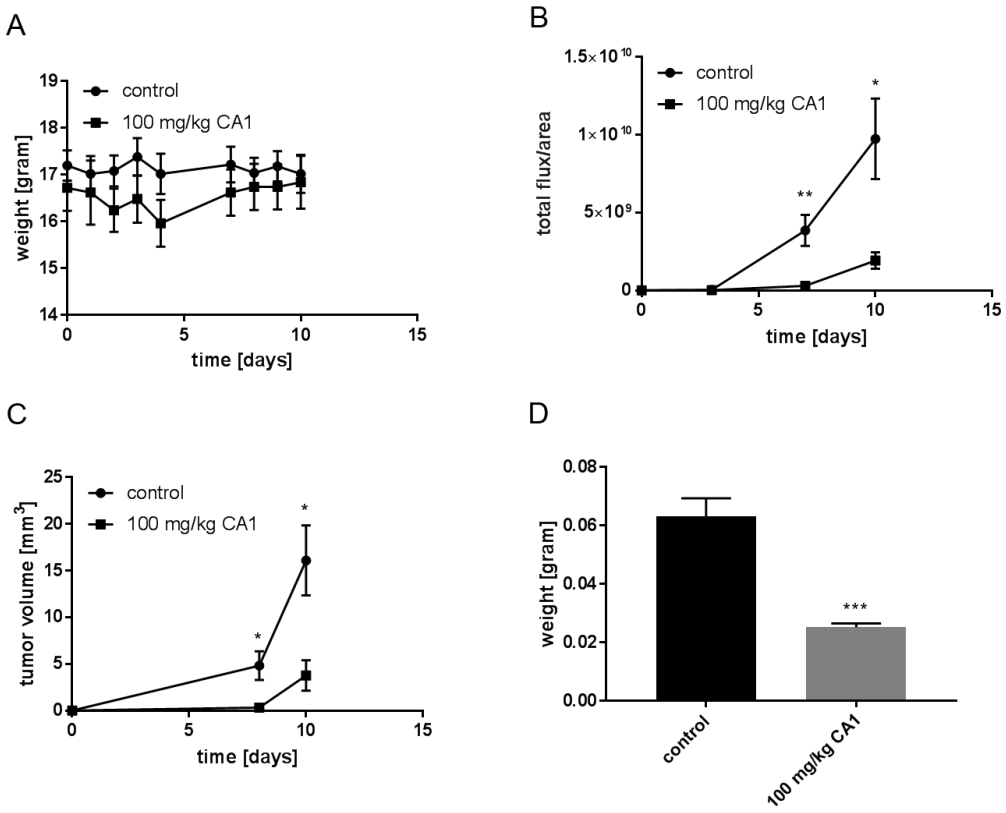

Figure 52: Results of HUH7 resi(+)-luc tumor growth experiment. A) Body weight development over time. Weight of mice during the experiment. Represented is the mean ± S.E.M. of five mice per group. **B)** Bioluminescence signal of s.c. HUH7 resi(+)-luc tumors treated with 100 mg/kg CA1 or solvent as control. Each curve represents the mean ± S.E.M. of five mice per group. **C)** Tumor growth over time measured with a digital caliper. Tumor volume of different HUH7 resi(+)-luc cells treated with 100 mg/kg CA1 or solvent as control three times a week. Each curve represents the mean ± S.E.M. of five mice per group. **D)** Tumor weight after resection on day 10. Significance was calculated by unpaired t-test (* $p < 0.05$, ** $p < 0.01$, *** $p < 0.001$).

5. Evaluation of a PDX cell leukemia model for AML-372

To evaluate the effects of PS89 and liposomal daunorubicin (DaunoXome®) on progression of acute myeloid leukemia, a mouse model with patient derived xenograft leukemia cells (AML-372) was performed. Details concerning the exact experimental setup can be seen in Table 5 on page 32. Before starting the treatment, the mouse body weight increased in all groups and the mice showed a physiological general condition without any abnormalities. During the treatment period, the mice in the control group and the PS89 treated group had a nearly constant body weight, whereas the mice in the daunorubicin group and the combination group showed reduction of weight (Figure 53). The duration of treatment differed between the four groups. The control mice and the mice which received PS89 were treated 13 to 20 days without abnormalities. The mice treated with liposomal daunorubicin were treated 8 to 13 days and had to be euthanized due to bad general condition in the majority of cases. In the same way the mice in the combination group were treated 8 to 15 days and were euthanized because of a decreasing general condition. Bioluminescence signal of the tumor burden was visible in the IVIS® spectrum in the femora, the humeri, the pelvis (in parts of the mice) and the sternum (in parts of the mice). In some mice the bioluminescence signal was diffuse at the end of the treatment period (Figure 55A). On day 12 of the treatment, the PS89 group showed a bioluminescence signal of $1.5x10^9$ total flux/area, the control group $1.3x10^9$ total flux/area, the combination group $1.2x10^9$ total flux/area, and the daunorubicin treated group $7.7x10^8$ total flux/area. On day 14 of the treatment, the daunorubicin treated group showed a bioluminescence signal of $1.0x10^9$ total flux/area, the PS89 group showed a bioluminescence signal of $9.4x10^9$ total flux/area (n=1), and the combination group $7.4x10^9$ total flux/area (n=1). The other mice of the daunorubicin and the combination group had to be euthanized before day 14 due to a decreasing general condition mainly caused by daunorubicin treatment. On day 17 the control group showed a bioluminescence signal of $8.0x10^9$ total flux/area and the PS89 treated group showed a bioluminescence signal of $2.4x10^9$ total flux/area (Figure 54 and Figure 55B). Unfortunately, comparison of leukemic tumor load between the different experimental groups was not possible after

an adequate treatment period. Furthermore, these data revealed the problematic side effects of multiple daunorubicin treatment in mice.

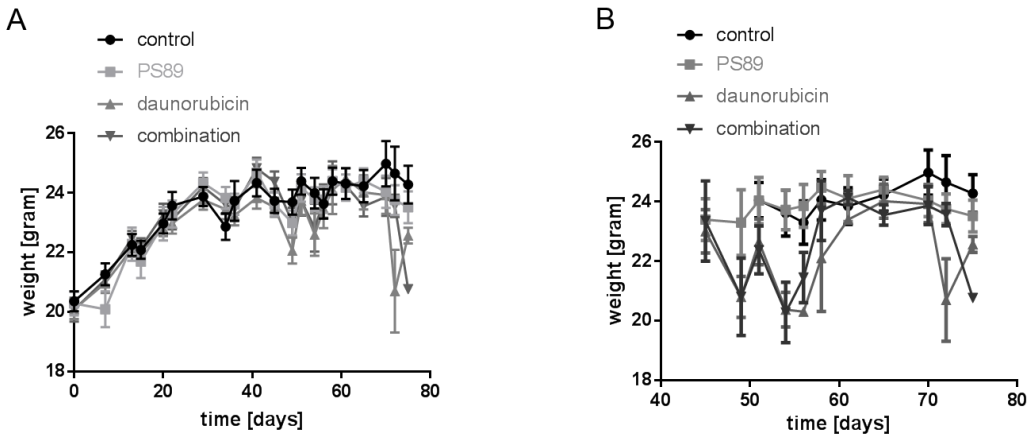

Figure 53: Body weight development over time. A) Weight of mice during the whole experimental period (day 0 – day 75). Represented is the mean ± SEM per group. **B)** Weight of mice during the treatment period. Represented is the mean ± S.E.M. per group.

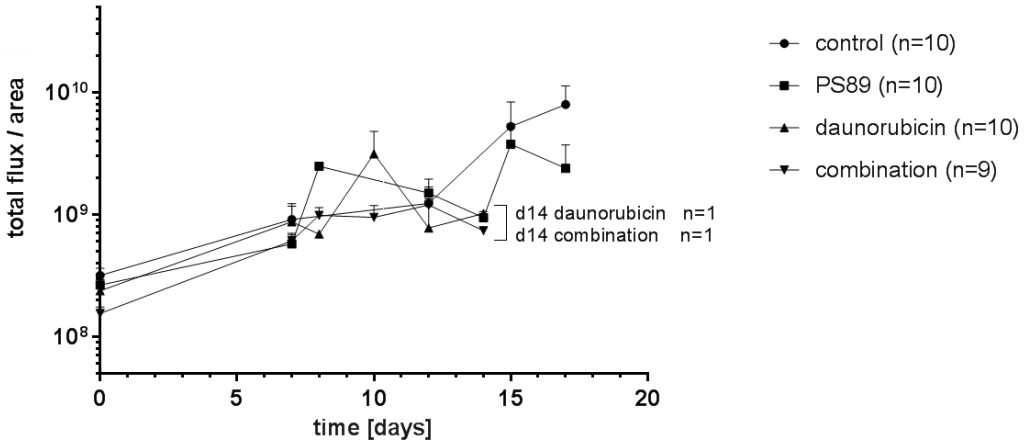

Figure 54: Results of bioluminescence imaging. Each curve represents the mean tumor load ± S.E.M. of nine or ten NSG mice per group. The treatment begins on day 0, when a bioluminescence signal of $1x10^8$ is reached. Analysis was done by Dr. Fabian Koczian.

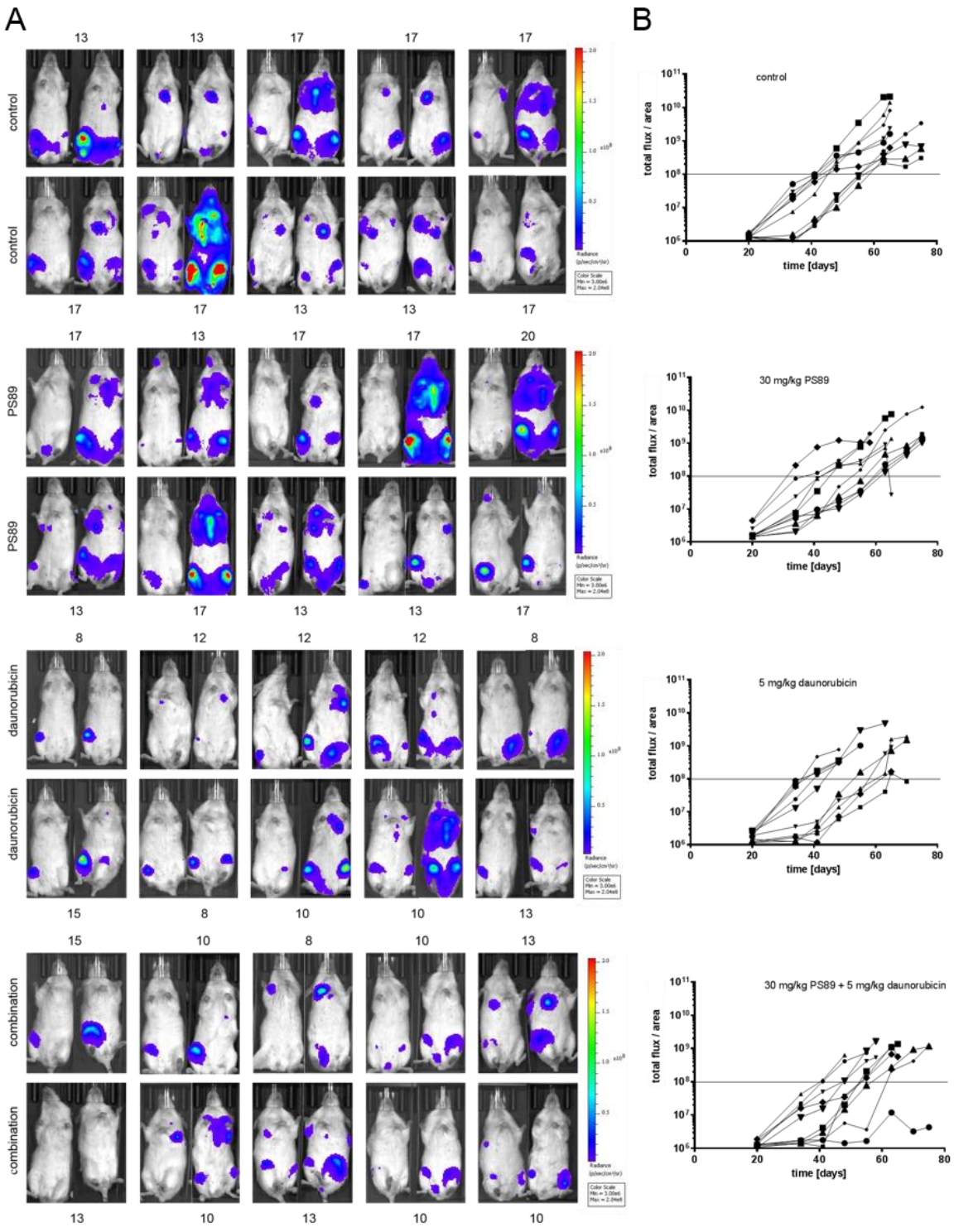

Figure 55: Bioluminescence imaging of AML-372 cells. A) Pictures of tumor burden in 40 NSG mice at the beginning of the treatment and prior to sacrifice. Days of treatment above or below the pictures. Pictures are taken in ventrodorsal position. **B)** Results of bioluminescence imaging. 10 mice per group were imaged once a week before treatment and twice a week during the treatment period. Treatment started when the bioluminescence signal reached $1x10^8$ total flux/area. Every curve represents the tumor load of one single NSG mouse. ROIs were drawn as whole-body ROIs.

6. Tumor metastasis evaluated in an orthotopic liver cancer model

To examine metastasis formation, we established an intrahepatic metastasis formation assay as described above for the first time in our lab. In a preliminary experiment two different murine liver cancer cell lines, Hep55c-luc and Ril175-luc (with two different numbers of cells), were tested. In every group one or two mice were treated with 10 mg/kg dinaciclib three times before cell injection (detailed conditions can be seen in Table 6 on page 34). All mice tolerated the surgery well and recovered completely within 24 hours afterwards. The surgical wound healed up without any complications. The body weight increased during the pretreatment (day -2 to day 0) but decreased after the surgery (day 0 to day 2). Two days after the surgery the body weight increased again until the end of the experiment (Figure 56). In the bioluminescence measurements tumor signals in the spleen and in the liver were detectable (Figure 57). Mice were imaged in ventrodorsal and dorsoventral position. As the Ril175-luc cells showed a reliable growth *in vivo* and dinaciclib was able to reduce tumor cell migration in this preliminary experiment, we decided to inject $1x10^6$ Ril175-luc cells in the main experiment.

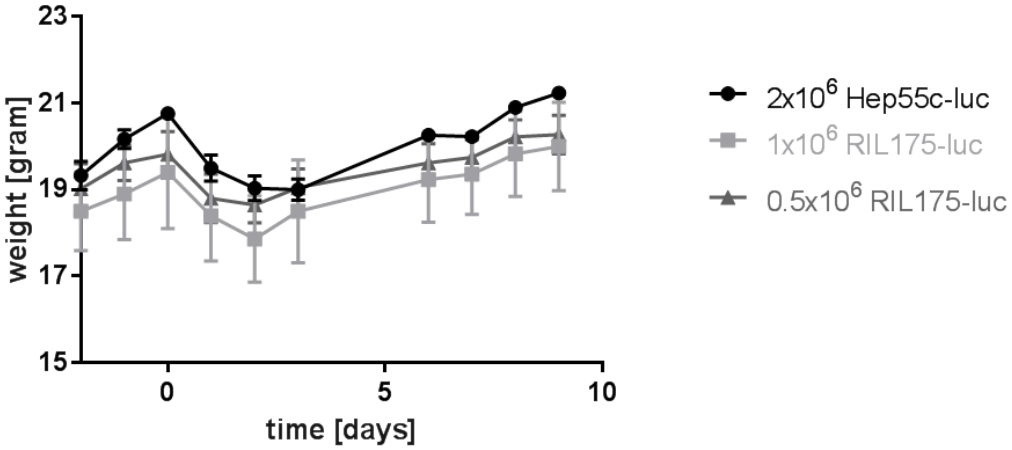

Figure 56: Body weight development. Weight of mice during the whole experimental period (day 0 – day 9). Represented is the mean ± S.E.M. of three or four mice per group.

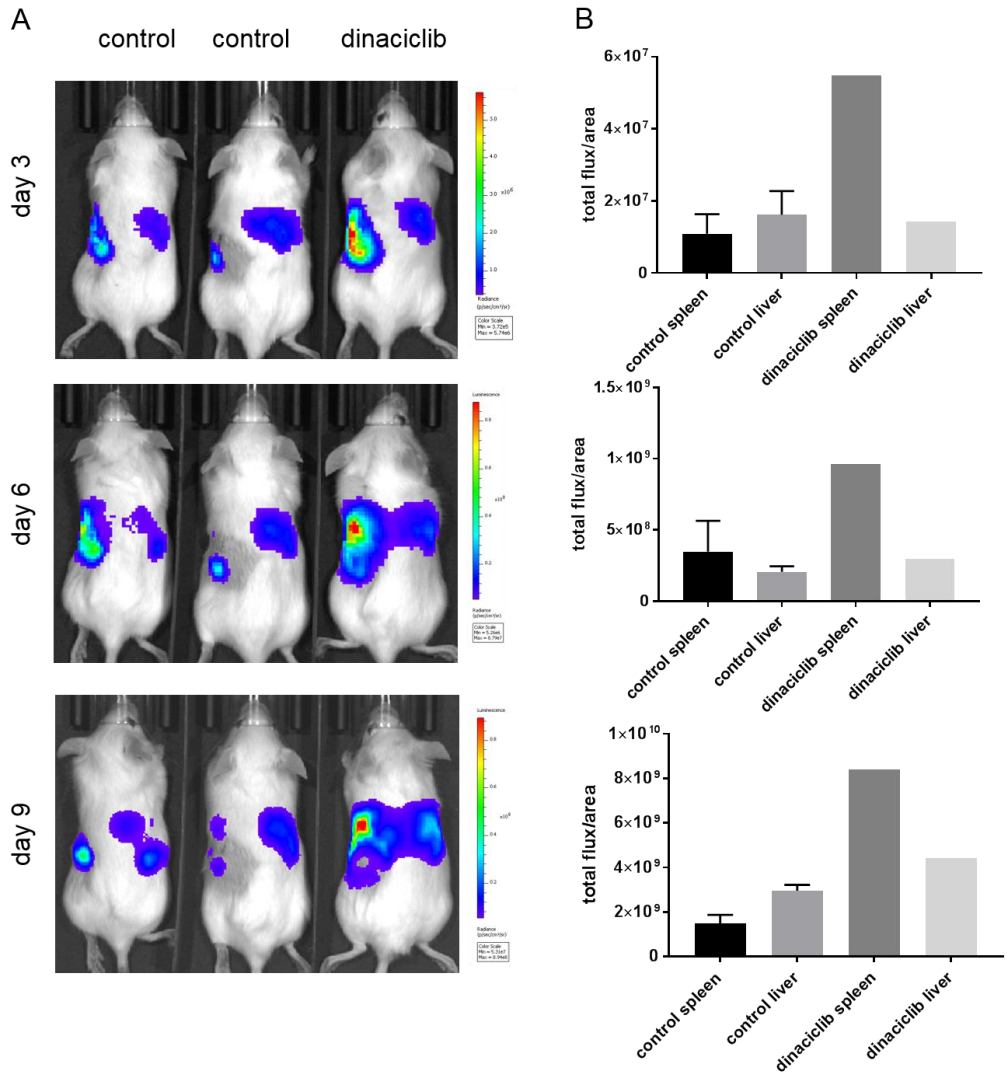

Figure 57: Bioluminescence imaging of preliminary intrahepatic metastasis model with 1x10^6 Ril175-luc cells injected into the spleen. A) Pictures of tumor cell migration in mice, taken on days 3, 6, and 9 in dorsoventral imaging position. **B)** Bioluminescence signals in total flux/area of spleen and liver on day 3, 6, and 9.

In the main experiment, inhibition of metastasis from spleen to liver was examined using 1x10^6 murine liver cancer cells Ril175-luc and pretreatment of mice with 10 mg/kg dinaciclib three times before cell injection. Ten mice served as control group and ten mice were pretreated with dinaciclib. The general condition during the pretreatment was without detectable abnormalities. After the surgery, the dinaciclib pretreated mice needed one day longer to recover than the control mice (Figure 58). Four mice of the dinaciclib treated group also opened their skin suture the day after the surgery, so that they had to be narcotized and the wound needed to be stitched again. In the dorsoventral imaging two split signals were detectable. The signal on the left side of the mouse was considered as spleen, the

signal on the right side was considered as liver. With this way of interpreting the signals, the bioluminescence signal on day 3 after the cell injection was higher in the spleen than in the liver in both groups. On day 6 the tumor signal of the dinaciclib treated group in the spleen was slightly higher ($3.6x10^8$ total flux/area) than in the liver ($3.0x10^8$ total flux/area), whereas the tumor signals in the control group were approximately equal in both organs (tumor signal in the spleen $2.5x10^8$ total flux/area, tumor signal in the liver $2.3x10^8$ total flux/area). This leads to the result, that tumor cell metastasis from spleen to liver could be reduced in comparison to the control group. However, unfortunately the *ex vivo* imaging of the solid organs showed a higher mean tumor signal in the liver than in the spleen on day 7 in both groups (Figure 59). Thus, we concluded that the combination of dinaciclib treatment, narcosis and surgery weakened the mice. Based on the *ex vivo* imaging, a reduction of intrahepatic metastasis formation by dinaciclib treatment was not detectable seven days after the cell injection.

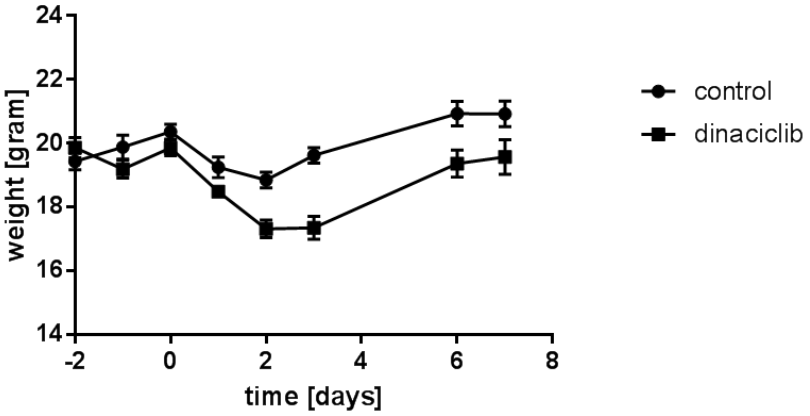

Figure 58: Body weight development. Weight of mice during the whole experimental period (day 0 – day 7). Represented is the mean ± S.E.M. of ten mice per group.

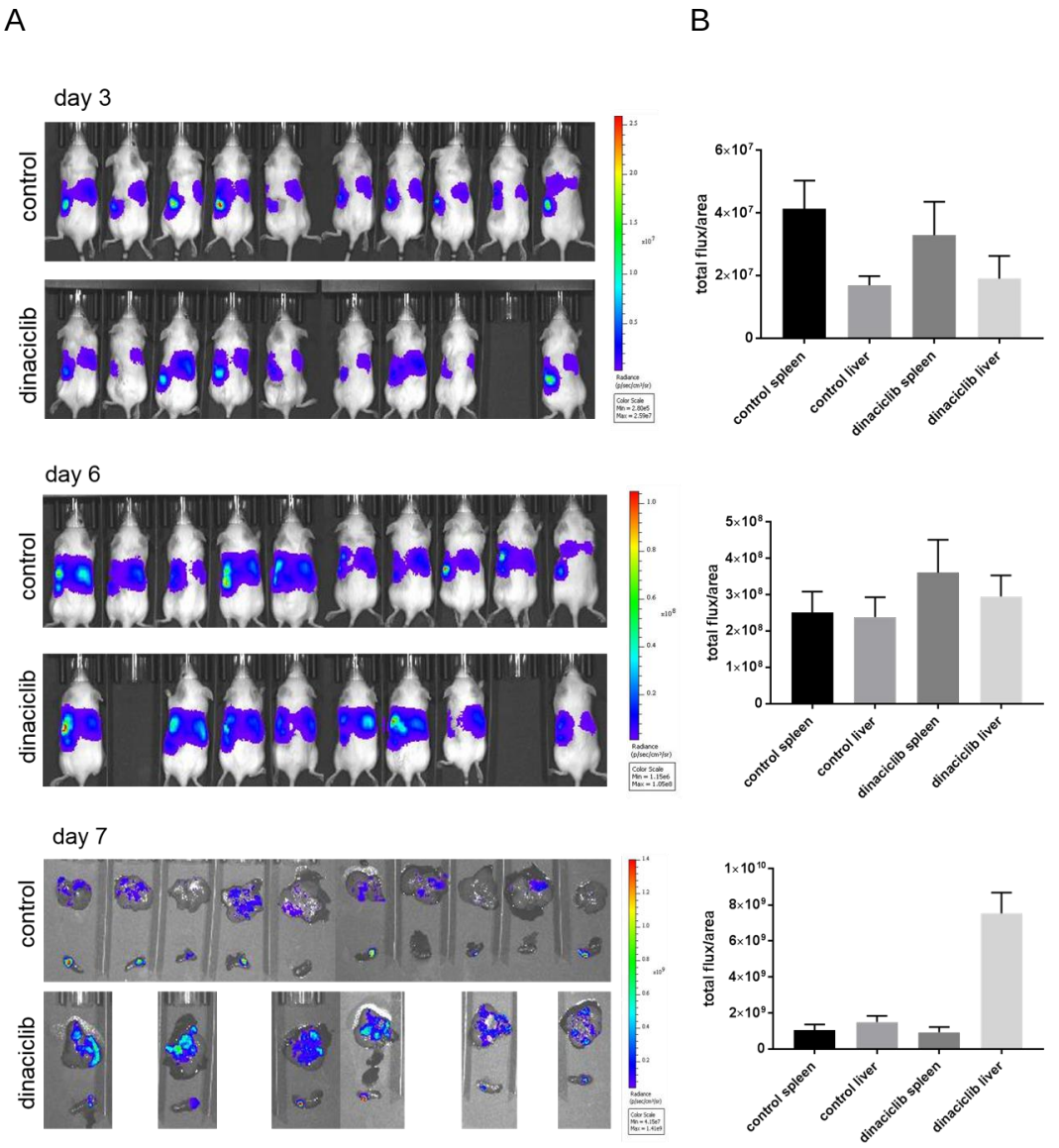

Figure 59: Bioluminescence signal measurement. A) Images in dorsoventral position of mice on day 3 and day 6, or imaging of the solid organs on day 7 after injection of 1x10^6 Ril175-luc cells into the spleen. **B)** Evaluation of tumor signals in the intrahepatic metastasis model on day 3, 6, and 7. Bioluminescence signals for spleen and liver shown in total flux/area. Represented is the mean ± S.E.M. per group.

IV. DISCUSSION

1. Neocarzilin A as a potential natural compound to impede tumor cell dissemination

Neocarzilin A showed promising *in vitro* effects against different cancer cell lines in our lab (data not published yet). Tested *in vivo* in a dissemination assay, neocarzilin A was able to reduce tumor dissemination of the murine breast cancer cell line 4T1-luc. In tumorigenesis, cancer cells have to detach from the primary tumor to reach the bloodstream. Consequently, they are transported to well circulated organs like the lung or the brain and are able to form metastases in these organs. Relating to solid tumors, these metastases are the cause of more than 90% of all cancer related deaths [106]. Tumor dissemination assays are simplified experiments to evaluate the behavior of tumor cells after they reach the bloodstream. In a dissemination assay the part of detachment and reaching the blood circulation is imitated by the intravenous injection of tumor cells. After getting into the lung, tumor cells attach there and begin to proliferate. Therefore, it is important to do bioluminescence imaging in a preferably short interval after the cell injection, to minimize the influence of tumor proliferation and to gain insights into the inhibiting effects on cell dissemination. In case of neocarzilin A it would be an interesting option to implement bioluminescence imaging already in shorter time after the cell injection to evaluate the effects on tumor cell dissemination less influenced by tumor cell proliferation or apoptosis. For further research, investigation of effects on tumor growth would also be of interest. As 10 mg/kg neocarzilin A were well tolerated during multiple injections a long-term treatment with neocarzilin A would also be feasible.

2. Two-pore channel inhibition as a novel strategy to reduce tumor cell dissemination

One team in our lab is investigating the roles of the endolysosomal system in development and treatment of cancer. The endolysosmal system of a cell plays a central role as cellular recycling center as well as central regulator of tumor growth and metastasis formation [107]. Furthermore, lysosomes are important for drug resistance in cancer cells and the autophagy-lysosome pathway [108]. In a recent review by Grimm et al. it is shown that there is a multitude of links between cancer and lysosomal function, but the exact mechanism how lysosomes influence tumorigenesis and cancer progression is still unclear [109]. Two-pore channels are endolysosomal membrane proteins with essential roles in endolysosomal trafficking and the autophagy-lysosome pathway. Moreover, they are part of the superfamily of voltage-gated ion channels. Two-pore channels exist in two subtypes, of which TPC1 is predominantly expressed on early endosomal membranes, whereas TPC2 is mainly found in lysosomal membranes [110]. We were able to show that pharmacological inhibition by Ned-19 as well as silencing TPC2 with siRNA reduced dissemination of murine breast cancer cells *in vivo* [55]. Moreover, loss of TPC2 function in murine liver cancer cells with TPC2 knock-out diminished tumor dissemination significantly. For future investigations, the influence of TPC2 on tumor growth *in vivo* would be of interest. Moreover, newly developed natural compounds, which have the same promising target as the experimental compound Ned-19, will be tested on their potential to inhibit tumor cell dissemination and tumor growth *in vivo*.

3. Cdk5 inhibition as a new approach against liver cancer

Cdk5 is a member of the cyclin-dependent kinase family, which are serine/threonine kinases playing an important role in the neuronal system, i.e. in the central nervous system as well as in axon guidance and synaptic function. Cdk5 contributes to neurodegenerative diseases like Alzheimer`s disease or amyotrophic lateral sclerosis [111]. In addition, Cdk5 turned out to have importance in non-neuronal tissues, especially in cancer cells [112-114]. Inhibition of Cdk5 is also a promising target in the therapy of hepatocellular carcinoma [115]. Recent findings in our lab showed that Cdk5 inhibition reduced HCC cell migration *in vitro* (data submitted). In a tumor dissemination experiment we were able to show a reduced dissemination of murine liver cancer cells Ril175-luc by pharmacologic inhibition of Cdk5 via dinaciclib treatment *in vivo*. In this experiment the Cdk5 inhibitor dinaciclib was injected three times intraperitoneally in a dose of 10 mg/kg into the mice, because of impairing side effects with higher dosages of dinaciclib observed in dose finding tests. Equally Cdk5 knockdown by the CRISPR/Cas9 system was able to reduce dissemination of Ril175-luc cells *in vivo*. Thus, inhibition of Cdk5 might be a promising tool in HCC therapy. Moreover, as dinaciclib is already clinically approved, it might be a treatment option also for HCC. These dissemination models represent a simple method to monitor effects on tumor cells *in vivo*. A more realistic approach to investigate liver cancer is represented by our intrahepatic metastasis model. Conducting this experiment for the first time in our lab, we were able to explore tumor cell migration from the spleen to the liver by bioluminescence imaging. Unfortunately, this approach led to two problems in the experimental setup. On the one hand the combination of dinaciclib treatment and burden of the surgery weakened the mice. Consequently, more postoperative problems appeared in the dinaciclib treated group. On the other hand, we had to recognize the risk that bioluminescence signals of spleen and liver might overlap and impede a correct evaluation of the tumor signals. Therefore, there is the need of imaging the solid organs as a control measurement in the end of the experiment. To overcome the problem of an overlapping primary tumor in the spleen and metastasis in

the liver, Rajendran et al. described a split-spleen approach, where one part of the spleen that includes the primary tumor is resected ten minutes after the cell injection. The residual part of the spleen is able to fulfill immune protective properties, but will not impair the possibility to appropriate the bioluminescence signal to the corresponding organ [116]. In future experiments it would be of interest if Cdk5 knockout in murine liver cancer cells could reduce the cell migration from spleen to liver in an orthotopic liver cancer model.

4. Sorafenib resistance in liver cancer cells evaluated in murine tumor models

One major field of research in our lab focuses on hepatocellular carcinoma (HCC). Different general challenges of chemotherapy are represented by treatment problems of HCC. Mostly diagnosed in advanced stage, sorafenib is the only approved treatment option [117]. Besides wearing side effects as hand-foot syndrome, diarrhea and hypertension, HCC shows acquired sorafenib resistance and rebound growth phenomena after sorafenib withdrawal [79, 118]. Moreover, patient`s survival benefit of less than three months with a median overall survival of 10.7 months compared to 7.9 months in the placebo group is still poor [118]. Therefore, one part of this thesis was the implementation of suitable mouse models for HCC and the evaluation of new treatment options. We showed that 20 mg/kg sorafenib administered every two days is sufficient to reduce subcutaneous growth of HUH7 wildtype tumors in SCID mice. Moreover, we described a phenotypic totally unequal tumor growth of different HUH7 cells *in vivo*. Whereas HUH7 wildtype tumors grew encapsulated and subcutaneously relocatable, HUH7 resistant cells showed an extremely invasive growth into deeper muscle layers. After tumor resection HUH7 wildtype tumors appeared well vascularized, whereas the resistant cell lines formed exsanguinous tumors. These findings led us to the presumption that vascularization might be altered in sorafenib resistant HUH7 cells. A reduced vascularization would on the one hand lead to a possibly reduced availability of chemotherapeutic drugs in these tumors, on the other hand the tumor volume measured via a caliper might be underestimated compared to HUH7 wildtype tumors with a

higher density of vasculature. In future experiments, differences in angiogenesis of HUH7 cell lines will be examined. Due to the very invasive tumor growth of HUH7 resistant cells, tumor measurement via a caliper was vague. Moreover, the different cell size of HUH7 wildtype and HUH7 sorafenib resistant cells could not be considered in these measurements. Therefore, we investigated a new experimental setup in which HUH7 luciferase tagged cells were injected subcutaneously in order to build tumors. Thereby bioluminescence measurement of the tumor signal was feasible. Thus, evaluation of tumor growth was more precise, examiner independent, and comparison of tumor growth was possible in short times after the cell injection. In this experimental setup we were also able to show that the experimental natural compound CA1 reduced tumor growth of HUH7 sorafenib resistant cells *in vivo*.

5. Patient-derived xenograft cells in a mouse model for acute myeloid leukemia

In this part of the thesis we implemented an *in vivo* model for acute myeloid leukemia in our lab. Therefore, we worked with patient-derived xenograft (PDX) cells. In contrast to tumor cell lines, which often show altered functional characteristics due to their longtime cultivation, PDX cells are an option more closely related to the clinics [20]. As PDX cells showed a reliable tumor growth in NSG mice, these severely immunocompromised mice were used in this project. Due to their immunodeficiency, strict barriers and aseptic handling of the mice was important during the whole experiment [119]. In our leukemia model we had to deal with an insufficient tumor growth after the first intravenous cell injection. Therefore, we had to inject tumor cells for a second time, which also led to an inhomogeneous tumor growth. Bioluminescence signal was detectable in the hematopoietic bones primarily in the femora, followed by humeri and in parts of the mice also the sternum and the pelvis. Moreover complicating, mice treated with the anthracycline DaunoXome® did not tolerate more than three intravenous injections. As anthracyclines in general are related to cardiotoxic effects [120, 121], the treatment period of mice treated with DaunoXome® or a combination consisting of DaunoXome® and our compound PS89 was

limited to approximately ten days. Thus, we were not able to compare the tumor load between all groups after a longer treatment period. We could show that intraperitoneal injection of PS89 did not harm the mice for a longer period of time. Moreover, PS89 was detectable in the blood plasma 15 minutes after intraperitoneal injection. For further experiments, different changes in the experimental setups might be possible. Based on *in vitro* data it would be a promising approach to combine PS89 with the chemotherapeutic agent etoposide, as there are no such negative side effects known as for anthracyclines. Furthermore, a clinically more relevant setup would consist in waiting for a very high tumor load, comparable with human patients at the timepoint of being diagnosed with acute myeloid leukemia. Then a short treatment period should start, with just one anthracycline treatment in large dose, combined with PS89 treatment. In our pharmacokinetic study, PS89 was not detectable any more 15 minutes after intravenous injection and 120 minutes after intraperitoneal injection. As we were only able to detect PS89 without further modification, potentially effective metabolites of PS89 were unconsidered in these measurements. For further investigation on PS89 it would be of interest, if effective metabolites of PS89 exist and could be detectable in the blood plasma of the mice. With these insights PS89 treatment could be planned more specifically.

V. SUMMARY

Cancer is one of the biggest health problems in our days. Due to growth and aging of the human population as well as multiple, omnipresent risk factors the number of cancer cases and cancer related deaths is still increasing. As current cancer survival rates are not satisfying and available treatment options have to deal with wearing side effects, there is necessity for novel therapeutic options and improvement of established therapies. Therefore, our lab is investigating the anti-cancer potential of natural and synthetic compounds to find out new chances to fight cancer.

In this project, compounds with promising *in vitro* findings were tested in murine tumor models to elucidate their potential *in vivo*. The aim of this thesis was the *in vivo* evaluation of auspicious experimental compounds in murine tumor models.

For a detailed *in vivo* characterization of our experimental compounds, they were tested in different experimental setups. We started with dose finding tests to figure out well tolerable dosages for *in vivo* treatments and pharmacokinetic studies to characterize compounds in more detail. Within this thesis we found adequate *in vivo* dosages for our compounds and their adjunction with approved drugs.

Concerning novel experimental approaches, it was part of this thesis to implement new experimental setups. Therefore, preliminary subcutaneous growth experiments with murine breast cancer cells 4T1-luc and rat hepatoma cells McA-RH7777 were conducted. Moreover, different modifications in the setup of dissemination assays were made, such as bioluminescence imaging of the murine liver cancer cell line Ril175-luc and imaging in short intervals after the cell injection, to examine essential procedures in the first hours after cell injection.

In dissemination assays we showed that the natural compound neocarzilin A reduced tumor cell dissemination of murine breast cancer cells 4T1-luc with a dosage of 10 mg/kg. Further, we showed that pharmacological inhibition of the two-pore channel TPC2 by Ned-19 or silencing TPC2 reduced tumor cell dissemination of 4T1-luc cells. Furthermore, both pharmacological inhibition by 10 mg/kg dinaciclib and

knockout of the cyclin dependent kinase Cdk5 via the CRISPR/Cas method reduced tumor cell dissemination of murine liver cancer cells Ril175-luc. To examine the influence of the Cdk5 inhibitor dinaciclib on metastasis formation, an intrahepatic metastasis model was conducted for the first time in our lab. Unfortunately, due to the wearing combination of dinaciclib treatment and surgery as well as problems by correlating the bioluminescence signal to the correct organ during the experiment, we were not able to show a reduction in metastasis formation under dinaciclib treatment.

In ectopic tumor models we focused on the investigation of hepatocellular carcinoma using different human HUH7 cell lines. Besides pharmacological inhibition of HUH7 wildtype tumor growth by 20 mg/kg sorafenib, we showed interesting differences in the phenotype of HUH7 wildtype and HUH7 sorafenib resistant tumors. Whereas HUH7 wildtype tumors grew subcutaneously relocatable and well vascularized, HUH7 sorafenib resistant tumors grew invasive and less vascularized. Moreover, we implemented a new bioluminescence imaging setup for subcutaneous HUH7 tumors using the IVIS® spectrum. Therefore, we were able to show that the experimental natural compound CA1 reduced subcutaneous tumor growth of HUH7 sorafenib resistant cells.

Within a leukemia project with patient derived xenograft (PDX) cells AML-372 we conducted an *in vivo* model for acute myeloid leukemia. With our experimental compound PS89 we tried to improve daunorubicin treatment, which is an approved treatment option for acute myeloid leukemia in humans. Unfortunately, due to less tolerance of daunorubicin treatment in mice, we were not able to show a positive effect of combination of PS89 and daunorubicin *in vivo*.

In conclusion, this thesis elucidated the anti-cancer potential of new natural and synthetic compounds and established murine tumor models for further investigations on the antitumoral activity of promising compounds.

VI. ZUSAMMENFASSUNG

Murine *in vivo* Tumormodelle zur Erforschung des anticancerogenen Potentials von Naturstoffen und synthetischen Compounds

Krebserkrankungen stellen eines der größten Gesundheitsprobleme unserer Zeit dar. Aufgrund des Bevölkerungswachstums und einer immer älter werdenden Gesellschaft, sowie einer Vielzahl omnipräsenter Risikofaktoren steigt die Anzahl der Krebserkrankungen und der damit verbundenen Todesfälle weiter an. Da momentane Überlebensraten nicht zufriedenstellend sind und verfügbare Behandlungsoptionen mit oftmals belastenden Nebenwirkungen zu kämpfen haben, besteht ein großer Bedarf an neuen Behandlungsmöglichkeiten und an Verbesserungen für etablierte Therapien. Daher erforscht unser Labor das anticancerogene Potential von Naturstoffen und synthetischen Wirkstoffen, um neue Möglichkeiten im Kampf gegen Krebserkrankungen zu finden.

In diesem Projekt werden Wirkstoffe mit vielversprechenden *in vitro* Ergebnissen in murinen Tumormodellen getestet, um ihr Potential *in vivo* aufzuklären. Das Ziel dieser Arbeit war die *in vivo* Evaluation von vielversprechenden experimentellen Compounds in murinen Tumormodellen.

Für eine detaillierte *in vivo* Charakterisierung wurden unsere experimentellen Compounds in verschiedenen Versuchen getestet. Zu Beginn standen Dosisfindungstests, um eine gut tolerierte Dosierung für *in vivo* Behandlungen herauszufinden. Die Pharmakokinetik wurde untersucht, um Wirkstoffe noch genauer charakterisieren zu können. Im Rahmen dieser Arbeit konnten wir für unsere Compounds und für Kombinationstherapien mit zugelassenen Medikamenten adäquate Dosierungen finden.

In Bezug auf neue experimentelle Herangehensweisen war es Teil dieser Arbeit einen neuen Versuchsaufbau für verschiedene Experimente zu verwirklichen. Es wurden Vorversuche zum subkutanen Tumorwachstum mit der murinen Mammakarzinomzelllinie 4T1-luc sowie mit der Rattenhepatomzelllinie McA-RH7777 durchgeführt. Des Weiteren wurden verschiedene Änderungen im Versuchsaufbau der Disseminationsversuche

durchgeführt. Es wurde die Biolumineszenzmessung der murinen Leberkrebszelllinie Ril175-luc etabliert, sowie ein Versuchsaufbau zur Messung der Biolumineszenz in kurzen Zeitintervallen nach der Zellinjektion entwickelt, um essentielle Vorgänge in den ersten Stunden nach der Tumorzellinjektion untersuchen zu können.

In Disseminationsversuchen konnten wir zeigen, dass der Naturstoff Neocarzilin A mit einer Dosierung von 10 mg/kg die Tumorzelldissemination der murinen Mammakarzinomzellen 4T1-luc reduziert. Des Weiteren konnten wir zeigen, dass sowohl pharmakologische Inhibierung durch Ned-19 sowie Silencing des „two-pore“ Kanals TPC2 die Dissemination von 4T1-luc Zellen reduziert. Überdies hinaus reduziert sowohl die pharmakologische Inhibierung durch 10 mg/kg Dinaciclib als auch der Knock-out der cyklinabhängigen Kinase Cdk5 mittels der CRISPR/Cas Methode die Tumorzelldissemination von murinen Leberkarzinomzellen Ril175-luc. Um den Einfluss des Cdk5 Inhibitors Dinaciclib auf die Metastasenbildung zu untersuchen, führten wir im Rahmen dieser Arbeit zum ersten Mal in unserem Labor ein intrahepatisches Metastasierungsmodel durch. Aufgrund der belastenden Kombination aus Behandlung mit Dinaciclib und Operation, sowie Problemen bei der korrekten Zuordnung des Biolumineszenzsignals zum jeweiligen Organ während des Experiments, war es leider nicht möglich eine Reduktion der Metastasierung durch Dinaciclib zu zeigen.

In ektopischen Tumormodellen fokussierten wir uns auf die Erforschung des hepatozellulären Karzinoms, indem wir verschiedene humane HUH7 Zelllinien verwendeten. Neben einer pharmakologischen Inhibierung des Wachstums von HUH7 Wildtyptumoren durch 20 mg/kg Sorafenib, konnten wir interessante Unterschiede im Phänotyp zwischen HUH7 Wildtyptumoren und HUH7 Tumoren mit Sorafenibresistenz feststellen. Während HUH7 Wildtyptumore subkutan verschieblich und gut vaskularisiert wuchsen, zeigten HUH7 Tumore mit Sorafenibresistenz ein invasives und scheinbar weniger gut vaskularisiertes Wachstum. Zudem erstellten und realisierten wir einen neuen Versuchsaufbau, um die Biolumineszenz von subkutanen HUH7 Tumoren mittels des IVIS® spectrum zu messen. Hierbei war es uns möglich zu zeigen, dass der experimentelle Naturstoff CA1 das subkutane Wachstum von HUH7

Tumoren mit Sorafenibresistenz reduziert.

Im Rahmen eines Leukämieprojektes mit den Patientenxenograftzellen AML-372 führten wir ein *in vivo* Model zur akuten myeloischen Leukämie durch. Mit unserem experimentellen Compound PS89 versuchten wir eine Behandlung mit Daunorubicin, welche für die akute myeloide Leukämie eine zugelassene Behandlungsmethode darstellt, zu verbessern. Die Behandlung mit Daunorubicin wurde von den Mäusen schlecht toleriert, wodurch wir leider keinen positiven Effekt durch die Kombination von PS89 mit Daunorubicin *in vivo* zeigen konnten.

Zusammenfassend zeigt diese Arbeit das anticancerogene Potential von Naturstoffen und synthetischen Compounds auf und etabliert murine Tumormodelle für die weitere Forschung an der antitumoralen Aktivität vielversprechender Wirkstoffe.

VII. REFERENCES

1. Torre, L.A., et al., *Global cancer statistics, 2012.* CA Cancer J Clin, 2015. **65**(2): p. 87-108.

2. https://www.cancer.org/content/dam/cancer-org/research/cancer-facts-and-statistics/global-cancer-facts-and-figures/global-cancer-facts-and-figures-3rd-edition.pdf.

3. Arnold, M., et al., *Global burden of cancer attributable to high body-mass index in 2012: a population-based study.* Lancet Oncol, 2015. **16**(1): p. 36-46.

4. Lippi, G., C. Mattiuzzi, and G. Cervellin, *Meat consumption and cancer risk: a critical review of published meta-analyses.* Crit Rev Oncol Hematol, 2016. **97**: p. 1-14.

5. Parkin, D.M., *The global health burden of infection-associated cancers in the year 2002.* Int J Cancer, 2006. **118**(12): p. 3030-44.

6. Turati, F., et al., *Alcohol and liver cancer: a systematic review and meta-analysis of prospective studies.* Ann Oncol, 2014. **25**(8): p. 1526-35.

7. Collaborative Group on Hormonal Factors in Breast Cancer, *Breast cancer and hormonal contraceptives: collaborative reanalysis of individual data on 53 297 women with breast cancer and 100 239 women without breast cancer from 54 epidemiological studies.* Lancet, 1996. **347**(9017): p. 1713-27.

8. Sergentanis, T.N., et al., *Risk for childhood leukemia associated with maternal and paternal age.* Eur J Epidemiol, 2015. **30**(12): p. 1229-61.

9. Jansen, L., et al., *Recent cancer survival in Germany: an analysis of common and less common cancers.* Int J Cancer, 2015. **136**(11): p. 2649-

58.

10. Frey, H.H., *Lehrbuch der Pharmakologie und Toxikologie für die Veterinärmedizin*. 2002: Enke.

11. Mak, I.W.Y., N. Evaniew, and M. Ghert, *Lost in translation: animal models and clinical trials in cancer treatment.* American Journal of Translational Research, 2014. **6**(2): p. 114-118.

12. Matthews, R.A., *Medical progress depends on animal models - doesn't it?* Journal of the Royal Society of Medicine, 2008. **101**(2): p. 95-98.

13. https://www.bmel.de/SharedDocs/Downloads/Tier/Tierschutz/Versuchstierdaten2015.pdf?__blob=publicationFile.

14. Cheon, D.J. and S. Orsulic, *Mouse models of cancer.* Annu Rev Pathol, 2011. **6**: p. 95-119.

15. Bryda, E.C., *The Mighty Mouse: The Impact of Rodents on Advances in Biomedical Research.* Missouri medicine, 2013. **110**(3): p. 207-211.

16. Fantozzi, A. and G. Christofori, *Mouse models of breast cancer metastasis.* Breast Cancer Res, 2006. **8**(4): p. 212.

17. He, L., et al., *Mouse models of liver cancer: Progress and recommendations.* Oncotarget, 2015. **6**(27): p. 23306-22.

18. Rashid, O.M. and K. Takabe, *Animal models for exploring the pharmacokinetics of breast cancer therapies.* Expert Opin Drug Metab Toxicol, 2015. **11**(2): p. 221-30.

19. Ito, R., et al., *Current advances in humanized mouse models.* Cell Mol Immunol, 2012. **9**(3): p. 208-14.

20. Vick, B., et al., *An advanced preclinical mouse model for acute myeloid leukemia using patients' cells of various genetic subgroups and in vivo bioluminescence imaging.* PLoS One, 2015. **10**(3): p. e0120925.

21. Waterston, R.H., et al., *Initial sequencing and comparative analysis of the mouse genome.* Nature, 2002. **420**(6915): p. 520-62.

22. Zuber, J., et al., *Mouse models of human AML accurately predict chemotherapy response.* Genes Dev, 2009. **23**(7): p. 877-89.

23. https://www.gesetze-im-internet.de/tierschg/TierSchG.pdf.

24. https://www.cancer.org/treatment/treatments-and-side-effects/treatment-types.html.

25. Bentzen, S.M., *Preventing or reducing late side effects of radiation therapy: radiobiology meets molecular pathology.* Nature Reviews Cancer, 2006. **6**: p. 702.

26. Al-Ghazal, S.K., L. Fallowfield, and R.W. Blamey, *Comparison of psychological aspects and patient satisfaction following breast conserving surgery, simple mastectomy and breast reconstruction.* European Journal of Cancer, 2000. **36**(15): p. 1938-1943.

27. Hansel, T.T., et al., *The safety and side effects of monoclonal antibodies.* Nat Rev Drug Discov, 2010. **9**(4): p. 325-38.

28. Coates, A., et al., *On the receiving end—patient perception of the side-effects of cancer chemotherapy.* European Journal of Cancer and Clinical Oncology, 1983. **19**(2): p. 203-208.

29. Longley, D.B. and P.G. Johnston, *Molecular mechanisms of drug resistance.* J Pathol, 2005. **205**(2): p. 275-92.

30. Gatti, L. and F. Zunino, *Overview of tumor cell chemoresistance mechanisms.* Methods Mol Med, 2005. **111**: p. 127-48.

31. Harvey, A.L., *Natural products in drug discovery.* Drug Discov Today, 2008. **13**(19-20): p. 894-901.

32. Newman, D.J. and G.M. Cragg, *Natural Products as Sources of New Drugs from 1981 to 2014.* J Nat Prod, 2016. **79**(3): p. 629-61.

33. Clark, A.M., *Natural Products as a Resource for New Drugs.* Pharmaceutical Research, 1996. **13**(8): p. 1133-1141.

34. Crane, E.A. and K. Gademann, *Capturing Biological Activity in Natural Product Fragments by Chemical Synthesis.* Angew Chem Int Ed Engl, 2016. **55**(12): p. 3882-902.

35. Otsuka, M., et al., *Cloning, sequencing, and functional analysis of an iterative type I polyketide synthase gene cluster for biosynthesis of the antitumor chlorinated polyenone neocarzilin in "Streptomyces carzinostaticus".* Antimicrob Agents Chemother, 2004. **48**(9): p. 3468-76.

36. Nozoe, S., et al., *Neocarzilins A and B, Novel Polyenones from Streptomyces Carzinostaticus.* Tetrahedron Letters, 1992. **33**(49): p. 7547-7550.

37. Tianqin, G., C. Chunlei, and W. Jingjing, *Synergistic Anti-glioma Effects in vitro and in vivo of Enediyne Antibiotic Neocarzinostatin and Paclitaxel via Enhanced Growth Delay and Apoptosis-Induction.* Biol Pharm Bull, 2016. **39**(10): p. 1623-1630.

38. Nozoe, S., et al., *Synthesis of neocarzilin A: An absolute streochemistry.* Tetrahedron Letters, 1992. **33**(49): p. 7551-7552.

39. Bubb, M.R., et al., *Effects of jasplakinolide on the kinetics of actin polymerization. An explanation for certain in vivo observations.* J Biol Chem, 2000. **275**(7): p. 5163-70.

40. Bubb, M.R., et al., *Jasplakinolide, a cytotoxic natural product, induces actin polymerization and competitively inhibits the binding of phalloidin to F-actin.* J Biol Chem, 1994. **269**(21): p. 14869-71.

41. Allingham, J.S., V.A. Klenchin, and I. Rayment, *Actin-targeting natural products: structures, properties and mechanisms of action.* Cellular and Molecular Life Sciences CMLS, 2006. **63**(18): p. 2119-2134.

42. Scott, V.R., R. Boehme, and T.R. Matthews, *New class of antifungal agents: jasplakinolide, a cyclodepsipeptide from the marine sponge, Jaspis species.* Antimicrob Agents Chemother, 1988. **32**(8): p. 1154-7.

43. Senderowicz, A.M., et al., *Jasplakinolide's inhibition of the growth of prostate carcinoma cells in vitro with disruption of the actin cytoskeleton.* J Natl Cancer Inst, 1995. **87**(1): p. 46-51.

44. Takeuchi, H., et al., *Jasplakinolide: interaction with radiation and hyperthermia in human prostate carcinoma and Lewis lung carcinoma.* Cancer Chemotherapy and Pharmacology, 1998. **42**(6): p. 491-496.

45. Trendowski, M., et al., *Tolerated doses in zebrafish of cytochalasins and jasplakinolide for comparison with tolerated doses in mice in the evaluation of pre-clinical activity of microfilament-directed agents in tumor model systems in vivo. In vivo*, 2014. **28**(6): p. 1021-31.

46. Helal, M.A., S. Khalifa, and S. Ahmed, *Differential binding of latrunculins to G-actin: a molecular dynamics study.* J Chem Inf Model, 2013. **53**(9): p. 2369-75.

47. Spector, I., et al., *Latrunculins: novel marine toxins that disrupt microfilament organization in cultured cells.* Science, 1983. **219**(4584): p. 493-5.

48. Coue, M., et al., *Inhibition of actin polymerization by latrunculin A.* FEBS Lett, 1987. **213**(2): p. 316-8.

49. Spector, I., et al., *Latrunculins--novel marine macrolides that disrupt microfilament organization and affect cell growth: I. Comparison with cytochalasin D.* Cell Motil Cytoskeleton, 1989. **13**(3): p. 127-44.

50. Konishi, H., et al., *Latrunculin a has a strong anticancer effect in a peritoneal dissemination model of human gastric cancer in mice.* Anticancer Res, 2009. **29**(6): p. 2091-7.

51. Macarron, R., et al., *Impact of high-throughput screening in biomedical research.* Nat Rev Drug Discov, 2011. **10**(3): p. 188-95.

52. Naylor, E., et al., *Identification of a chemical probe for NAADP by virtual screening.* Nat Chem Biol, 2009. **5**(4): p. 220-6.

53. Genazzani, A.A. and A. Galione, *A Ca2+ release mechanism gated by the novel pyridine nucleotide, NAADP.* Trends in Pharmacological Sciences, 1997. **18**(4): p. 108-110.

54. Coxon, C.H., et al., *NAADP regulates human platelet function.* Biochem J, 2012. **441**(1): p. 435-42.

55. Nguyen, O.N., et al., *Two-Pore Channel Function Is Crucial for the Migration of Invasive Cancer Cells.* Cancer Res, 2017. **77**(6): p. 1427-1438.

56. Hood, J.D. and D.A. Cheresh, *Role of integrins in cell invasion and migration.* Nat Rev Cancer, 2002. **2**(2): p. 91-100.

57. Favia, A., et al., *NAADP-Dependent Ca(2+) Signaling Controls Melanoma Progression, Metastatic Dissemination and Neoangiogenesis.* Sci Rep, 2016. **6**: p. 18925.

58. https://www.tocris.com/products/trans-ned-19_3954#product-citations.

59. Eirich, J., et al., *A small molecule inhibits protein disulfide isomerase and triggers the chemosensitization of cancer cells.* Angew Chem Int Ed Engl, 2014. **53**(47): p. 12960-5.

60. Kim, I., W. Xu, and J.C. Reed, *Cell death and endoplasmic reticulum stress: disease relevance and therapeutic opportunities.* Nat Rev Drug Discov, 2008. **7**(12): p. 1013-30.

61. Paruch, K., et al., *Discovery of Dinaciclib (SCH 727965): A Potent and Selective Inhibitor of Cyclin-Dependent Kinases.* ACS Med Chem Lett, 2010. **1**(5): p. 204-8.

62. Parry, D., et al., *Dinaciclib (SCH 727965), a novel and potent cyclin-dependent kinase inhibitor.* Mol Cancer Ther, 2010. **9**(8): p. 2344-53.

63. Nguyen, T. and S. Grant, *DINACICLIB (SCH727965) INHIBITS THE UNFOLDED PROTEIN RESPONSE (UPR) THROUGH A CDK1 AND CDK5-DEPENDENT MECHANISM.* Molecular cancer therapeutics, 2014. **13**(3): p. 662-674.

64. Rajput, S., et al., *Inhibition of cyclin dependent kinase 9 by dinaciclib suppresses cyclin B1 expression and tumor growth in triple negative breast cancer.* Oncotarget, 2016. **7**(35): p. 56864-56875.

65. Baker, A., et al., *The CDK9 Inhibitor Dinaciclib Exerts Potent Apoptotic and Antitumor Effects in Preclinical Models of MLL-Rearranged*

Acute Myeloid Leukemia. Cancer Res, 2016. **76**(5): p. 1158-69.

66. Desai, B.M., et al., *The Anti-Melanoma Activity of Dinaciclib, a Cyclin-Dependent Kinase Inhibitor, Is Dependent on p53 Signaling.* PLoS ONE, 2013. **8**(3): p. e59588.

67. Feldmann, G., et al., *Cyclin-dependent kinase inhibitor Dinaciclib (SCH727965) inhibits pancreatic cancer growth and progression in murine xenograft models.* Cancer Biology & Therapy, 2011. **12**(7): p. 598-609.

68. Gojo, I., et al., *Clinical and laboratory studies of the novel cyclin-dependent kinase inhibitor dinaciclib (SCH 727965) in acute leukemias.* Cancer Chemotherapy and Pharmacology, 2013. **72**(4): p. 897-908.

69. Stephenson, J.J., et al., *Randomized phase 2 study of the cyclin-dependent kinase inhibitor dinaciclib (MK-7965) versus erlotinib in patients with non-small cell lung cancer.* Lung Cancer, 2014. **83**(2): p. 219-23.

70. Mita, M.M., et al., *Randomized phase II trial of the cyclin-dependent kinase inhibitor dinaciclib (MK-7965) versus capecitabine in patients with advanced breast cancer.* Clin Breast Cancer, 2014. **14**(3): p. 169-76.

71. http://www.ema.europa.eu/docs/en_GB/document_library/Orphan_designation/2011/10/WC500116529.pdf.

72. Wilhelm, S., et al., *Discovery and development of sorafenib: a multikinase inhibitor for treating cancer.* Nat Rev Drug Discov, 2006. **5**(10): p. 835-844.

73. Wilhelm, S.M., et al., *BAY 43-9006 exhibits broad spectrum oral antitumor activity and targets the RAF/MEK/ERK pathway and receptor tyrosine kinases involved in tumor progression and angiogenesis.* Cancer Res, 2004. **64**(19): p. 7099-109.

74. Sharma, A., et al., *Mutant V599EB-Raf regulates growth and vascular development of malignant melanoma tumors.* Cancer Res, 2005. **65**(6): p. 2412-21.

75. Carlomagno, F., et al., *BAY 43-9006 Inhibition of Oncogenic RET Mutants.* JNCI: Journal of the National Cancer Institute, 2006. **98**(5): p. 326-334.

76. Chang, Y.S., et al., *Sorafenib (BAY 43-9006) inhibits tumor growth and vascularization and induces tumor apoptosis and hypoxia in RCC xenograft models.* Cancer Chemotherapy and Pharmacology, 2007. **59**(5): p. 561-574.

77. Liu, L., et al., *Sorafenib blocks the RAF/MEK/ERK pathway, inhibits tumor angiogenesis, and induces tumor cell apoptosis in hepatocellular carcinoma model PLC/PRF/5.* Cancer Res, 2006. **66**(24): p. 11851-8.

78. Escudier, B., et al., *Sorafenib in advanced clear-cell renal-cell carcinoma.* N Engl J Med, 2007. **356**(2): p. 125-34.

79. Llovet , J.M., et al., *Sorafenib in Advanced Hepatocellular Carcinoma.* New England Journal of Medicine, 2008. **359**(4): p. 378-390.

80. Rimassa, L. and A. Santoro, *Sorafenib therapy in advanced hepatocellular carcinoma: the SHARP trial.* Expert Review of Anticancer Therapy, 2009. **9**(6): p. 739-745.

81. Cheng, A.L., et al., *Efficacy and safety of sorafenib in patients with advanced hepatocellular carcinoma according to baseline status: subset analyses of the phase III Sorafenib Asia-Pacific trial.* Eur J Cancer, 2012. **48**(10): p. 1452-65.

82. Brose, M.S., et al., *Sorafenib in radioactive iodine-refractory, locally*

advanced or metastatic differentiated thyroid cancer: a randomised, double-blind, phase 3 trial. Lancet, 2014. **384**(9940): p. 319-28.

83. http://www.ema.europa.eu/docs/en_GB/document_library/EPAR_-_Product_Information/human/000690/WC500027704.pdf.

84. Giovannini, C., et al., *Notch3 inhibition enhances sorafenib cytotoxic efficacy by promoting GSK3b phosphorylation and p21 down-regulation in hepatocellular carcinoma.* Oncotarget, 2013. **4**(10): p. 1618-31.

85. http://www.medchemexpress.com/Sorafenib.html.

86. Arcamone, F., et al., *Adriamycin, 14-hydroxydaimomycin, a new antitumor antibiotic from S. Peucetius var. caesius.* Biotechnology and Bioengineering, 1969. **11**(6): p. 1101-1110.

87. Gewirtz, D., *A critical evaluation of the mechanisms of action proposed for the antitumor effects of the anthracycline antibiotics adriamycin and daunorubicin.* Biochemical Pharmacology, 1999. **57**(7): p. 727-741.

88. Burnett, A.K., et al., *A randomized comparison of daunorubicin 90 mg/m(2) vs 60 mg/m(2) in AML induction: results from the UK NCRI AML17 trial in 1206 patients.* Blood, 2015. **125**(25): p. 3878-3885.

89. https://www.fachinfo.de/suche/fi/002977.

90. Forssen, E.A., et al., *Fluorescence imaging studies for the disposition of daunorubicin liposomes (DaunoXome) within tumor tissue.* Cancer Res, 1996. **56**(9): p. 2066-75.

91. Forssen, E.A., D.M. Coulter, and R.T. Proffitt, *Selective in vivo localization of daunorubicin small unilamellar vesicles in solid tumors.*

Cancer Res, 1992. **52**(12): p. 3255-61.

92. Latagliata, R., et al., *Liposomal daunorubicin versus standard daunorubicin: long term follow-up of the GIMEMA GSI 103 AMLE randomized trial in patients older than 60 years with acute myelogenous leukaemia.* Br J Haematol, 2008. **143**(5): p. 681-9.

93. http://www.ema.europa.eu/ema/index.jsp?curl=pages/medicines/landing/orphan_search.jsp&mid=WC0b01ac058001d12b&source=homeMedSearch&keyword=daunorubicin&isNewQuery=true.

94. Petre, C.E. and D.P. Dittmer, *Liposomal daunorubicin as treatment for Kaposi's sarcoma.* Int J Nanomedicine, 2007. **2**(3): p. 277-88.

95. Cummings, J., et al., *The molecular pharmacology of doxorubicin in vivo.* European Journal of Cancer and Clinical Oncology, 1991. **27**(5): p. 532-535.

96. Ito, H., et al., *Doxorubicin selectively inhibits muscle gene expression in cardiac muscle cells in vivo and in vitro.* Proceedings of the National Academy of Sciences, 1990. **87**(11): p. 4275-4279.

97. Sharpe, M., et al., *Polyethylene glycol-liposomal doxorubicin: a review of its use in the management of solid and haematological malignancies and AIDS-related Kaposi's sarcoma.* Drugs, 2002. **62**(14): p. 2089-126.

98. Ren, S., et al., *Comparison of pharmacokinetics, tissue distribution and pharmacodynamics of liposomal and free doxorubicin in tumour-bearing mice following intratumoral injection.* J Pharm Pharmacol, 2014. **66**(9): p. 1231-9.

99. http://www.ema.europa.eu/ema/index.jsp?curl=pages/medicines/lan

ding/epar_search.jsp&mid=WC0b01ac058001d124&source=homeMedSearch&keyword=doxorubicin&category=human&isNewQuery=true.

100. https://www.medchemexpress.com/Doxorubicin.html.

101. http://www.envigo.com/.

102. http://www.criver.com/.

103. Vieira, J., L. Pinto da Silva, and J.C.G. Esteves da Silva, *Advances in the knowledge of light emission by firefly luciferin and oxyluciferin.* Journal of Photochemistry and Photobiology B: Biology, 2012. **117**: p. 33-39.

104. Lauber, D.T., et al., *State of the art in vivo imaging techniques for laboratory animals.* Lab Anim, 2017. **51**(5): p. 465-478.

105. https://mbi-ctac.sites.medinfo.ufl.edu/files/2013/04/IVIS.jpg.

106. Gupta, G.P. and J. Massagué, *Cancer Metastasis: Building a Framework.* Cell, 2006. **127**(4): p. 679-695.

107. Davidson, S.M. and M.G. Vander Heiden, *Critical Functions of the Lysosome in Cancer Biology.* Annu Rev Pharmacol Toxicol, 2017. **57**: p. 481-507.

108. Piao, S. and R.K. Amaravadi, *Targeting the lysosome in cancer.* Ann N Y Acad Sci, 2016. **1371**(1): p. 45-54.

109. Grimm, C., et al., *Endolysosomal Cation Channels and Cancer—A Link with Great Potential.* Pharmaceuticals, 2018. **11**(1): p. 4.

110. Patel, S., *Function and dysfunction of two-pore channels.* Sci Signal, 2015. **8**(384): p. re7.

111. Dhavan, R. and L.H. Tsai, *A decade of CDK5.* Nat Rev Mol Cell Biol, 2001. **2**(10): p. 749-59.

112. Liebl, J., et al., *Twice switched at birth: cell cycle-independent roles of the "neuron-specific" cyclin-dependent kinase 5 (Cdk5) in non-neuronal cells.* Cell Signal, 2011. **23**(11): p. 1698-707.

113. Feldmann, G., et al., *Inhibiting the cyclin-dependent kinase CDK5 blocks pancreatic cancer formation and progression through the suppression of Ras-Ral signaling.* Cancer Res, 2010. **70**(11): p. 4460-9.

114. Lin, H., et al., *Cdk5 regulates STAT3 activation and cell proliferation in medullary thyroid carcinoma cells.* J Biol Chem, 2007. **282**(5): p. 2776-84.

115. Ehrlich, S.M., et al., *Targeting cyclin dependent kinase 5 in hepatocellular carcinoma--A novel therapeutic approach.* J Hepatol, 2015. **63**(1): p. 102-13.

116. Rajendran, S., et al., *Murine bioluminescent hepatic tumour model.* J Vis Exp, 2010(41).

117. Kudo, M., *Signaling Pathway and Molecular-Targeted Therapy for Hepatocellular Carcinoma.* Digestive Diseases, 2011. **29**(3): p. 289-302.

118. Llovet, J.M., et al., *Sorafenib in advanced hepatocellular carcinoma.* N Engl J Med, 2008. **359**(4): p. 378-90.

119. https://www.jax.org/jax-mice-and-services/find-and-order-jax-mice/nsg-portfolio/housing-and-breeding-considerations-for-nsg-mice.

120. Liu, Y. and D. Wang, *Administration of Chromium(III) and Manganese(II) as a Potential Protective Approach Against Daunorubicin-*

Induced Cardiotoxicity: in vitro and in vivo Experimental Evidence. Biological Trace Element Research, 2013. **156**(1): p. 253-261.

121. Volkova, M. and R. Russell, *Anthracycline Cardiotoxicity: Prevalence, Pathogenesis and Treatment.* Current Cardiology Reviews, 2011. **7**(4): p. 214-220.

VIII. HOMEPAGES

www.bmel.de

www.cancer.org

www.criver.com

http://ctac.mbi.ufl.edu/

www.emea.europa.eu/ema/

www.envigo.com

www.fachinfo.de

www.gesetze-im-internet.de

www.jax.org

www.medchemexpress.com

www.toris.com

IX. APPENDIX

Publications:

O.N. Nguyen, C. Grimm, L. S. Schneider, Y. K Chao, C. Atzberger, K. Bartel, A. Watermann, M. Ulrich, D. Mayr, C. Wahl-Schott, M. Biel, A. M. Vollmar

Two-Pore Channel Function Is Crucial for the Migration of Invasive Cancer Cells. 2017 January 20, Cancer Research.

Maximilian A. Ardelt, Thomas Fröhlich, Emanuele Martini, Martin Müller, Veronika Kanitz, Carina Atzberger, Laura Posselt, Thorsten Lehr, Melanie Ulrich, Georg J. Arnold, Lars König, Sara Sigismund, Dario Parazzoli, Stefan Zahler, Simon Rothenfußer, Doris Mayr, Alexander Gerbes, Giorgio Scita, Angelika M. Vollmar, Johanna Pachmayr

Inhibition of Cyclin-dependent Kinase 5 – a Novel Strategy to Improve Sorafenib Response in HCC Therapy. 2018 July 23, Hepatology.

Submitted:

L. Pfitzer, C. Moser, F. Foerster, C. Atzberger, T. Zisis, R. Kubisch-Dohmen, J. Busse, R. Smith, G. Timinszky, O. Kalinina, R. Müller, E. Wagner, A. M. Vollmar, S. Zahler

Targeting actin inhibits repair of chemotherapy induced DNA damage: a novel therapeutic approach for combination therapy.

In preparation:

Neocarzilin interrogates VAT-1's interaction with PI3-Kinase and inhibits cancer cell motility

Targeting of Two-Pore Cannel 2 Using Bisbenzylisoquinoline Derivates Inhibits Cancer Cell Growth in Vitro and in Vivo

X. ACKNOWLEDGEMENTS

Mein allergrößter Dank geht an Frau Prof. Dr. Angelika Vollmar für die Möglichkeit an ihrem Lehrstuhl für Pharmazeutische Biologie meine Dissertation anfertigen zu können. Ich möchte mich bei Ihnen für das entgegengebrachte Vertrauen im Hinblick auf die experimentelle Arbeit sowie die Verantwortung für unsere Labormäuse bedanken. Vielen Dank für Ihr jederzeit offenes Ohr und Ihre wertschätzende Art.

Herrn Prof. Dr. Eckhard Wolf gilt mein größter Dank dafür, dass Sie mein Betreuer an der Tierärztlichen Fakultät München sind und Sie meine Dissertation angenommen haben.

Im ganz besonderen Maße möchte ich mich bei Frau Prof. Dr. Johanna Pachmayr für die Betreuung meiner Arbeit am Institut und meiner Dissertation bedanken. Ich danke dir vielmals für deine stets verfügbare Unterstützung.

Herrn Prof. Dr. Martin Biel und Herrn PD Dr. Stylianos Michalakis gilt mein großer Dank dafür, dass ich ihren Tierstall für meine Labormäuse nutzen durfte.

Im Besonderen möchte ich mich bei den Kooperationspartnern des Arbeitskreises Vollmar bedanken. Vielen Dank an Frau Prof. Dr. Irmela Jeremias und Frau Dr. Binje Vick für die Kooperation im Projekt AML-372, für die Expertise mit NSG-Mäusen und die Unterstützung während des Leukämieprojektes. Großer Dank gilt auch Herrn Dr. Christoph Müller und Frau Anna Niedrig für die Messungen der Pharmakokinetik, ebenso Herrn Dr. Sebastian Kobold für die Kooperation zur Tumorzelldissemination, sowie Herrn PD Dr. Hans Zischka und Frau Dr. Sabine Schmitt für die Kooperation zum subkutanen Tumormodel mit McA-RH7777. Mein größter Dank gilt Frau Laura Posselt für die Durchführung der Operation im Model zur intrahepatischen Metastasierung.

Ebenso möchte ich mich herzlich bei Frau Dr. Simone Braig bedanken. Danke für deine Unterstützung und dein Engagement bezüglich des Enrichments bei unseren Mäusen.

Großer Dank gilt den Tierpflegern des Arbeitskreises Biel, Mariella, Selina, Jessica, Katharina und Pierre für ihre Arbeit im Tierstall.

Als einziger Tierarzt im Arbeitskreis ist eine gute Einarbeitung von enormem Wert. Frau Dr. Melanie Ulrich, ich bin dir dankbar, dass du dir Zeit genommen hast, mich in meine neuen Aufgaben einzuarbeiten.

Alleine wäre es unmöglich gewesen, Versuche in diesem Umfang durchzuführen. Liebe Kerstin, ich danke dir von ganzem Herzen für deine Unterstützung, deinen Rat, deine Geduld und deine Freundschaft.

Die Planung der Tierexperimente erfolgte oftmals in Zusammenarbeit mit anderen Doktoranden und Mitarbeitern. An dieser Stelle sollen zwei Kollegen besondere Erwähnung finden. Liebe Phuong, ich danke dir für deine Hilfe in allem was PC-Technik und Datenaufbereitung betrifft. Lieber Max, ich danke dir im Besonderen für deine Hilfe bei allen Tumorfotographien und deinen enormen Enthusiasmus vor und während gemeinsamer Versuche.

Liebe Sarah, ich danke dir vielmals für das aufmerksame Korrekturlesen meiner Dissertation.

Besonderer Dank für die angenehme Zeit in unserem gemeinsamen Labor gilt meinen Mitdoktorandinnen Christina, Lisa und Caro.

Dem kompletten Arbeitskreis Vollmar möchte ich für das freundschaftliche und immer hilfsbereite Miteinander danken.

Mein herzlichster Dank gilt meinen Eltern Anita und Harald für ihre Unterstützung, meinen eigenen Weg zu gehen und ihr Vertrauen in meine Entscheidungen. Ohne eure Unterstützung wäre mein Ziel nicht umsetzbar gewesen.

Lieber Christopher, ich danke dir besonders für deine Unterstützung, dein Verständnis für ein zeitintensives Studium und deine beruhigende Art zur rechten Zeit.